Multi-omic Landscape of Extracellular Vesicles in Human Carotid Atherosclerotic Plaque Reveals Endothelial Communication Networks

Sneha Raju, MD, PhD,[1, 2, 3, 4] Mandy E Turner, PhD,[5] Christian Cao,[4] Majed Abdul-Samad, BSc,[6] Neil Punwasi, MSc,[7] Mark C Blaser, PhD,[5] Rachel ME Cahalane, PhD,[5,8] Steven R Botts, MSc,[1,2,4] Kamal Prajapati, BSc,[1,6] Sarvatit Patel, PhD,[1] Ruilin Wu, MSc,[1,6] Dakota Gustafson, PhD,[1] Natalie J Galant, PhD,[9] Lindsey Fiddes, PhD,[4] Melody Chemaly, PhD,[10] Ulf Hedin, MD, PhD,[10] Ljubica Matic, PhD,[10] Michael Seidman, MD, PhD,[6,7] Vallijah Subasri, PhD,[7] Sasha A Singh, PhD,[5] Elena Aikawa, MD, PhD,[5,11] Jason E Fish, PhD,[1,2,6,7] *Kathryn L Howe, MD, PhD,[1,2,3,4,6,7]

Institutions:

[1] Toronto General Hospital Research Institute, University Health Network, Toronto, Canada.

[2] Institute of Medical Science, University of Toronto, Toronto, Canada.

[3] Division of Vascular Surgery, Toronto General Hospital, Toronto, Canada.

[4] Faculty of Medicine, University of Toronto, Toronto ON, Canada.

[5] Center for Interdisciplinary Cardiovascular Sciences, Cardiovascular Division, Department of Medicine, Brigham and Women's Hospital, Harvard Medical School, Boston, MA, USA

[6] Department of Laboratory Medicine and Pathobiology, University of Toronto, Toronto, ON, Canada

[7] Peter Munk Cardiac Centre, Toronto General Hospital, Toronto, Canada

[8] Mechanobiology and Medical Device Research group (MMDRG), Biomedical Engineering, College of Science and Engineering, University of Galway, Galway, Ireland.

[9] Princess Margaret Cancer Center, Toronto, ON, Canada

[10] Vascular Surgery Division, Department of Molecular Medicine and Surgery, Karolinska University Hospital and Karolinska Institut, Stockholm, Sweden.

[11] Center for Excellence in Vascular Biology, Brigham and Women's Hospital, Harvard Medical School, Boston, MA, USA

Short-Title: Endothelial messaging in carotid atherosclerosis

Correspondence:

Kathryn L. Howe (Kathryn.howe@uhn.ca)

Peter Munk Cardiac Centre, University Health Network

6EN 220-200 Elizabeth Street, Toronto General Hospital, Toronto, ON, M5G 2C4, Canada

Word Count: 14,759

Abstract

Background: Carotid atherosclerosis is a multifaceted disease orchestrated by a myriad of cell-cell communication that drives progression along a clinical continuum (asymptomatic to symptomatic). Extracellular vesicles (EVs) are lipid bilayer membrane-enclosed cell-derived nanoparticles that represent a new paradigm in cellular communication. Little is known about their biological cargo, cellular origin/destination, and functional roles in human atherosclerotic plaque.

Methods: EVs were enriched via size exclusion chromatography from human carotid endarterectomy samples dissected into plaque and marginal zones (n= 29 patients, paired plaque and marginal zone; symptomatic n=16, asymptomatic n=13), with further density gradient ultracentrifugation for proteomic analysis. EV cargoes were assessed via whole transcriptome miRNA sequencing and mass spectrometry-based proteomics. EV multi-omics were integrated with publicly available bulk and single cell RNA-sequencing (scRNA-seq) datasets to predict EV cellular origin and ligand-receptor interactions and multi-modal biological network integration of EV-cargo was completed. EV functional impact was assessed with endothelial angiogenesis assays.

Results: Human carotid plaques contained greater quantities of EVs than adjacent marginal zones. EV-miRNA and protein content was different in diseased plaque versus adjacent marginal zones, with differential functions in key atherogenic pathways. EV cellular origin analysis suggested that tissue EV signatures originated from endothelial cells (EC), smooth muscle cells (SMC), and immune cells. Furthermore, EV signatures

from SMCs and immune cells were most enriched in the marginal and plaque zones, respectively. Integrated tissue vesiculomics and scRNA-seq indicated complex EV-vascular cell communication strategies that changed with disease progression and plaque vulnerability (i.e., symptomatic disease). Plaques from symptomatic patients, but not asymptomatic patients, were characterized by increased involvement of endothelial pathways and more complex ligand-receptor interactions, relative to their marginal zones. Plaque-EVs were predicted to mediate communication with ECs. Pathway enrichment analysis delineated a strong endothelial signature with potential roles in angiogenesis and neovascularization – well-known indices of plaque instability. This was corroborated functionally, wherein human carotid symptomatic plaque EVs induced sprouting angiogenesis in comparison to their matched marginal zones.

Conclusion: Our findings indicate that EVs may drive dynamic changes in plaques through EV-vascular cell communication and effector functions that typify vulnerability to rupture, precipitating symptomatic disease. The discovery of endothelial-directed processes mediated by EVs creates new avenues for novel therapeutics in atherosclerosis.

Key Words: carotid atherosclerosis, extracellular vesicles, microRNAs, proteomics, endothelial cells

Non-Standard Abbreviations

cryo-EM	cryogenic electron microscopy
EC	endothelial cell
EV	extracellular vesicle
GO	Gene Ontology
KEGG	Kyoto Encyclopedia of Genes and Genomes
NTA	nanoparticle tracking analysis
miRNA	microRNA
MISEV	Minimal information for studies of extracellular vesicles
MZ	marginal zone
PZ	plaque zone
scRNA-seq	single cell RNA-sequencing
SEC	size exclusion chromotography
SMC	smooth muscle cell
TEM	transmission electron microscopy

63 **Introduction**

64 Atherosclerosis is a multi-cellular biological process of lipid accumulation, unresolved
65 inflammation, and plaque development in the arterial wall.[1,2] While some plaques
66 enlarge and impede blood flow, plaques can also become unstable and rupture, thereby
67 releasing atheroembolic material that occludes an end-artery leading to a transient
68 ischemic attack (TIA, i.e. neurologic recovery) or stroke.[1,3] Atherosclerosis exists along
69 a disease continuum wherein much of the disease process is silent and presents as
70 asymptomatic disease; low-density lipoprotein accumulation and endothelial dysfunction
71 initiates the disease process, followed by recruitment of adaptive and innate immune
72 cells and migration of smooth muscle cells (SMCs) leading to plaque progression and
73 development of the necrotic core, followed by eventual fibrous cap rupture and
74 thrombosis causing clinical events such as myocardial infarction or stroke.[2] Altered
75 cellular communication is a critical linchpin of atherogenesis.[4-7] Recent work has
76 identified the importance of endothelial cells (ECs) in directing differential, polarized
77 messaging with cells found in circulation and those in the vessel wall.[8] Given that
78 several types of plaque cells exist in transitory states (ECs, SMCs, macrophages), are
79 highly dynamic, and can alter their phenotype in the active plaque microenvironment, an
80 exciting possibility is that cellular states dictate and result from changes in cell-cell
81 communication[9-12]

82

83 Much of the early and late stages of atherosclerotic disease is silent or asymptomatic,
84 creating challenges in patient stratification. Unlike management of symptomatic carotid
85 atherosclerotic disease, which is well established and includes surgical removal of the

plaque (carotid endarterectomy) or endovascular carotid stenting with the goal of secondary stroke prevention ~~[13-16]~~, management of patients with asymptomatic carotid disease is more nuanced, as interventions have an upfront risk of stroke and we have not yet solved how to accurately predict plaque rupture.[17,18] Current non-operative management with lipid reduction, anti-hypertensive therapy, and lifestyle modifications (i.e. smoking cessation) reduces stroke risk, but some patients progress despite meeting these targets.[17,19] Prior studies have employed whole-tissue proteomics, transcriptomics, and metabolomics to identify major shifts in plaque biology with disease progression.[20-23] However, despite ongoing research, there are still no universally reliable means to identify the patient at risk and novel therapeutic targets need to be unveiled through a better understanding of plaque biology as it evolves along the disease continuum.

Given the multi-cellular environment of the atherosclerotic plaque, cell-cell communication is a major factor driving the biology of the disease. Extracellular vesicles (EVs) are lipid bilayered membrane-enclosed cell-derived nanoparticles that carry bioactive molecules such as microRNAs (miRNAs) and proteins from a donor to a recipient cell, where they participate in EV-ligand based interactions or are endocytosed and release contents that can modulate recipient cell phenotype.[24] Given the clinical potential of this field, the development of Minimal Information for the Study of Extracellular Vesicles (MISEV) guidelines has been crucial for improving clarity, consistency in reporting, and interpretation of EV-based studies.[25,26] Previous studies in atherosclerotic plaques have examined larger EV particles (i.e., microparticles; primarily

109 >200 nm) and provided early insights into their importance in atherosclerotic biology.[27,28]
110 However the evolution of EV isolation and technical progress in EV cargo analysis
111 mandates a fresh examination of their biological roles, particularly with respect to small
112 EVs (<200 nm) given their abundant numbers and potential for therapeutic
113 modulation.[29,30] Recently, a proteomics study of human carotid plaque-derived EVs
114 small and large identified their role in advanced atherosclerotic calcification, and found
115 that EV-proteomics can identify additional phenotypes than those at the whole plaque
116 level, warranting independent investigation.[31] Our understanding of carotid tissue
117 vulnerability as modulated by EV cellular source, EV-cell communication, and the
118 impact of EVs on downstream cellular processes is limited. There is a need to
119 understand the holistic biological niche of stable and vulnerable carotid plaques in these
120 contexts, with the goal of identifying novel targets for preventing rupture through plaque
121 stabilization.
122
123 The intraplaque environment is dynamic, changes over time, and there is a significant
124 role for cell-cell communication. EVs contain cargo that serve as important mediators of
125 cell-cell communication with functional effects that alter cell biology in recipient cells.[32-34]
126 What is not known however, are the alterations to cell-cell communication that render an
127 atherosclerotic plaque vulnerable to rupture. Patients with symptomatic carotid disease
128 have demonstrated clinical consequences of carotid plaque vulnerability where
129 atheroembolic events have caused transient ischemic events or stroke.[35] Here, we
130 performed a novel analysis to uncover the transcriptomic and proteomic EV profile in
131 carotid plaque and adjacent marginal zones, in both asymptomatic and symptomatic

132 disease states. By integrating our data with scRNA-seq datasets, we identified the
133 predicted EV-cell communication pathways that may be enriched in asymptomatic and
134 symptomatic (vulnerable) carotid plaques. Furthermore, we found a strong endothelial
135 signature and demonstrated a functional role for plaque EVs in regulating angiogenesis
136 and neovascularization – well-known precursors of plaque instability.[36-38] Importantly,
137 symptomatic plaques were studied within 30 days of the last neurologic event, with
138 pathological evaluation of a subset that clearly demonstrated intraplaque hemorrhage,
139 consistent with the EV angiogenesis experiments pursued. Together, our data suggest
140 that EVs may contribute to dynamic changes seen in plaques - through EV-cell
141 communication and effector functions - including neovascularization and angiogenesis
142 that contribute to plaque destabilization. The discovery of an endothelial-centric process
143 that could be mediated by EVs points towards novel therapeutics targeting this highly
144 accessible and strategic cellular layer.
145
146
147 **Methods**
148 Detailed methods are provided in the Supplemental Material. Human carotid
149 endarterectomy specimens were obtained from patients undergoing surgery for
150 asymptomatic and symptomatic disease. Samples were handled under the institutional
151 research ethics board protocols set by University Health Network, Toronto Canada (18-
152 5282). Patients gave written informed consent and procedures were followed in
153 accordance with institutional guidelines. Tissues were separated by plaque and
154 marginal (non-atheromatous) zones and EV enrichment performed according to

155 MISEV2023 guidelines. Transcriptomics (next-generation miRNA sequencing) and
156 proteomics (mass spectrometry-based) data are deposited in GEO and
157 ProteomeXChange Consortium via the PRIDE repository (publicly available at the time
158 of publication), respectively. Cell-cell communication was evaluated by integrating data
159 with the TISSUES database[39] and a publicly available scRNA-sequencing dataset of
160 carotid endarterectomy specimens containing plaque and marginal zones
161 (GSE159677).[20] Multi-omic network analysis was performed using BIONIC.[40] Functional
162 validation of predicted roles for EVs on angiogenesis was performed in Human
163 Umbilical Vein Endothelial Cell (HUVEC) spheroid-based sprouting assays.
164

165 **Statistical Analysis**

166 The Fisher's exact test tested the prevalence of gene ontology (GO) terms in whole
167 tissue proteomics. For non-omics data with sample sizes <10, a two-sided Mann-
168 Whitney or Wilcoxon (for paired samples) test was completed and for n≥10, data
169 distribution was assessed and differences between two groups were tested using a two-
170 tailed unpaired Student's *t*-test. For comparisons between three or more groups, a one-
171 way ANOVA was used with Šidák multiple comparisons test . Differences were
172 significant for values of $p<0.05$ and are indicated in the figures. Proteomics (tissue and
173 EV) were quantified using Discover (Version 2.5) and peptides were filtered based on a
174 1.0% FDR. A minimum of at least 2 unique peptides for each protein was required for
175 the protein to be included in the analyses. Differential enrichment analysis was
176 performed using Qlucore Omics Explorer statistical software (Version 3.9; Qlucore,
177 Sweden) and differentially enriched proteins were calculated using a two-group

178 comparison with a Benjamini-Hochberg false discovery rate (FDR)-corrected p-value
179 (i.e., q-value) <0.05. Transcriptomic data (miRNA) was quantified in Partek Flow
180 (v10.0.23.0326) including trimming of adaptors, sequence alignment to genome (h38
181 assembly, Homo Sapiens, BioProject PRJNA31257, Bowtie), and quantification
182 (miRBase mature miRNAs, Version 22). Differential expression of miRNA in
183 experimental conditions was determined via DESeq2 with adjustment for multiple
184 comparisons using Benjamini and Hochberg's FDR step-up (adjusted p-value<0.05).
185 Predicted messenger RNA (mRNA) targets of differentially expressed EV-miRNA were
186 identified using MicroRNA Enrichment Turned Network (MIENTURNET version 2019-11-
187 25) using the miRTarBase database. Pathway analysis of differentially enriched EV-
188 miRNAs and EV-proteins were completed using Enrichr using the Gene Ontology
189 (Biological Process and Cellular Component) and Kyoto Encyclopedia of Genes and
190 Genomes(KEGG) databases with multiple testing correction using the Benjamini-
191 Hochberg procedure (adjusted p<0.05). Protein-protein interaction analysis was
192 completed in STRING v12.0. The TISSUES and Tabula Sapiens databases were
193 accessed through STRING v12.0 and Enrich, respectively. EV cellular identity
194 enrichement analysis was completed using the AddModule score function in Seurat
195 (Version 5.0.1) to assess the enrichment of EV protein signatures among different cell
196 types. The 'CellChat' R package (version 1.6.0) was used to infer cell interaction
197 networks by filtering the CellChat cell-cell communication ligand database for genes
198 associated with EV protein gene IDs. Comparison of fold enrichments between cohorts
199 regarding endothelial-related GO biological processes were performed using ANOVA
200 and Tukey's honest significant difference.

201 **Results**

202

203 **Atherosclerotic tissue proteome and extracellular vesicle (EV) concentration**

204 **identify a potential role for EVs in modulating the disease continuum**

205

206 As recently shown by Alsaigh et al., single cell RNA sequencing (scRNA-seq) of

207 matched human carotid marginal zones and plaque zones harbour different cellular

208 subpopulations, revealing distinct microenvironments, and cellular communication

209 strategies that may provide insights into disease progression.[20] To begin understanding

210 the continuum of disease in carotid atherosclerosis, we delineated EV-based biology in

211 plaque versus marginal zones from all patients (asymptomatic and symptomatic).

212 Human carotid endarterectomy specimens for whole tissue proteomics (n=5) were

213 dissected into plaque zones (PZ) and marginal zones (MZ) based on gross morphology

214 by a single trained surgeon (Dr. S. Raju), with another 59 paired samples similarly

215 dissected for EV enrichment and characterization (Figure 1A). Tissue histopathology

216 with hematoxylin and eosin and Movat pentachrome stains delineated plaque and

217 marginal zones to be different with distinguishing features of advanced atherosclerotic

218 plaque morphology (e.g. necrotic core, intraplaque hemorrhage) visualized exclusively

219 in plaque regions (Figure S1A-B).

220

221 Tissue proteomes (Figure S2A) from the plaque zones and marginal zones clustered

222 separately by principal component analysis (Figure 1B donor corrected; Figure S2C

223 donor uncorrected), with 514 differentially enriched proteins identified by zone (Figure

224 S2B). Pathway analysis of differentially enriched proteins in the marginal and plaque
225 zone (p_{adj}<0.05) using Gene Ontology (GO) and Kyoto Encyclopedia of Genes and
226 Genomes (KEGG) revealed atherogenic signatures, while GO terms containing 'vesicle'
227 were increased in plaque zones specifically (Figure 1C, S2D-F, S3A-B). We next
228 pursued EV enrichment in plaque and marginal zones separately. EVs were enriched
229 using size exclusion chromatography that included an additional density
230 ultracentrifugation step to remove extracellular matrix co-isolation[31] and was validated in
231 accordance with the MISEV2023 criteria (Figure 1D-G, S4A-F, S5A, S6). Briefly, EVs
232 were enriched in fractions 7-10 as evidenced by single vesicle analysis using
233 nanoparticle tracking analysis (NTA) and as a protein peak using the bicinchoninic acid
234 assay (Figure S4E). The secondary protein peak (Figure S4E) represents smaller
235 proteins that elute in the later fractions.[41] The presence of common EV protein markers
236 in per-fraction proteomics, including CD63, CD81, CD9, FLOT1, and an absence of the
237 cell protein marker calnexin confirmed successful EV isolation in our fractions of interest
238 (Figure 1D, left and right panels respectively; Figure S5A). Several vesicle-related
239 pathways were enriched in plaque zones compared to marginal zones (Figure S5B),
240 which may suggest increased EV processes taking place. We confirmed EV
241 morphology via direct visualization using cryogenic electron microscopy (cryo-EM),
242 which revealed bilayered nanoparticles with dense cores, as well as several muti-
243 compartmented vesicles, recently seen to be released by cells (Figure 1E).[42] We did not
244 observe any morphological or size differences between EV isolates from plaque and
245 marginal zones (Figure 1F). Paired plaque regions liberated similar EV size distribution,
246 but a larger quantity of EVs per milligram of tissue relative to marginal zones (Figure

247 1G). Notably, we found minimal lipoprotein (APOA1[43] and APOB100, enzyme-linked
248 immunosorbent assay, Figure S4C-D) and no whole-cell (flow cytometry, Figure S4F)
249 inclusion in vesicle preparations. Given EVs in marginal and plaque zones have the
250 potential to contribute to the local milieu, we next compared the biological cargo of EVs
251 between these two anatomical locations to help delineate the potential functional effects
252 of the EV-vesiculome in carotid atherosclerotic disease progression.
253
254
255 **Carotid plaque EV-vesiculome (miRNA transcriptome and proteome) is distinct in**
256 **plaque versus marginal zones and drives pathways known to govern plaque**
257 **progression**
258
259 Given that EV miRNA and protein cargo can mediate their functional effects on recipient
260 cells in local environments,[32-34] we performed next-generation miRNA sequencing and
261 proteomic analysis of EVs enriched from carotid plaque zones and marginal zones
262 (Figures S6, S7). Exploratory analysis with donor-corrected principal component
263 analysis (PCA) revealed that the EV-vesiculome clustered by location; specifically
264 plaque zone (PZ, purple) and marginal zones (MZ, pink; Figure 2A-B; donor
265 uncorrected Figure S7F). Differentially enriched protein pathway analysis predicted
266 biological interconnectability in plaque-derived EVs, as seen by greater than expected
267 protein-protein interactions (Figure 2C). Differential expression analysis between EV-
268 miRNA in plaque versus marginal zones revealed 371 EV-miRNA enriched in plaque
269 zones and 290 EV-miRNA enriched in marginal zones, across 20 paired patient

270 samples (Figure 2D). Top differentially expressed upregulated miRNA in the plaque
271 zones included miR-146a, miR-155, let-7a, miR-200b, miR-223, and miR181b, known to
272 have roles in secretion and response to inflammatory mediators and cell proliferation
273 and differentiation.[44-54] Among differentially enriched proteins, we found 282 proteins
274 enriched in plaque zones, and 379 enriched in marginal zones, across 23 paired patient
275 samples (Figure 2E). Like the EV-miRNAs, several known mediators of plaque
276 progression including metalloproteinases (MMP9), cell adhesion proteins (ICAM1),
277 lipoprotein metabolism proteins (LPL), complement and coagulation proteins (F2, F10),
278 and inflammatory mediators (CRP, SAA2-4, BLVRA, BLVRB) were more abundant in
279 EVs from plaque environments (Figure 2E).
280
281 To explore the potential functions of EV-miRNA and protein cargo, we queried KEGG
282 pathways using the Enrichr interface comparing plaque zone versus marginal zone EV
283 cargo.[55] Carotid plaque EV-cargo represented 155 unique KEGG pathways
284 (FDR<0.05), with 60 pathways specific to EV-miRNAs and 60 pathways specific to EV-
285 proteins (Figure 2F, Venn diagram). Top unique pathways predicted to be modulated by
286 plaque EV-miRNA included cell cycle, apoptosis, and inflammatory signaling pathways
287 (TNF, T cell receptor, TGF-β, chemokine, NFκB; Figure 2F, top right panel). Conversely,
288 top unique pathways of differentially expressed plaque EV-proteins include complement
289 and coagulation, phagosome, cholesterol metabolism, cell adhesion, and vascular
290 smooth muscle contraction (Figure 2F, bottom right panel). Key pathways involved in
291 atherosclerotic plaque progression shared between the EV-miRNA and EV-proteome
292 included cellular senescence, cell adhesion and migration, leukocyte transendothelial

293 migration, fluid shear stress and atherosclerosis, lipid and atherosclerosis, and amino
294 acid and pyruvate metabolism (Figure 2F, bottom left panel). These data suggest that in
295 the plaque the differentially enriched EV-vesiculome (i.e., protein and miRNA) may
296 function together, as well as independently, to modulate several pathways known to be
297 involved in driving plaque biology. Given EVs are a vector of cell-cell communication
298 between donor and recipient cells, we next attempted to determine the cellular origin of
299 human plaque EVs to delineate the cellular contributors to plaque EV and further, how
300 they might change with disease progression from marginal to plaque zones.
301
302
303 **Total EV-proteomics suggests diverse EV cell of origin and potential targets**
304 **modulated in recipient cells**
305
306 EVs carry cargo and membrane proteins that are reflective of their cell of origin.[56,57]
307 Cells secrete EVs with distinct biological cargo to relay specific messages to recipient
308 cells. To date, little is known about the cellular communication occurring *in vivo* within
309 the plaque niche via EVs. We used two complementary approaches to infer the EV cell
310 of origin using our EV proteomics. We started by exploring our total EV proteomics (i.e.
311 plaque and marginal regions combined) within the TISSUES database[39] which
312 integrates evidence on tissue expression from proteomic and transcriptomic screens.
313 The predicted cellular EV origin included a range of expected cells including endothelial
314 (neointima), several immune (B-lymphoblastoid, plasma cell, bone marrow cell, and
315 foam cell), and smooth muscle cells (Figure 3A; Figure S8A,C). The analysis was then

316 refined with EV-protein signature enrichment analysis among carotid artery cells
317 specifically, by integrating our complete list of total detected EV-proteins with a publicly
318 available scRNA-seq dataset containing paired plaque and marginal region samples
319 (n=6 samples, Figure S9A-G).[20] Data integration corroborated the EV cell of origin,
320 identifying strong EV signatures from vascular smooth muscle cells, endothelial cells,
321 dendritic cells, macrophages and lymphocytes (Figure 3B). Likewise, examination of
322 EV-miRNA normalized counts in our plaque and marginal zones identified several
323 miRNAs that are frequently ascribed to endothelial,[45,58-62] smooth muscle,[63-65] and
324 lymphocyte cells,[47,66-70] suggesting EV cell of origin signatures that align with those
325 predicted by the EV-proteome (Figure S10A).
326
327 Beyond the suspected cell of origin, EV surface proteins and protein cargo deliver
328 ligands to recipient cells within the atherosclerotic plaque environment – the biological
329 consequences of this interaction will depend on the protein repertoire of the recipient
330 cell. Using CellChat[71], we predicted EV ligand communication (incoming signaling) with
331 recipient cells that would be found in atherosclerosis using the same publicly available
332 scRNA-seq dataset as above. Global EV-cell communication analysis was performed by
333 specifically filtering for known receptor-ligand interactions where ligands were derived
334 from EV proteomics and receptors from scRNA-seq. When the total EV proteome was
335 applied to scRNA-seq data annotated as plaque or marginal, it identified the predicted
336 distribution of cellular EV source by each region (Figure 3C). Inferred cell
337 communication pathways used total EV-associated ligands with total scRNA-seq (i.e.
338 present in both plaque and marginal regions) (Figure 3D), as well as total EV-ligands

339 separated by marginal and plaque regions (Figure S10C). The strongest global EV-cell
340 interactions were seen among immune cells including macrophages and T-cells, with
341 the enrichment of inflammatory signaling patterns (CypA, MIF, MHC-I, CXCL,
342 prostaglandin, MHC-II). The predicted distribution of enriched global EV signaling
343 pathways place ApoE, tenascin, cholesterol, and visfatin more likely within plaque zones
344 (Figure S10B), while cord diagrams demonstrate predicted global EV ligand-receptor
345 pairs with endothelial, macrophage, and vascular SMC populations (Figure S10D left,
346 middle, and right panels, respectively).
347
348 Approaching EV-miRNA communication within tissue is more complex. Using the
349 predicted messenger RNA (mRNA) targets of EV-miRNA, the genes that could be
350 altered can be determined and correlated with single cell transcriptomics to understand
351 potential EV-miRNA communication to recipient cells. We similarly used two approaches
352 to annotate expected cellular targets of plaque EV-miRNAs - Tabula Sapiens database[72]
353 (vascular tissue) and the publicly available scRNA-seq carotid dataset as above (Figure
354 3E-F). All differentially expressed EV-miRNA had over 1956 (FDR<0.05) experimentally
355 validated (miRTarBase)[73] mRNA targets expressed in lymphocytes, endothelial cells,
356 SMCs and macrophages (Figure 3E). Plaque EV-miRNA to mRNA gene-set enrichment
357 analysis with the carotid scRNA-seq dataset corroborated these findings, wherein
358 targets of plaque EV-miRNAs were enriched in lymphocytes, endothelial cells, vascular
359 SMCs, and macrophages (Figure 3F).
360
361

362 **Plaque and marginal zone EV-proteomes predict different EV cells of origin,**
363 **recipient cell repertoires, and expected communication with vascular cells**
364
365 As the microenvironments of plaque and marginal zones are likely distinct (also
366 implicated by initial exploration, Figure 3C), we recapitulated our approach to infer EV
367 cellular origin and predicted targets in recipient cells by region using differentially
368 enriched EV-proteins and differentially expressed EV-miRNA between plaque versus
369 marginal zones. When delineated by region, plaque zones appear to have greater
370 representation of macrophages as sources of EVs than marginal zones, where vascular
371 SMCs predominated (Figure 4A-B). TISSUES database supported this finding, with our
372 plaque and marginal zones highlighting diverse cellular EV sources that ranked
373 differently by region (Figure 4C-D, S8B-C), predominantly reflecting cells that would be
374 found in atherosclerosis despite the broader tissue sources included in this dataset.
375
376 We then pursued EV-cell communication signals within plaque and marginal regions
377 separately, by filtering EV ligands as either plaque-enriched EV-proteins or marginal-
378 enriched EV-proteins. Known ligand-receptor interactions were then explored using
379 CellChat as above. In comparison to marginal zones (Figure 4E), plaque enriched EV-
380 protein ligands were predicted to participate in more diverse and distinct cellular
381 communication strategies when paired with total scRNA-seq (i.e. present in both plaque
382 and marginal regions) (Figure 4F). For example, several predicted inflammatory ligand-
383 receptor interactions emerged in the plaque zone with ApoE, complement, ICAM,
384 cathepsin (CTSG), and cholesterol signatures. Similar increased communication

385 diversity was predicted in plaque zones when analysis was restricted to single cells in
386 marginal and plaque regions separately (Figure S11A-B). Chord communication
387 diagrams were then created to explore region-specific cell-cell communication.
388 Differentially enriched EV-protein ligands from our marginal and plaque zones were
389 paired with publicly available single cell transcripts (potential receptor recipients) from
390 either endothelial cells (Figure 4G), vascular SMCs (Figure 4H), or macrophages
391 (Figure S11C) found in respective marginal regions (left panels) or plaque regions (right
392 panels). For each cell type examined, plaque zones exhibited increased predicted
393 ligand-receptor interactions relative to marginal zones. Notably, proposed plaque EV-
394 cell communication included endothelial integrins (needed for cell motility), vascular
395 SMC integrins and AXL (phagocytosis), and macrophage complement and cell adhesion
396 (C3AR1, CD44). Together, EVs are predicted to communicate with several
397 atherosclerosis-relevant cell types, with regional (plaque and marginal) differences in
398 communication patterns.
399
400
401 **Carotid plaque EVs are increased in number and contain EV-cargo (miRNA and**
402 **protein) that are differentially enriched based on plaque vulnerability**
403
404 Understanding the biological potential and EV-cell communication that takes place
405 along the continuum of asymptomatic to symptomatic carotid disease will provide new
406 insights into this complex clinical problem. We assessed differences in EV-cargo
407 between asymptomatic (n=10 patients) and symptomatic (n=10-13 patients) groups by

408 anatomical zones (marginal and plaque; Figure 5A). Blinded pathological grading
409 performed by a staff pathologist (Dr. M. Seidman) of a representative plaque samples
410 (n=5) demonstrated fibroatheroma and calcification in all (AHA grade V-VI),[38,74] with
411 evidence of intraplaque hemorrhage reported in all symptomatic patients (Figure 5B,
412 S12A). While both asymptomatic and symptomatic plaque zones contained more EVs
413 per milligram of tissue compared to their matched marginal zones, only symptomatic
414 patients achieved statistical significance (Figure 5C-D, S12B). Morphologically, carotid
415 EVs were similar in symptomatic and asymptomatic groups (size and cryo-EM, Figure
416 5E). Direct comparisons by symptom status within plaque and marginal zones did not
417 yield significant differences in EV quantification highlighting the importance of matched
418 marginal zone controls (Figure S12C-D).
419
420 When analysis of EV-cargos was performed, there were consistently larger numbers of
421 differentially enriched EV-miRNA and EV-proteins in the symptomatic group in both
422 marginal zones (delineated by negative fold change) and plaque zones (delineated by
423 positive fold change) (Figure 5F-I – volcano plots), suggesting increased biological
424 complexity in clinically vulnerable plaques and their corresponding marginal regions for
425 symptomatic patients.
426
427 We next assessed specific differences in EV-cargo between asymptomatic plaques
428 versus paired marginal zones and separately, EV-cargo differences between
429 symptomatic plaques versus paired marginal zones (Figure 6). There were 306 unique
430 differentially expressed EV-miRNAs in symptomatic tissue compared to only 33 unique

431 EV-miRNA in asymptomatic tissue (Figure 6A). Overlap was seen with 364 differentially
432 expressed EV-miRNAs in the two groups. Pathway analysis of unique EV-miRNA
433 symptomatic predicted targets revealed more GO and KEGG pathways (Figure 6B).
434 Unique signatures in asymptomatic tissues included steroid biosynthesis, ABC
435 transporters, and the AMPK signaling pathway (Figure 6C). Pathways derived using
436 unique symptomatic EV-miRNAs were numerous and included lipid and atherosclerosis,
437 inflammatory signalling (HIF-1, TGFβ, TNF) and NOTCH signaling (endothelial
438 angiogenesis) (Figure 6D). Similarly, 435 unique differentially enriched EV-proteins were
439 seen in symptomatic tissue, compared to 6 in asymptomatic (Figure 6E) and functioned
440 with a high degree of biological interconnectibility (Figure S12E). Similar to the EV-
441 miRNA analysis, there were an increased number of GO and KEGG pathways
442 modulated by the symptomatic plaque EV-protein contents (Figure 6F). KEGG pathway
443 analysis of the unique EV-proteins from asymptomatic tissue identified 6 KEGG
444 pathways functioning in amino acid and nutrient metabolism, antigen presentation, renin
445 secretion, and complement and coagulation with only a single EV-protein (annotated in
446 figure) contributing to each pathway protein (Figure 6G). The unique EV-proteins from
447 symptomatic tissue identified several biological pathways with the top differentially
448 expressed pathways including complement and coagulation, cell motility (regulation of
449 actin cytoskeleton, focal adhesion, ECM-receptor interaction, leukocyte transendothelial
450 migration), and cholesterol metabolism (Figure 6H, left panel). Several proteins were
451 enriched in the symptomatic plaque EVs that demonstrated protein-protein interactions,
452 forming three units (complement and coagulation cascades, cholesterol metabolism,
453 and regulation of actin cytoskeleton) predicted to modulate these pathways (Figure 6H,

454 right panel). Together, these vesiculomic data highlight the potential for EVs to govern
455 several well-known aspects of plaque biology, with increasing complexity as the disease
456 continuum progresses.
457
458
459 **Predicted EV-based cell communication in the symptomatic plaque reveals the**
460 **emergence of an endothelial cell signature with functional effects on**
461 **angiogenesis**
462
463 The differences in EV cargo between asymptomatic and symptomatic groups led us to
464 query differences in predicted cellular communication based on symptom status. EV
465 cellular identity was inferred by integrating our enriched EV-protein signatures from
466 either marginal or plaque zones according to symptom status with carotid marginal and
467 plaque scRNA-seq data (Figure 7A-D). Greater endothelial cell (EC) enrichment was
468 predicted in symptomatic plaque signatures relative to asymptomatic plaque signatures
469 (purple bars highlight each EC subpopulation, with increasing prevalence noted as a
470 shift to the left; Figure 7B,D), possibly suggesting a heightened role of endothelial cell-
471 derived EVs in governing EV-cell communication with atherosclerotic plaque
472 progression. No notable differences in cell type enrichment was observed for marginal
473 signatures (Figure 7A,C). Potential recipient cell repertoires available in asymptomatic
474 and symptomatic plaques was also explored through EV-miRNA-mRNA predicted
475 targets (Figure S13).
476

477 We then explored differences in asymptomatic and symptomatic plaque EV-cell
478 communication with CellChat, by similarly examining EV-proteins as the ligands in
479 known ligand-receptor interactions, where receptors were predicted from scRNA-seq in
480 marginal and plaque zones (Figure 7E-F). Although asymptomatic plaques shared all
481 EV-cell signaling pathways with the symptomatic group (Figure 7E-F), symptomatic
482 plaque EV-protein ligands also exhibited unique signaling involving ApoE, galectin, and
483 visfatin. Specifically, EV/visfatin to endothelial cell-based communication was unique to
484 symptomatic plaques – notable given angiogenesis can be modulated through visfatin-
485 based secretion of vascular endothelial growth factor (VEGF) and fibroblast growth
486 factor 2 (FGF-2),[75,76] monocyte recruitment through monocyte chemoattractant protein 1
487 (MCP-1),[77] and extracellular matrix remodelling via matrix metalloproteinase
488 expression.[78,79] We then explored specific ligand-receptor pairs between asymptomatic
489 and symptomatic plaque EVs and recipient cell repertoires that might be available in
490 ECs (Figure 8A, S14A), SMCs (Figure S14B-D), and macrophages (Figure S14E-G).
491 Cell-cell communication strategies predicted in the asymptomatic plaques were mostly
492 recapitulated in the symptomatic group, with symptomatic plaques exhibiting more
493 complex EV-recipient cell signaling (Figure 8A, S14D,G). As an approach to externally
494 validate some of our cell communication predictions, we examined the EV marker CD63
495 as well as CD63-normalized visfatin and CD63-normalized VEGFA in a cohort of 18
496 carotid endarterectomy specimens (Biobank of Karolinska Endarterectomy, BiKE) where
497 proteomics had been completed on plaque zones and marginal zones (*n*=9
498 symptomatic, *n*=9 asymptomatic).[37] While these were bulk tissue proteomics, more of
499 the common EV marker CD63 protein was detected in symptomatic plaques and

500 increased visfatin (NAMPT) and VEGFA was detected in symptomatic carotid tissue
501 when normalized to CD63 protein by zone (Figure S15A-C).
502
503 Given the distinct EV-based communication strategies predicted in symptomatic versus
504 asymptomatic tissues, we then assessed the potential functional consequences through
505 analysis by GO and KEGG pathways for EV-miRNA, EV-proteins, and EV-vesiculome
506 (integrated analysis) (Figure S16A,B). We found differences in pathways predicted to be
507 modulated by EVs in symptomatic compared to asymptomatic plaques. Key EV-miRNA
508 based pathways enriched in symptomatic plaque included inflammatory signaling (TCR
509 signaling, NFkB, HIF-1, TNF, TGFβ), apoptosis, cell senescence, and cell
510 migration/motility (adherens junctions, VEGF) (Figure S16A,B left panels). Enriched
511 pathways in symptomatic plaques predicted to be modulated by EV-proteins included
512 complement and coagulation (includes fibrinolysis, iron metabolism), cholesterol
513 metabolism (includes lipid transport, response to low density lipoprotein particle
514 stimulus), and amino acid metabolism (Figure S16 A,B middle panels). Network analysis
515 integrating EV-miRNA and EV-protein content identified the importance of metabolic
516 pathways (amino acid biosynthesis, RNA synthesis and turnover, steroid biosynthesis,
517 cholesterol), complement and coagulation, and inflammatory pathways (antigen
518 processing and presentation, macrophage proliferation, neutrophil degranulation) as
519 shared targets of EV-contents in symptomatic plaques (Figure S16 A-B right panels).
520 Likewise, overrepresentation analysis of differentially enriched EV-miRNA and EV-
521 protein predicted differential representation of GO and KEGG pathways that based on
522 symptom status (Figure S17A-D). Upon closer examination there was a clear

523 endothelial and angiogenic signature in EV-miRNA-mRNA overrepresentation analysis
524 in symptomatic versus asymptomatic EVs with overrepresented predicted pathways in
525 angiogenesis, blood vessel development, sprouting angiogenesis and VEGF signaling
526 (Figure 8B, S18A-B), while EV-protein and EV-vesiculomics overrepresentation analysis
527 were more varied (Figure S18C-F, S19A-D).
528
529 As significantly more endothelial angiogenesis-related pathways were identified in
530 symptomatic plaque zones versus their respective marginal zones (Figure 8C, p-value =
531 $1.84X10^{-23}$), we tested the functional effects of symptomatic plaque EVs (n=3) using an
532 endothelial spheroid-based sprouting assay (Figure 8D-F, S19E-J). Endothelial sprouts
533 were significantly increased in number (110.2±4.34 versus. 92.3±2.59; $p=2.7X10^{-2}$)
534 (Figure 8E) as well as total sprout length (244.9±5.06 versus 179.7±4.27 μm; $p<1.0X10^{-}$
535 ^{10}) (Figure 8F) and average sprout length (Figure S19G) after treatment with
536 symptomatic plaque EVs compared to matched marginal zone EVs. Controls included
537 eluates (negative control, Figure 8E-F, S19F-G) and VEGF (positive control, Figure
538 S19F,H-J). Taken together, these results highlight the biologically relevant EV-protein
539 and EV-miRNA cargoes that exist within the plaque and marginal zones of carotid tissue
540 along the continuum of asymptomatic to symptomatic disease.
541
542 **Discussion**
543
544 It is currently unknown what renders a carotid atherosclerotic plaque vulnerable to
545 rupture and leads to stroke. Cell-cell communication – including through extracellular

546 vesicles (EVs)[31] – may play a role. Our study evaluates carotid tissue EV-
547 transcriptomics and EV-proteomics to understand changes in EV-cargo in diseased
548 states (plaque versus marginal zones) along the clinical continuum (asymptomatic to
549 symptomatic) to predict EV source, potential recipient cell responses, and a relevant
550 biological functional effect based upon these predictions. Increased numbers of EVs
551 containing distinct cargos were discovered in carotid plaque versus matched adjacent
552 marginal zones, implicating their role in governing plaque biology. Given EV-based cell-
553 cell communication necessitates an EV donor and an EV recipient cell, we integrated
554 publicly available datasets (TISSUES[39], Tabula Sapiens[72] and carotid plaque scRNA-
555 seq datasets[20]) with our region-specific carotid EV-vesiculomics to gain insight into the
556 cellular drivers of EV-based communication within the plaque. As plaque vulnerability
557 increased from asymptomatic to symptomatic disease states, there was a greater
558 degree of EV communication suggested in the symptomatic plaques. Our *in silico*
559 analysis suggested an increased abundance of endothelial cell-derived EVs with plaque
560 progression and predicted a greater number of unique EV-endothelial cell ligand-
561 receptor pairs in symptomatic plaques known to function in angiogenesis, with
562 downstream overrepresentation analysis corroborating increased endothelial-based
563 pathways. Intriguingly, we discovered an EV-derived endothelial/neovascularization
564 'signature' in symptomatic carotid plaques and then showed for the first time, that
565 human symptomatic carotid plaque EVs induce angiogenesis in a model of endothelial
566 sprouting. Taken together, these exciting data illustrate a complex communication
567 network, with renewed focus on the role of EVs and the endothelium.
568

569 EVs are mediators of cardiovascular disease states and have previously been shown to
570 be increased in patient samples.[31,80-84] Here, we optimized and validated a protocol to
571 enrich tissue-entrapped atherosclerotic plaque-derived EVs using size exclusion
572 chromatography and validated our EVs in accordance with the MISEV2023 criteria,[26] in
573 alignment with our previous EV isolation approaches using similar methodology.[31] We
574 found increased EVs per gram of tissue from plaque regions in comparison to their
575 matched adjacent marginal regions. Recent work has delineated an increase in EV
576 signature based on pathway analysis of differential protein expression from diseased
577 areas (carotid plaque and aortic valve).[31] EVs mediate their effects via delivering their
578 cargo such as miRNAs and proteins to recipient cells.[32-34] In carotid tissue, this has
579 been difficult to test empirically. To date, there is evidence that carotid plaque-derived
580 microparticles are thrombogenic[27] and that candidate EV-cargo (from multiomics
581 analysis of carotid tissue) can increase calcification in cultured human carotid SMCs.[31]
582 Given the challenges working with EVs[31,85], there has been no study to date using
583 human carotid plaque derived EVs in functional assays to determine the biological
584 consequences of altered EV-cargo in diseased states. By examining the EV-vesiculome
585 within our carotid plaque versus marginal zones, plaque EV-contents were predicted to
586 be involved in several pro-atherogenic pathways such as complement and coagulation,
587 fluid shear stress, cellular senescence, cell proliferation and differentiation, and immune
588 pathways. As EVs carry proteins that are indicative of their cell of origin,[56,86] we
589 harnessed an opportunity to examine our unique dataset within publicly available single
590 cell RNA -sequencing datasets to explore potential EV-based cell-cell communication in
591 the carotid atherosclerotic plaque milieu.

592

593 To assess EV-based communication in the plaque microenvironment, we layered our
594 EV-vesiculomics with the only published carotid plaque scRNA-seq dataset that
595 contained site-specific data (plaque zone and marginal zone) to reveal potential EV
596 donor cell identities and communication partners in our two zones of interest.[20,56,86] Site-
597 specific layering is important in atherosclerotic disease given the cellular plasticity seen
598 in plaque progression.[12,87,88] Leveraging tissue-specific scRNA-seq data to inform the
599 probable cell of origin of EVs has recently gained acceptance as a starting point in
600 complex human tissue.[57] The differences in EV cell of origin identity with vascular SMCs
601 predominating in marginal zones and immune cells in plaques zones is in keeping with
602 recent reports of different identities and quantities of various cell populations found in
603 plaques versus the adjacent region.[20] The role of SMCs in regulating atherosclerotic
604 plaque progression through phenotypic switching in atherogenic environments[11,87] is
605 well characterized and our data now suggest that SMCs could also be important
606 sources of EVs in marginal zones, beyond their roles within advanced plaques.[12,20,88,89]
607 The role of immune cells in governing advanced plaque biology is similarly
608 acknowledged, and likely explains the increased EV contribution predicted from these
609 cells in plaque regions.[90,91] Intriguingly, the ligand-receptor communication strategies
610 (using EV-protein cargo as ligands and recipient cell repertoires from scRNA-seq) that
611 were predicted in the plaque versus marginal zones suggested increasing complexity of
612 the biological milieu along the disease continuum.[20,31] Our analysis implicates EVs as
613 integral mediators of atherosclerotic plaque progression and EV-based communication
614 as a potential target to modulate plaque biology.

615

616 Assessment and treatment of vulnerable carotid atherosclerotic plaques represents a
617 continuing clinical challenge with opportunities to improve.[92] With symptomatic plaques
618 representing culprit lesions with advanced vulnerable atherosclerotic disease where
619 participation from resident and circulating cells that are phenotypically dynamic
620 contribute to the EV-pool, disease progression lends itself to multifaceted
621 communication patterns.[93] We defined a predicted role for endothelial cells at both
622 facets (donor and recipient) of the EV cell-cell communication paradigm in symptomatic
623 plaques, where endothelial cells featured prominently as both potential sources of EVs
624 and responders to EVs – specifically with communication signaling known to function in
625 neovascularization and angiogenesis. Neovascularization in atherosclerotic plaque
626 occurs as a result of hypoxemia and leads to the growth of immature and leaky vessels
627 causing intra-plaque hemorrhage, a well known contributor to plaque instability and
628 rupture.[37,94-96] While not unique to symptomatic plaques, it does predominate in this
629 group of patients.[97] With this insight, we corroborated our predictions functionally and
630 showed for the first time that symptomatic human carotid plaque zone EVs induce
631 angiogenesis using an optimized low-input human endothelial spheroid sprouting assay.
632

633 The importance of endothelial EV-based communication in driving atherosclerotic
634 plaque instability represents an opportunity to understand the disease process from the
635 less-studied endothelial-centric lens. Endothelial cell-EVs are intimately involved in
636 autocrine and paracrine communication with cells of the atherosclerotic plaque where
637 they orchestrate upregulation of adhesion molecules, and activation, proliferation, and

638 migration of vascular cells.[7,98-104] In the atherosclerotic milieu, endothelial cells are
639 exposed to disturbed flow and inflammatory mediators, and can undergo endothelial-to-
640 mesenchymal transition wherein they lose endothelial identify and adopt mesenchymal
641 properties.[9,10,105] In the scRNA-seq dataset from Alsaigh *et al*, there were three
642 endothelial cell populations contributing to plaque-derived EVs as seen in the original
643 scRNA-sequencing dataset that represented quiescent, activated, and
644 transdifferentiated endothelial cells.[20] Given the quiescent endothelium has been shown
645 to participate in atheroprotective EV-messaging[104], it would be beneficial to resolve the
646 differences in communication between these cell types and understand how to shift the
647 messaging to a quiescent phenotype. The important role of endothelial cell-based EV
648 communication in carotid atherosclerotic plaque combined with the accessibility of the
649 endothelial layer, emphasizes the potential of endothelial-EV targeted therapeutics in
650 atherosclerotic vascular disease.
651
652 Our study explored EV-based cell-cell communication in human atherosclerotic disease
653 and how this might dictate plaque vulnerability in part through the functional role of EVs
654 in endothelial angiogenesis. There are limitations, however. While we completed tissue
655 EV-transcriptomics and EV-proteomics, it was not possible to generate matched scRNA-
656 sequencing that would have allowed us to annotate the cells and communication
657 occurring within the same carotid tissue.[57] The external dataset selected was the only
658 publicly available scRNAseq on plaque and marginal zones, however it did not contain
659 symptomatic patients. Given the cell identity changes seen with plaque progression, cell
660 annotations and ligand-receptor interactions may not have captured the diversity of the

661 symptomatic plaque cell populations specifically. *In silico* analysis only enables
662 predictions for delineating EV cells of origin and potential recipient cell responses, which
663 could be a limitation across all samples – regardless of patient symptom status. Lastly,
664 EVs are one of many extracellular signals in the plaque microenvironment. While it is
665 encouraging that increased CD63 (common EV marker) was similarly detected in
666 symptomatic plaque zones in the BiKE dataset, and was significantly increased in the
667 most severe Cluster 3 carotid plaques described by Mokry et al,[106] the role of
668 lipoproteins, non-EV inflammatory or angiogenic processes, and metabolites cannot be
669 excluded.[107] Our work does not preclude the role of other signalling molecules, nor can
670 it account for the dynamic, spatial, and other physical elements taking place. As
671 technologies progress, it may become possible to validate our findings at a single EV-
672 level.
673
674
675 **Conclusions**
676
677 This work was pursued with the challenging goal of establishing an important
678 conversation around EVs in carotid plaque biology. Crucially, vulnerable symptomatic
679 carotid disease was characterized by an increased concentration of EVs in plaque
680 zones, with increased contribution from endothelial cell sources. Furthermore, EVs
681 harbored a signature for specific EV-based communication with endothelial cells, with
682 predicted impact on angiogenic pathways. These predictions were corroborated
683 functionally by demonstrating symptomatic carotid plaque zone EVs increase

684 endothelial sprouting angiogenesis – a signature that might imply neovascularization
685 and plaque rupture potential. These provocative results underscore the importance of
686 the endothelium in governing vulnerable biology and highlight unique opportunities to
687 consider the role of EVs as a therapeutic target in plaque stabilizing therapies.
688
689

690 **Acknowledgements**

691

692 The authors thank the patients, surgical teams, and stroke neurology colleagues at
693 University Health Network and Sunnybrook Health Sciences. For assistance with
694 pathology: Ms. Melanie Peralta (UHN). Electron microscopy imaging of EVs was
695 performed in the Harvard Medical School Electron Microscopy Facility.

696

697 **Sources of Funding**

698 This work was supported by Canadian Institutes of Health Research (CIHR) Project
699 Grants PJT178006 (K. Howe) and PJT148487 (J. Fish), a Tier II Canada Research
700 Chair from CIHR (J. Fish), Heart and Stroke Foundation of Canada (New Investigator
701 Award, K. Howe), Vascular Cures (Wylie Scholar Award, K. Howe), Blair Early Career
702 Professorship in Vascular Surgery (K. Howe), Peter Munk Cardiac Centre (K. Howe),
703 University Health Network (K. Howe) and Vanier Canada Graduate Scholarship (S.
704 Raju). Infrastructure funding was obtained from the John R. Evans Leaders Fund (J.
705 Fish). E. Aikawa lab is supported by NIH grants (R01 HL136431, R01 HL141917, R01
706 HL147095. M. E. Turner is supported by a CIHR Banting Fellowship. L.M. is the
707 recipient of fellowships and awards from the Swedish Research Council [VR, 2023-
708 02724, 2019-02027], Karolinska Institute Consolidator program, Swedish Heart-Lung
709 Foundation [HLF, 20240094, 20230357, 20210466, 20200621, 20200520, 20180244,
710 20180247, 201602877], Swedish Society for Medical Research [SSMF, P13-0171]. L.M.
711 also acknowledges funding from Mats Kleberg's, Sven and Ebba-Christina Hagberg's,
712 Tore Nilsson's, Magnus Bergvall's and Karolinska Institute research (KI Fonder) and

713 doctoral education (KID) foundations. Project funding was also obtained by U.H. from
714 the Swedish Heart-Lung Foundation (20180036, 20170584), the Swedish Research
715 Council (2017-01070, 2019-02027), and King Gustav Vth and Queen Victoria's
716 Foundation.

717

718

719

720 **Disclosures**

721 Natalie Galant is co-founder and CEO of Paradox Immunotherapeutics, but the content
722 of this manuscript is unrelated to the work of this company.

723

724

725 **Clinical Perspective**

726

727 **What Is New?**

728 - First analysis of extracellular vesicle (EV) miRNA and proteomics in carotid
729 atherosclerosis by region (plaque zone and marginal zone) across the clinical
730 spectrum (asymptomatic and symptomatic disease).
731 - Integration with single-cell RNA-sequencing of carotid plaque and marginal
732 zones revealed predicted EV cell of origins and EV-ligand-receptor interactions
733 with an endothelial signature involved in neovascularization of vulnerable
734 (symptomatic) plaque zones.
735 - Functional assays corroborated the endothelial *in silico* predictions, with EVs
736 from symptomatic carotid plaque zones increasing endothelial sprouting (number
737 and length) compared to matched marginal zone EVs or controls.

738

739 **What Are the Clinical Implications?**

740 - Cell-cell communication in atherosclerotic plaques reflects a dynamic milieu that
741 can eventually render a plaque vulnerable to rupture and cause stroke, but needs
742 further study to better reveal novel therapeutic targets for plaque stabilization.
743 - Tissue-based EVs are an increasingly recognized means for cell-cell
744 communication, with EVs from donor cells (source) being taken up by
745 neighboring cells (recipients) to govern their function – these communication
746 patterns need to be understood along the continuum of cellular identity and local
747 plaque environments.

748 • Discovery of an endothelial EV communication network in symptomatic carotid
749 plaques capable of neovascularization represents a new approach to consider for
750 plaque stabilization therapies.
751

References

1. Libby P. The changing landscape of atherosclerosis. *Nature.* 2021;592(7855):524-533.
2. Libby P, Buring JE, Badimon L, et al. Atherosclerosis. *Nature Reviews Disease Primers.* 2019;5(1):56.
3. Shahjouei S, Sadighi A, Chaudhary D, et al. A 5-decade analysis of incidence trends of ischemic stroke after transient ischemic attack: a systematic review and meta-analysis. *JAMA neurology.* 2021;78(1):77-87.
4. Howe KL, Cybulsky M, Fish JE. The Endothelium as a Hub for Cellular Communication in Atherogenesis: Is There Directionality to the Message? *Front Cardiovasc Med.* 2022;9:888390.
5. Yu L, Xu L, Chu H, et al. Macrophage-to-endothelial cell crosstalk by the cholesterol metabolite 27HC promotes atherosclerosis in male mice. *Nat Commun.* 2023;14(1):4101.
6. Yurdagul A, Jr. Crosstalk Between Macrophages and Vascular Smooth Muscle Cells in Atherosclerotic Plaque Stability. *Arterioscler Thromb Vasc Biol.* 2022;42(4):372-380.
7. Hergenreider E, Heydt S, Tréguer K, et al. Atheroprotective communication between endothelial cells and smooth muscle cells through miRNAs. *Nature cell biology.* 2012;14(3):249-256.
8. Raju S, Botts SR, Blaser MC, et al. Directional Endothelial Communication by Polarized Extracellular Vesicle Release. *Circulation Research.* 2024;134(3):269-289.
9. Chen P-Y, Qin L, Baeyens N, et al. Endothelial-to-mesenchymal transition drives atherosclerosis progression. *The Journal of clinical investigation.* 2015;125(12):4514-4528.
10. Evrard SM, Lecce L, Michelis KC, et al. Endothelial to mesenchymal transition is common in atherosclerotic lesions and is associated with plaque instability. *Nature communications.* 2016;7(1):11853.
11. Gomez D, Owens GK. Smooth muscle cell phenotypic switching in atherosclerosis. *Cardiovascular research.* 2012;95(2):156-164.
12. Alencar GF, Owsiany KM, Karnewar S, et al. Stem cell pluripotency genes Klf4 and Oct4 regulate complex SMC phenotypic changes critical in late-stage atherosclerotic lesion pathogenesis. *Circulation.* 2020;142(21):2045-2059.
13. Group ECSTC. Randomised trial of endarterectomy for recently symptomatic carotid stenosis: final results of the MRC European Carotid Surgery Trial (ECST). *The Lancet.* 1998;351(9113):1379-1387.
14. stenosis Beoceispwh-gc. North American symptomatic carotid endarterectomy trial collaborators. *N Engl J Med.* 1991;325(7):445-453.
15. Walker MD, Marler JR, Goldstein M, et al. Endarterectomy for asymptomatic carotid artery stenosis. *Jama.* 1995;273(18):1421-1428.
16. Brott TG, Hobson RW, Howard G, et al. Stenting versus endarterectomy for treatment of carotid-artery stenosis. *New England Journal of Medicine.* 2010;363(1):11-23.
17. Hackam DG. Optimal medical management of asymptomatic carotid stenosis. *Stroke.* 2021;52(6):2191-2198.

794 18. Committee W. European Society for Vascular Surgery (ESVS) 2023 Clinical Practice
795 Guidelines on Radiation Safety. *European Journal of Vascular and Endovascular Surgery.*
796 2022.
797 19. Goessens BM, Visseren FL, Kappelle LJ, Algra A, van der Graaf Y. Asymptomatic carotid
798 artery stenosis and the risk of new vascular events in patients with manifest arterial
799 disease: the SMART study. *Stroke.* 2007;38(5):1470-1475.
800 20. Alsaigh T, Evans D, Frankel D, Torkamani A. Decoding the transcriptome of calcified
801 atherosclerotic plaque at single-cell resolution. *Communications biology.*
802 2022;5(1):1084.
803 21. Theofilatos K, Stojkovic S, Hasman M, et al. Proteomic atlas of atherosclerosis: the
804 contribution of proteoglycans to sex differences, plaque phenotypes, and outcomes.
805 *Circulation Research.* 2023;133(7):542-558.
806 22. Tomas L, Edsfeldt A, Mollet IG, et al. Altered metabolism distinguishes high-risk from
807 stable carotid atherosclerotic plaques. *European heart journal.* 2018;39(24):2301-2310.
808 23. Vaisar T, Hu JH, Airhart N, et al. Parallel murine and human plaque proteomics reveals
809 pathways of plaque rupture. *Circulation research.* 2020;127(8):997-1022.
810 24. Colombo M, Raposo G, Théry C. Biogenesis, secretion, and intercellular interactions of
811 exosomes and other extracellular vesicles. *Annual review of cell and developmental*
812 *biology.* 2014;30:255-289.
813 25. Théry C, Witwer KW, Aikawa E, et al. Minimal information for studies of extracellular
814 vesicles 2018 (MISEV2018): a position statement of the International Society for
815 Extracellular Vesicles and update of the MISEV2014 guidelines. *Journal of extracellular*
816 *vesicles.* 2018;7(1):1535750.
817 26. Welsh JA, Goberdhan DC, O'Driscoll L, et al. Minimal information for studies of
818 extracellular vesicles (MISEV2023): From basic to advanced approaches. *Journal of*
819 *extracellular vesicles.* 2024;13(2):e12404.
820 27. Leroyer AS, Isobe H, Lesèche G, et al. Cellular origins and thrombogenic activity of
821 microparticles isolated from human atherosclerotic plaques. *Journal of the American*
822 *College of Cardiology.* 2007;49(7):772-777.
823 28. Rautou P-E, Leroyer AS, Ramkhelawon B, et al. Microparticles from human
824 atherosclerotic plaques promote endothelial ICAM-1–dependent monocyte adhesion
825 and transendothelial migration. *Circulation research.* 2011;108(3):335-343.
826 29. Haraszti RA, Didiot M-C, Sapp E, et al. High-resolution proteomic and lipidomic analysis
827 of exosomes and microvesicles from different cell sources. *Journal of extracellular*
828 *vesicles.* 2016;5(1):32570.
829 30. Stamatikos A, Knight E, Vojtech L, et al. Exosome-mediated transfer of anti-miR-33a-5p
830 from transduced endothelial cells enhances macrophage and vascular smooth muscle
831 cell cholesterol efflux. *Human gene therapy.* 2020;31(3-4):219-232.
832 31. Blaser MC, Buffolo F, Halu A, et al. Multiomics of tissue extracellular vesicles identifies
833 unique modulators of atherosclerosis and calcific aortic valve stenosis. *Circulation.*
834 2023;148(8):661-678.
835 32. Valadi H, Ekström K, Bossios A, Sjöstrand M, Lee JJ, Lötvall JO. Exosome-mediated
836 transfer of mRNAs and microRNAs is a novel mechanism of genetic exchange between
837 cells. *Nature cell biology.* 2007;9(6):654-659.

838 33. Jiang S, Li X, Li Y, et al. APOE from patient-derived astrocytic extracellular vesicles
839 alleviates neuromyelitis optica spectrum disorder in a mouse model. *Science*
840 *Translational Medicine.* 2024;16(736):eadg5116.
841 34. Antounians L, Catania VD, Montalva L, et al. Fetal lung underdevelopment is rescued by
842 administration of amniotic fluid stem cell extracellular vesicles in rodents. *Science*
843 *translational medicine.* 2021;13(590):eaax5941.
844 35. Barrett KM, Brott TG. Stroke caused by extracranial disease. *Circulation research.*
845 2017;120(3):496-501.
846 36. Goncalves I, Sun J, Tengryd C, et al. Plaque vulnerability index predicts cardiovascular
847 events: a histological study of an endarterectomy cohort. *Journal of the American Heart*
848 *Association.* 2021;10(15):e021038.
849 37. Matic LP, Jesus Iglesias M, Vesterlund M, et al. Novel multiomics profiling of human
850 carotid atherosclerotic plaques and plasma reveals biliverdin reductase B as a marker of
851 intraplaque hemorrhage. *JACC: Basic to Translational Science.* 2018;3(4):464-480.
852 38. Stary HC, Chandler AB, Dinsmore RE, et al. A definition of advanced types of
853 atherosclerotic lesions and a histological classification of atherosclerosis: a report from
854 the Committee on Vascular Lesions of the Council on Arteriosclerosis, American Heart
855 Association. *Circulation.* 1995;92(5):1355-1374.
856 39. Palasca O, Santos A, Stolte C, Gorodkin J, Jensen LJ. TISSUES 2.0: an integrative web
857 resource on mammalian tissue expression. *Database.* 2018;2018:bay003.
858 40. Forster DT, Li SC, Yashiroda Y, et al. BIONIC: biological network integration using
859 convolutions. *Nature Methods.* 2022;19(10):1250-1261.
860 41. Hong P, Koza S, Bouvier ES. A review size-exclusion chromatography for the analysis of
861 protein biotherapeutics and their aggregates. *Journal of liquid chromatography &*
862 *related technologies.* 2012;35(20):2923-2950.
863 42. Petersen JD, Mekhedov E, Kaur S, Roberts DD, Zimmerberg J. Endothelial cells release
864 microvesicles that harbour multivesicular bodies and secrete exosomes. *Journal of*
865 *Extracellular Biology.* 2023;2(4):e79.
866 43. Organization WH. *Strategy for optimizing national routine health information systems:*
867 *strengthening routine health information systems to deliver primary health care and*
868 *universal health coverage.* World Health Organization; 2024.
869 44. Cheng HS, Besla R, Li A, et al. Paradoxical suppression of atherosclerosis in the absence
870 of microRNA-146a. *Circulation research.* 2017;121(4):354-367.
871 45. Cheng HS, Sivachandran N, Lau A, et al. Micro RNA-146 represses endothelial activation
872 by inhibiting pro-inflammatory pathways. *EMBO molecular medicine.* 2013;5(7):1017-
873 1034.
874 46. Raitoharju E, Lyytikäinen L-P, Levula M, et al. miR-21, miR-210, miR-34a, and miR-146a/b
875 are up-regulated in human atherosclerotic plaques in the Tampere Vascular Study.
876 *Atherosclerosis.* 2011;219(1):211-217.
877 47. Nazari-Jahantigh M, Wei Y, Noels H, et al. MicroRNA-155 promotes atherosclerosis by
878 repressing Bcl6 in macrophages. *The Journal of clinical investigation.* 2012;122(11):4190-
879 4202.
880 48. Yang Y, Yang L, Liang X, Zhu G. MicroRNA-155 promotes atherosclerosis inflammation via
881 targeting SOCS1. *Cellular Physiology and Biochemistry.* 2015;36(4):1371-1381.

882 49. Huang S, Zeng Z, Sun Y, et al. Association study of hsa_circ_0001946, hsa-miR-7-5p and
883 PARP1 in coronary atherosclerotic heart disease. *International journal of cardiology.*
884 2021;328:1-7.
885 50. Reddy MA, Jin W, Villeneuve L, et al. Pro-inflammatory role of microrna-200 in vascular
886 smooth muscle cells from diabetic mice. *Arteriosclerosis, thrombosis, and vascular*
887 *biology.* 2012;32(3):721-729.
888 51. Zhang F, Cheng N, Du J, Zhang H, Zhang C. MicroRNA-200b-3p promotes endothelial cell
889 apoptosis by targeting HDAC4 in atherosclerosis. *BMC cardiovascular disorders.*
890 2021;21:1-12.
891 52. An T-H, He Q-W, Xia Y-P, et al. MiR-181b antagonizes atherosclerotic plaque vulnerability
892 through modulating macrophage polarization by directly targeting Notch1. *Molecular*
893 *Neurobiology.* 2017;54:6329-6341.
894 53. Di Gregoli K, Mohamad Anuar NN, Bianco R, et al. MicroRNA-181b controls
895 atherosclerosis and aneurysms through regulation of TIMP-3 and elastin. *Circulation*
896 *research.* 2017;120(1):49-65.
897 54. Sun P, Li L, Liu Y-Z, et al. MiR-181b regulates atherosclerotic inflammation and vascular
898 endothelial function through Notch1 signaling pathway. *European Review for Medical &*
899 *Pharmacological Sciences.* 2019;23(7).
900 55. Kuleshov MV, Jones MR, Rouillard AD, et al. Enrichr: a comprehensive gene set
901 enrichment analysis web server 2016 update. *Nucleic acids research.* 2016;44(W1):W90-
902 W97.
903 56. Hallal S, Tűzesi Á, Grau GE, Buckland ME, Alexander KL. Understanding the extracellular
904 vesicle surface for clinical molecular biology. *Journal of extracellular vesicles.*
905 2022;11(10):e12260.
906 57. He R, Zhu J, Ji P, Zhao F. SEVtras delineates small extracellular vesicles at droplet
907 resolution from single-cell transcriptomes. *Nature Methods.* 2024;21(2):259-266.
908 58. Wang S, Aurora AB, Johnson BA, et al. The endothelial-specific microRNA miR-126
909 governs vascular integrity and angiogenesis. *Developmental cell.* 2008;15(2):261-271.
910 59. Fish JE, Santoro MM, Morton SU, et al. miR-126 regulates angiogenic signaling and
911 vascular integrity. *Developmental cell.* 2008;15(2):272-284.
912 60. Vasa-Nicotera M, Chen H, Tucci P, et al. miR-146a is modulated in human endothelial cell
913 with aging. *Atherosclerosis.* 2011;217(2):326-330.
914 61. McCann JV, Xiao L, Kim DJ, et al. Endothelial miR-30c suppresses tumor growth via
915 inhibition of TGF-β-induced Serpine1. *J Clin Invest.* 2019;129(4):1654-1670.
916 62. Yang ZJ, Liu R, Han XJ, et al. Knockdown of the long non-coding RNA MALAT1 ameliorates
917 TNF-α-mediated endothelial cell pyroptosis via the miR-30c-5p/Cx43 axis. *Mol Med Rep.*
918 2023;27(4).
919 63. Afzal TA, Luong LA, Chen D, et al. NCK Associated Protein 1 Modulated by mi RNA-214
920 Determines Vascular Smooth Muscle Cell Migration, Proliferation, and Neointima
921 Hyperplasia. *Journal of the American Heart Association.* 2016;5(12):e004629.
922 64. Cordes KR, Sheehy NT, White MP, et al. miR-145 and miR-143 regulate smooth muscle
923 cell fate and plasticity. *Nature.* 2009;460(7256):705-710.

924 65. Cheng Y, Liu X, Yang J, et al. MicroRNA-145, a novel smooth muscle cell phenotypic
925 marker and modulator, controls vascular neointimal lesion formation. *Circulation*
926 *research.* 2009;105(2):158-166.
927 66. O'Connell RM, Zhao JL, Rao DS. MicroRNA function in myeloid biology. *Blood, The*
928 *Journal of the American Society of Hematology.* 2011;118(11):2960-2969.
929 67. Das A, Ganesh K, Khanna S, Sen CK, Roy S. Engulfment of apoptotic cells by
930 macrophages: a role of microRNA-21 in the resolution of wound inflammation. *The*
931 *Journal of Immunology.* 2014;192(3):1120-1129.
932 68. Maurya M, Barthwal MK. MicroRNA-99a: a potential double-edged sword targeting
933 macrophage inflammation and metabolism. *Cellular & Molecular Immunology.*
934 2021;18(9):2290-2292.
935 69. Rodriguez A, Vigorito E, Clare S, et al. Requirement of bic/microRNA-155 for normal
936 immune function. *Science.* 2007;316(5824):608-611.
937 70. Seeley JJ, Baker RG, Mohamed G, et al. Induction of innate immune memory via
938 microRNA targeting of chromatin remodelling factors. *Nature.* 2018;559(7712):114-119.
939 71. Jin S, Guerrero-Juarez CF, Zhang L, et al. Inference and analysis of cell-cell
940 communication using CellChat. *Nature communications.* 2021;12(1):1088.
941 72. Consortium* TTS, Jones RC, Karkanias J, et al. The Tabula Sapiens: A multiple-organ,
942 single-cell transcriptomic atlas of humans. *Science.* 2022;376(6594):eabl4896.
943 73. Hsu S-D, Lin F-M, Wu W-Y, et al. miRTarBase: a database curates experimentally validated
944 microRNA–target interactions. *Nucleic acids research.* 2011;39(suppl_1):D163-D169.
945 74. Stary HC. Natural history and histological classification of atherosclerotic lesions: an
946 update. *Arteriosclerosis, thrombosis, and vascular biology.* 2000;20(5):1177-1178.
947 75. Adya R, Tan BK, Punn A, Chen J, Randeva HS. Visfatin induces human endothelial VEGF
948 and MMP-2/9 production via MAPK and PI3K/Akt signalling pathways: novel insights into
949 visfatin-induced angiogenesis. *Cardiovascular research.* 2008;78(2):356-365.
950 76. Bae Y-H, Bae M-K, Kim S-R, Lee JH, Wee H-J, Bae S-K. Upregulation of fibroblast growth
951 factor-2 by visfatin that promotes endothelial angiogenesis. *Biochemical and biophysical*
952 *research communications.* 2009;379(2):206-211.
953 77. Adya R, Tan BK, Chen J, Randeva HS. Pre-B cell colony enhancing factor (PBEF)/visfatin
954 induces secretion of MCP-1 in human endothelial cells: role in visfatin-induced
955 angiogenesis. *Atherosclerosis.* 2009;205(1):113-119.
956 78. Adya R, Tan BK, Chen J, Randeva HS. Nuclear factor-κB induction by visfatin in human
957 vascular endothelial cells: its role in MMP-2/9 production and activation. *Diabetes care.*
958 2008;31(4):758-760.
959 79. Kim S-R, Bae Y-H, Bae S-K, et al. Visfatin enhances ICAM-1 and VCAM-1 expression
960 through ROS-dependent NF-κB activation in endothelial cells. *Biochimica et Biophysica*
961 *Acta (BBA)-Molecular Cell Research.* 2008;1783(5):886-895.
962 80. Sinning J-M, Losch J, Walenta K, Böhm M, Nickenig G, Werner N. Circulating
963 CD31+/Annexin V+ microparticles correlate with cardiovascular outcomes. *European*
964 *heart journal.* 2011;32(16):2034-2041.
965 81. Arteaga RB, Chirinos JA, Soriano AO, et al. Endothelial microparticles and platelet and
966 leukocyte activation in patients with the metabolic syndrome. *The American journal of*
967 *cardiology.* 2006;98(1):70-74.

968 82. Chironi G, Simon A, Hugel B, et al. Circulating leukocyte-derived microparticles predict
969 subclinical atherosclerosis burden in asymptomatic subjects. *Arteriosclerosis,*
970 *thrombosis, and vascular biology.* 2006;26(12):2775-2780.
971 83. Koga H, Sugiyama S, Kugiyama K, et al. Elevated levels of VE-cadherin-positive
972 endothelial microparticles in patients with type 2 diabetes mellitus and coronary artery
973 disease. *Journal of the American College of Cardiology.* 2005;45(10):1622-1630.
974 84. Amabile N, Cheng S, Renard JM, et al. Association of circulating endothelial
975 microparticles with cardiometabolic risk factors in the Framingham Heart Study.
976 *European Heart Journal.* 2014;35(42):2972-2979.
977 85. Crescitelli R, Lässer C, Lötvall J. Isolation and characterization of extracellular vesicle
978 subpopulations from tissues. *Nature Protocols.* 2021;16(3):1548-1580.
979 86. Dixson AC, Dawson TR, Di Vizio D, Weaver AM. Context-specific regulation of
980 extracellular vesicle biogenesis and cargo selection. *Nature Reviews Molecular Cell*
981 *Biology.* 2023;24(7):454-476.
982 87. Shankman LS, Gomez D, Cherepanova OA, et al. KLF4-dependent phenotypic modulation
983 of smooth muscle cells has a key role in atherosclerotic plaque pathogenesis. *Nature*
984 *medicine.* 2015;21(6):628-637.
985 88. Pan H, Xue C, Auerbach BJ, et al. Single-cell genomics reveals a novel cell state during
986 smooth muscle cell phenotypic switching and potential therapeutic targets for
987 atherosclerosis in mouse and human. *Circulation.* 2020;142(21):2060-2075.
988 89. Bennett MR, Sinha S, Owens GK. Vascular smooth muscle cells in atherosclerosis.
989 *Circulation research.* 2016;118(4):692-702.
990 90. Fernandez DM, Rahman AH, Fernandez NF, et al. Single-cell immune landscape of human
991 atherosclerotic plaques. *Nature medicine.* 2019;25(10):1576-1588.
992 91. Milei J, Parodi J, Barone A, et al. Carotid atherosclerosis. Immunocytochemical analysis
993 of the vascular and cellular composition in endarterectomies. *Cardiologia (Rome, Italy).*
994 1996;41(6):535-542.
995 92. Soehnlein O, Libby P. Targeting inflammation in atherosclerosis—from experimental
996 insights to the clinic. *Nature reviews Drug discovery.* 2021;20(8):589-610.
997 93. Libby P. The biology of atherosclerosis comes full circle: lessons for conquering
998 cardiovascular disease. *Nature Reviews Cardiology.* 2021;18(10):683-684.
999 94. Gao P, Chen Z-q, Bao Y-h, Jiao L-q, Ling F. Correlation between carotid intraplaque
1000 hemorrhage and clinical symptoms: systematic review of observational studies. *Stroke.*
1001 2007;38(8):2382-2390.
1002 95. Parma L, Baganha F, Quax PH, de Vries MR. Plaque angiogenesis and intraplaque
1003 hemorrhage in atherosclerosis. *European journal of pharmacology.* 2017;816:107-115.
1004 96. Wadén K, Karlöf E, Narayanan S, et al. Clinical risk scores for stroke correlate with
1005 molecular signatures of vulnerability in symptomatic carotid patients. *Iscience.*
1006 2022;25(5).
1007 97. Larson AS, Benson JC, Brinjikji W, et al. Variations in the presence of carotid Intraplaque
1008 hemorrhage across age categories: what age groups are Most likely to benefit from
1009 plaque imaging? *Frontiers in neurology.* 2020;11:603055.

98. Arderiu G, Peña E, Badimon L. Angiogenic microvascular endothelial cells release microparticles rich in tissue factor that promotes postischemic collateral vessel formation. *Arteriosclerosis, thrombosis, and vascular biology.* 2015;35(2):348-357.
99. Boyer MJ, Kimura Y, Akiyama T, et al. Endothelial cell-derived extracellular vesicles alter vascular smooth muscle cell phenotype through high-mobility group box proteins. *Journal of extracellular vesicles.* 2020;9(1):1781427.
100. Charla E, Mercer J, Maffia P, Nicklin S. Extracellular vesicle signalling in atherosclerosis. *Cellular signalling.* 2020;75:109751.
101. He S, Wu C, Xiao J, Li D, Sun Z, Li M. Endothelial extracellular vesicles modulate the macrophage phenotype: Potential implications in atherosclerosis. *Scandinavian journal of immunology.* 2018;87(4):e12648.
102. Jansen F, Yang X, Baumann K, et al. Endothelial microparticles reduce ICAM-1 expression in a micro RNA-222-dependent mechanism. *Journal of cellular and molecular medicine.* 2015;19(9):2202-2214.
103. Liang H, Li S, Chen H. GW28-e0938 Endothelial microparticles-mediated transfer of microRNA-19b, a novel messenger in cell-cell communication, plays a key role in endothelial migration and angiogenesis. *Journal of the American College of Cardiology.* 2017;70(16S):C34-C34.
104. Njock M-S, Cheng HS, Dang LT, et al. Endothelial cells suppress monocyte activation through secretion of extracellular vesicles containing antiinflammatory microRNAs. *Blood, The Journal of the American Society of Hematology.* 2015;125(20):3202-3212.
105. Botts SR, Fish JE, Howe KL. Dysfunctional vascular endothelium as a driver of atherosclerosis: emerging insights into pathogenesis and treatment. *Frontiers in pharmacology.* 2021;12:787541.
106. Mokry M, Boltjes A, Slenders L, et al. Transcriptomic-based clustering of human atherosclerotic plaques identifies subgroups with different underlying biology and clinical presentation. *Nature cardiovascular research.* 2022;1(12):1140-1155.
107. Seeley EH, Liu Z, Yuan S, et al. Spatially resolved metabolites in stable and unstable human atherosclerotic plaques identified by mass spectrometry imaging. *Arteriosclerosis, thrombosis, and vascular biology.* 2023;43(9):1626-1635.

1048 **Figure Legends**

1049

1050 **Figure 1. Whole tissue proteomics identifies a potential role for EVs in modulating**
1051 **plaque biology corroborated with increased enrichment of tissue resident EVs**
1052 **from human atherosclerotic carotid plaques. A.** Experimental overview. Carotid
1053 endarterectomy specimens (*n*=64*)* were collected from the operating room and
1054 dissected into plaque and marginal zones for downstream analysis. **B.** Principal
1055 component analysis of carotid tissue proteomes between the PZ and MZ (donor
1056 matched *n*=5; donor uncorrected in Figure S2C). **C.** Percent incidence of Gene
1057 Ontology (GO; Biological Process and Cellular Component) terms (false discovery rate
1058 <0.05) containing "vesicle" derived from differentially enriched proteins (q-value<0.05)
1059 from plaque and marginal zones (left panel; *n*=5). Right panel lists top 26 (by adjusted
1060 p-value) GO Biological Process terms where vesicle-associated terms from plaque
1061 regions are highlighted (marginal zone in Figure S2D). **D.** Heatmap representing per-
1062 fraction proteomics identifies prototypical EV markers enriched in fractions 7-10 (left
1063 panel). Protein abundance was Z-score normalized by protein (Representative sample,
1064 *n*=4 in Figure S5A). Western blot analysis depicting EV markers (CD63, CD81, CD9,
1065 and Flot1) in EV-enriched fractions (7-10) isolated from human atherosclerotic plaque
1066 tissue (right panel, *n*=1). **E.** Cryo-EM of EVs isolated from plaque and adjacent
1067 marginal zones. Arrows indicate select EV structures as bilayered nanoparticles with
1068 dense cores (Representative Sample, *n*=4). Scale bar = 200nm. **F.** Quantification of EV
1069 mean diameter by nanoparticle tracking analysis (NTA; *n*=20). **G.** Nanoparticle
1070 concentration (normalized to tissue weight, NTA dilution factor, and total EV-enriched

1071 volume; *n*=11) binned by particle size from plaque (PZ, purple) and marginal zones (MZ,
1072 pink). Quantification of nanoparticle concentration across all sizes by NTA (*n*=11, right
1073 panel). Bar graphs show mean ± SEM. Statistical significance assessed by Fisher's
1074 exact test (C) and a two-tailed paired t-test (11-20 pairs; F,G).
1075
1076 **Figure 2. Carotid plaque EV-vesiculome is zone-specific (plaque versus marginal)**
1077 **with differentially expressed EV-miRNA and proteins associated with pro-**
1078 **atherogenic functions. A-B.** Donor corrected principal component analysis (PCA)
1079 showing EV-miRNA **(A)** and EV-protein **(B)** profiles of EVs enriched from carotid plaque
1080 zones (PZ, purple) versus marginal zones (MZ, pink) (miRNA *n*=20 pairs; protein *n*=23
1081 pairs). **C.** Edge quantification of protein-protein interaction network with all differentially
1082 enriched EV-proteins (n=661) in plaque versus marginal zones. Represents full STRING
1083 network wherein edges indicate both functional and physical protein interactions with a
1084 medium confidence interaction score and nodes represent proteins. **D-E.** Volcano plot of
1085 carotid tissue derived EV-miRNA **(D)** and EV-protein **(E)** contents with positive and
1086 negative fold change (FC) representing miRNAs and proteins enriched in plaque versus
1087 marginal zones, respectively (FDR step up/q-value<0.05). Highlighted in red are
1088 miRNAs and proteins known to function in inflammation. **F.** Kyoto Encyclopedia of
1089 Genes and Genomes (KEGG) pathway analysis of all differentially expressed (FDR/q-
1090 value <0.05) predicted EV-miRNA targets (mRNA, miRTarBase via MIENTURNET) and
1091 EV-proteins. Venn diagram of unique and shared KEGG pathways between predicted
1092 EV-miRNA targets and EV-proteins (top left panel). Bubble plots of KEGG pathways that
1093 were significantly (FDR<0.05) modulated by all differentially enriched plaque EV-

1094 miRNAs (top right panel) and EV-proteins (bottom right panel), with all pathways that
1095 were shared by EV-miRNA and EV-proteins shown in bottom left panel. Labeled are
1096 pathways of interest (FDR<0.05). Cancer-, and infection- associated pathways were
1097 excluded from analysis.
1098
1099 **Figure 3. *In silico* analysis of human atherosclerotic tissue derive EV-cell-of-origin**
1100 **and global communication strategies in plaque and marginal zones. A.** Pictorial
1101 representation of cell of origin using the TISSUES database with all EV-proteins. Top 11
1102 cells by strength metric calculated as a ratio of observed and background gene count
1103 after inclusion of cell types only (tissue annotations filtered out; further details in Figure
1104 S8A). **B.** Box plot of global EV-protein signature enrichment among cells from
1105 atherosclerotic plaques, informed by integrating all detected EV-proteins (global EV
1106 signature) with single cell RNA sequencing (scRNA-seq) of carotid atherosclerotic
1107 plaques. **C.** Stacked bar plot visualizing total number of predicted cell-cell
1108 communication interactions in plaque (purple) and marginal (pink) zones with CellChat.
1109 **D.** Heatmap depicting EV-cell signaling strength employed by all EV-proteins to both
1110 plaque and marginal single cells. Strength of EV-derived signaling molecule and cell
1111 type shown on right and top bar graph, respectively, and represents communication
1112 probability. **E.** Cell type annotations derived using the Tabula Sapiens database
1113 (vascular tissue) by inputting all significant (adjusted p-value <0.05) predicted mRNA
1114 targets of all differentially expressed EV-miRNA in plaque and marginal zones combined
1115 (FDR<0.05). **F.** Box plot of predicted EV-miRNA-mRNA target signature enrichment

among cells of the atherosclerotic plaque, informed by integrating differentially detected EV-miRNA - mRNA targets with scRNA-seq of carotid atherosclerotic plaques.

Figure 4. Site specific (plaque versus marginal zone) differences in EV cell of origin, recipient cell communication strategies and directed communication with vascular cells (ECs, SMCs, macrophages). A-B. Box plot of differential marginal **(A)** and plaque **(B)** EV-protein signature enrichment among cells of the atherosclerotic plaque, informed by integrating differentially enriched EV-proteins with scRNA-seq of carotid atherosclerotic plaques. **C-D.** Pictorial representation of cell of origin using the TISSUES database with differentially expressed EV-proteins in marginal **(C)** and plaque **(D)** zones. Top 10 cells by strength metric calculated as a ratio of observed and background gene count after filtering for tissues (further details in Figure S8B). **E-F.** Heatmap depicting differential marginal and plaque EV to cell signaling strength employed by differentially enriched EV proteins in marginal **(E)** and plaque **(F)** zones to all atherosclerotic single cells in plaque and marginal regions. Strength of EV-derived signaling molecule and cell type shown on right and top bar graph, respectively. **G-H.** Chord diagrams representing differentially expressed EV ligands to EC **(G)** and SMC **(H)** ligand-receptor pairs to single cells in marginal zones (left panels) and plaque zones (right panels). Arrows represent EV-ligand interactions. Individual cell populations annotated in legend.

Figure 5. EV concentration and greater differential EV cargo (miRNA and protein) discriminates between symptomatic and asymptomatic atherosclerotic plaques.

1139 **A.** Schematic of experimental design. Carotid endarterectomy specimens from
1140 symptomatic and asymptomatic patients were dissected into plaque and marginal
1141 zones, followed by EV-enrichement, quantification, and miRNA transcriptomics and
1142 proteomics. **B.** Hematoxylin and eosin (H&E) and Movat pentachrome stain of
1143 asymptomatic (top panel) and symptomatic (bottom panel) of carotid plaque specimens
1144 (Patient 1 and 2). Large, calcified plaque with calcified/necrotic center, but with no
1145 significant intraplaque hemorrhage (top panel). Large, calcified plaque with
1146 calcified/necrotic center with intraplaque hemorrhage (bottom panel). H&E staining with
1147 intraplaque hemorrhage indicated by green arrowheads (bottom left panel) and Movat
1148 pentachrome staining with intraplaque hemorrhage indicated by cyan arrowheads
1149 (bottom right panel). Scale bar (500 μm) as shown. **C-D.** Nanoparticle tracking analysis
1150 (NTA) of nanoparticle concentration in asymptomatic **(C)** and symptomatic **(D)**
1151 atherosclerotic plaque versus marginal zones. **E.** Assessment of EV size and
1152 morphology. NTA of mean diameter of nanoparticles enriched from asymptomatic (left
1153 panel) and symptomatic (middle panel) carotid plaques. Cryogenic electron microscopy
1154 (cryo-EM) of EVs from asymptomatic (right panel, top) and symptomatic (right panel,
1155 bottom) carotid plaques (*n*=1-2 per group). Arrows indicate select EV structures as
1156 bilayered nanoparticles with dense cores. Scale bar = 200nm. **F-G.** Volcano plot of
1157 carotid tissue resident EV-miRNA transcriptome in asymptomatic **(F)** and symptomatic
1158 **(G)** with positive and negative fold change (FC) representing miRNAs enriched in
1159 plaque versus marginal zones (FDR step up<0.05). **H-I.** Volcano plot of carotid tissue
1160 resident EV-proteome in asymptomatic **(H)** and symptomatic **(I)** with positive and
1161 negative fold change (FC) representing EV-proteins enriched in plaque versus marginal

zones (q-value<0.05). Bar graphs show mean ± SEM. Statistical significance assessed by non-parametric paired Wilcoxon test **(C-E)**.

Figure 6. Differential plaque EV-secretome highlights key pathways involved in plaque vulnerability. A. Venn diagram depicting shared and unique plaque derived EV-miRNA in asymptomatic (green) and symptomatic (purple) conditions (FDR step-up<0.05, filtered for miRNAs<1000). **B.** Total numbers of significant Gene Ontology (GO) and Kyoto Encyclopedia of Genes and Genomes (KEGG) pathways (adjusted p-value<0.05) modulated by the predicted mRNA targets (miRTarBase via MIENTURNET, threshold of minimum interactions 1; FDR<0.05) of differentially expressed plaque EV-miRNAs in asymptomatic (green), symptomatic (purple), and shared (brown) conditions. **C.** Dot plot of all KEGG pathways derived from unique asymptomatic plaque-derived predicted EV-miRNA mRNA targets (p-value<0.05). Labelled are significant (adjusted p-value<0.05) pathways graphed by odds ratio. **D.** Dot plot of KEGG pathway analysis from unique symptomatic plaque-derived predicted EV-miRNA mRNA targets. Graphed are top 42 significant (adjusted p-value<0.05) pathways by odds ratio (total 120 pathways with adjusted p-value<0.05). **E.** Venn diagram depicting shared and unique plaque derived EV-proteins in asymptomatic (green) and symptomatic (purple) conditions (q-value<0.05). **F.** Total numbers of significant GO and KEGG pathways (adjusted p-value<0.05) modulated by differentially expressed plaque EV-proteins (q-value<0.05) in asymptomatic (green), symptomatic (purple), and shared (brown) conditions. **G.** Bar graph of all significant KEGG pathways (adjusted p-value<0.05) from unique asymptomatic plaque-derived EV-proteins (adjusted p-value<0.05). **H.** Bar graph

1185 of all significant KEGG pathways (adjusted p-value<0.05) from unique symptomatic
1186 plaque-derived EV-proteins (adjusted p-value<0.05). STRING (db version 12.0) used to
1187 generate protein-protein interaction maps (right panel) of pathways of interest. Cancer-,
1188 and infection- associated pathways were excluded from analysis.
1189
1190 **Figure 7. Endothelial cells (ECs) are cellular players modulating cell-cell**
1191 **communication through EVs in vulnerable plaques. A-D.** Box plots of symptom and
1192 regional EV-protein signature enrichment among cells of the atherosclerotic plaque,
1193 informed by integrating differentially expressed EV-proteins in asymptomatic and
1194 symptomatic, marginal versus plaque zones with scRNA-seq of carotid atherosclerotic
1195 plaques. Asymptomatic marginal **(A)** and plaque **(B)** zone signature enrichment among
1196 cells of the atherosclerotic plaque. Symptomatic marginal **(C)** and plaque **(D)** zone
1197 signature enrichment among cells of the atherosclerotic plaque. **E-F.** Heatmap depicting
1198 differential asymptomatic plaque- **(E)** and symptomatic plaque- **(F)** EV-cell signaling
1199 strength employed by differentially expressed EV-proteins in asymptomatic and
1200 symptomatic cohorts with plaque cells. Strength of EV-derived signaling molecule and
1201 cell type shown on right and top bar graph, respectively.
1202
1203 **Figure 8. Overrepresentation analysis identifies angiogenesis and**
1204 **neovascularization as functional effects of vulnerable (symptomatic) plaque EVs**
1205 **with support from a functional EC sprouting assay. A.** Chord diagrams representing
1206 ligand-receptor pairs between differentially enriched EV-proteins (ligands) to ECs
1207 (receptor) in asymptomatic (top panel) and symptomatic (bottom panel) plaques. Red

1208 arrows represent EV-ligand to receptor interactions. Individual cell populations
1209 annotated in legend. **B.** Filtered inquiry of EC, angiogenesis, and neovascularization
1210 specific pathways from Gene Ontology (GO) overrepresentation analysis of differentially
1211 expressed predicted EV-miRNA-mRNA targets in asymptomatic and symptomatic
1212 groups. Fold enrichment represented in legend. **C.** Pairwise comparison of mean fold
1213 enrichment of EC-specific pathways in symptomatic versus asymptomatic plaques. **D-F.**
1214 Functional effect of symptomatic marginal zone (MZ) and plaque zone (PZ) EVs on
1215 endothelial cell angiogenesis. Representative confocal microscopy images of HUVEC-
1216 spheroid angiogenesis after addition of EVs (2-4X10^{10} EVs; 24 h), or assay control **(D)**.
1217 Scale bar 100 μm. Representative grayscale images with annotations for sprout number
1218 **(E, left panel)** and quantification of sprout number per spheroid (*n*=7-10 from 3
1219 independent experiments; **E, right panel**). Representative grayscale images with
1220 tracings representing individual sprout lengths **(F, left panel)** and quantification (*n*=188-
1221 331 sprouts from 7–10 spheroids from 3 independent experiments). Bar graphs shows
1222 the mean±SEM. Violin plots show median ± interquartile range. Statistical significance
1223 assessed by 1-way ANOVA with Sidak multiple comparisons test **(**adjusted p-values
1224 shown; **E,F)**. P-values meeting significance (<0.05) shown in bolded text.
1225
1226
1227
1228
1229
1230

1231 **Supplemental Figure Legends**

1232

1233 **Supplemental Figure 1. Histopathology validates tissue dissection (plaque and**
1234 **marginal zones) and identifies characteristic features of late-stage**
1235 **atherosclerosis predominantly in plaque zones. A.** Hematoxylin and eosin (H&E)
1236 and Movat pentachrome stain of plaque and marginal zones from patient one. Area
1237 adjacent to plaque (marginal zone; 1-2). H&E staining: intimal hyperplasia (green
1238 bracket), media with moderate degenerative changes (cyan bracket; 1). Movat
1239 pentachrome staining: intimal hyperplasia (blue bracket), media with moderate
1240 degenerative changes (cyan bracket; 2). Middle zone of large, calcified plaque (3-4).
1241 H&E staining: surface calcification (green octagon), fibrous cap (green star), and
1242 necrotic center (yellow octagon); media (yellow star; 3). Movat pentachrome staining:
1243 surface calcification (blue octagon), fibrous cap (blue star), necrotic center (cyan
1244 octagon), media (cyan star; 4).
1245 Edge zone of large, calcified plaque (5-6). H&E staining: calcification (green star; 5).
1246 Movat pentachrome staining: calcification (cyan star; 6). **B.** H&E and Movat
1247 pentachrome stain of plaque and marginal zones from patient two. Area adjacent to
1248 plaque from (marginal zone; 1-2) H&E staining: intimal hyperplasia (green bracket),
1249 media with moderate degenerative changes (cyan bracket;1). Movat pentachrome
1250 staining: intimal hyperplasia (blue bracket), media with moderate degenerative changes
1251 (cyan bracket; 2). Middle zone of large, calcified plaque (3-4). H&E staining: surface
1252 calcification (green octagon), fibrous cap (green stars), and necrotic center (yellow
1253 octagon); media (yellow star; 3). Movat pentachrome staining: surface calcification (blue

1254 octagon), fibrous cap (blue star), necrotic center (cyan octagon), media (cyan star, 4).
1255 Edge zone of large, calcified plaque (5-6). H&E staining: media with marked disruption
1256 of the subintimal layer by plaque (green bracket), plaque (artifactually displaced from
1257 the rest of the tissue) with fibrous cap (cyan star) and intraplaque hemorrhage (green
1258 star, 5). Movat pentachrome staining: media with marked disruption of the subintimal
1259 layer by plaque (cyan bracket), plaque (artifactually displaced from the rest of the
1260 tissue) with fibrous cap (cyan star) and intraplaque hemorrhage (blue star; 6). Scale bar
1261 (500 μm) as shown.
1262
1263 **Supplemental Figure 2. Carotid tissue proteomics delineates differential protein**
1264 **enrichment in plaque versus marginal zones with pathway analysis identifying**
1265 **atherogenic signatures. A.** Proteomic data pre-processing and per-sample violin plots
1266 for carotid tissue proteomes of the plaque zone and marginal zone (*n*=10). Following
1267 valid value filtering, data was median normalized, log2 transformed, and imputed from a
1268 Gaussian distribution. **B.** Volcano plot of carotid plaque and marginal zone proteome
1269 with purple and pink representing plaque and marginal enriched, respectively (q-
1270 value<0.05). **C.** Donor uncorrected principal component analysis of label-free
1271 proteomics of whole-tissue carotid plaque (purple) and marginal zones (pink; *n*=5). **D.**
1272 Percent incidence of Gene Ontology (GO; Biological Process and Cellular Component)
1273 terms (false discovery rate <0.05) containing “vesicle” resulting from all differentially
1274 expressed proteins (q-value<0.05) from plaque and marginal zones (right panel; *n*=5,
1275 repeated from Figure 1C). Left panel lists top 26 (by adjusted p-value) GO Biological
1276 Process terms and highlighted are vesicle-associated terms from marginal zones. **E.**

1277 Top 25 (by adjusted p-value) GO Cellular Component pathways derived from all
1278 differentially enriched proteins in plaque zones. **F.** Top 25 (by adjusted p-value) Kyoto
1279 Encyclopedia of Genes and Genomes pathways derived from all differentially enriched
1280 proteins in plaque zones. Statistical significance assessed by Fisher's exact test (D)
1281
1282 **Supplemental Figure 3. Marginal zone pathway analysis features vesicle related**
1283 **and atherogenic pathways. A.** Top 25 (by adjusted p-value) Gene Ontology Cellular
1284 Component pathways derived from all differentially enriched proteins in marginal zones.
1285 **B.** Top 25 (by adjusted p-value) Kyoto Encyclopedia of Genes and Genomes pathways
1286 derived from all differentially enriched proteins in marginal zones.
1287
1288 **Supplemental Figure 4. Carotid Plaque EV-enrichment protocol and validation of**
1289 **purity. A.** Representative images showing dissection of whole carotid plaque into
1290 marginal and plaque zones. **B.** Schematic for EV isolation from atherosclerotic carotid
1291 plaque tissue. Briefly, tissues were collected in Hanks balanced salt solution (HBSS)
1292 and dissected into plaque and adjacent marginal zones. Subsequently, tissues were
1293 prepared for size exclusion chromatography (SEC) by enzymatic digestion, and
1294 centrifugation and filtration to remove cellular debris. EVs were enriched via SEC in
1295 fractions 7-10 and concentrated using ultrafiltration to a desired volume. EVs destined
1296 for proteomics underwent an additional purification step with ultracentrifugation and
1297 density gradient ultracentrifugation. **C-D.** Lipoprotein co-isolation in EV preparations via
1298 enzyme-linked immunosorbent assay (ELISA) for ApoA1 (HDL; **C**) and ApoB100 (LDL;
1299 **D**; *n*=1 plaque). **E.** Fractional analysis of nanoparticle isolation via nanoparticle tracking

1300 analysis (NTA) and bicinchoninic acid assay (*n*=1). **F.** Flow Cytometry based
1301 assessment of whole cell co-isolation with Hoechst nuclei stain. Bone marrow cells
1302 (positive control) and plaque-derived EV fractions depicted on left and right panel,
1303 respectively. EV, extracellular vesicle (*n*=1).
1304
1305 **Supplemental Figure 5. Proteomics of EVs enriched from carotid tissue identifies**
1306 **several EV markers. A.** Prototypical EV markers are enriched in fractions 7-10.
1307 Abundance Z-score normalized by protein in four samples. **B.** Bubble plot of GO
1308 pathway analysis of all differentially expressed EV-proteins between plaque zone and
1309 marginal zone filtered by vesicle-related terms. Data points are sized by combined
1310 score, and size-scaled by genes altered in pathway/total number of unique genes in
1311 analysis and color-scaled by biological processes and cellular locations.
1312
1313 **Supplemental Figure 6. Density gradient ultracentrifugation (DGUC) after size**
1314 **exclusion chromatography (SEC) enriches for EVs and depletes extracellular**
1315 **matrix proteins.** N=3 matched sample pre- and post-DGUC. **A.** After DGUC, 85.4%
1316 (958/1121) of proteins IDs remain, 158 protein IDs were no longer identified, and 4 were
1317 uniquely identified. Markers of EVs were retained following DGUC. **B.** SEC and DGUC
1318 cluster separately in principal component analysis (PCA) after using a generalized linear
1319 model to account for matched sample variability. **C.** Extracellular matrix proteins were
1320 differentially enriched in samples prior to DGUC (Total: N=206 differentially enriched in
1321 SEC pre DGUC, N=58 differentially enriched post DGUC). p-value threshold of 0.1. **D.**
1322 Transmission electron microscopy confirms the removal of debris indicative of

1323 extracellular matrix and retention of EV structures. Representative image, *n*=3 samples.
1324 Scale bars = 200 nm **E.** Post-DGUC nanoparticle tracking analysis identified particles
1325 with a size distribution consistent with the TEM imaging in both marginal zone (MZ) and
1326 plaque zone (PZ)**.** Graphs shows mean ± SEM. **F.** Proteomic data pre-processing and
1327 per-sample violin plots for EVs derived from carotid tissue plaque zone and marginal
1328 zone (*n*=46). Following valid value filtering, data was median normalized, log2
1329 transformed, and imputed from a Gaussian distribution.
1330
1331 **Supplemental Figure 7. EV-miRNA transcriptomics data post-alignment quality**
1332 **metrics. A.** Alignment breakdown chart features each sample as a column. The
1333 percentage of reads with different alignment outcomes (unique paired, non-unique,
1334 unaligned) is quantified by the y-axis and visualized by colored stacked columns. **B.**
1335 Coverage plot showing average read depth for each sample. **C.** Total reads plot
1336 showing total reads for each sample. **D.** Average base quality per read plot displays the
1337 proportion of reads with a given Phred quality score wherein all base quantities within
1338 the read are averaged. Lines represent individual samples. **E.** Average base quality per
1339 position plot displays the average Phred score for each position in the reads. Lines
1340 represent individual samples. **F.** Donor uncorrected principal component analysis (PCA)
1341 showing EV-miRNA (top panel) and EV-protein (bottom panel) profiles of EVs enriched
1342 from carotid plaque zones (PZ, purple) versus marginal zones (MZ, pink) (miRNA *n*=20
1343 pairs; protein *n*=23 pairs).
1344

1345 **Supplemental Figure 8. TISSUES Database identifies known cell and tissues**
1346 **types driving atherosclerotic vascular disease. A-B.** Dot plot of top (by strength
1347 metric, FDR<0.05) cell type and tissue annotations derived from inputting all EV-
1348 proteins **(A)** and all differentially enriched EV-proteins in marginal **(B,** top panel**)** and
1349 plaque zones **(B,** bottom panel**)**. **C.** Proteins used to inform cell annotations (SMC, foam
1350 cell, and B-lymphoblastoid cell) in the TISSUES database. Colored nodes represent
1351 query proteins and edges represent protein-protein interactions (curated and
1352 experimentally validated) with line thickness indicating the strength of data support.
1353
1354 **Supplemental Figure 9. Publicly available carotid scRNA-sequencing data**
1355 **identifies over 17,000 single cells that can be annotated to distinct cell types**
1356 **based on gene signatures. A-C.** Uniform manifold approximation and projection
1357 (UMAP) of 17,000 plaque- and marginal-region derived single cells labelled by sample
1358 **(A)**, region **(B)**, and cell-type **(C)**. **D-F.** Dot plot of marker gene expression for T cells
1359 **(D)**, macrophages and dendritic cells **(E)**, and vascular smooth muscle cells (VSMCs;
1360 **F**). Dot size and color darkness indicate the percentage of gene-expressing cells, and
1361 average expression, respectively. **G)** UMAP of markers *MS4A1*, *MZB1*, *TPSAB1*, *VWF*
1362 for identifying B-cell lymphocytes, plasma cells, mast cells, and endothelial cells (ECs),
1363 respectively.
1364

1365 **Supplemental Figure 10. Global atherosclerotic plaque EV communication**
1366 **patterns. A.** Normalized (DeSeq2 median normalization) counts of EV-miRNAs by
1367 identity in plaque and marginal zones. **B-D:** Integration with publicly available carotid
1368 plaque scRNA-seq dataset. **B.** Stacked bar plot visualizing enriched signaling pathways
1369 by overall information flow from global EV-proteome to plaque (purple) and marginal
1370 (pink) single cells. Pathways are colored by their dominance within the plaque or
1371 marginal regions. **C.** Heatmap depicting EV-cell signaling strength employed by all EV-
1372 proteins to atherosclerotic single cells in plaque (right panel) and marginal (left panel)
1373 regions. **D.** Chord diagrams representing global EV ligand to EC (left), macrophage
1374 (center), and SMC (right) ligand-receptor pairs. Arrows represent EV-receptor to ligands
1375 interactions. Individual cell populations annotated in legend. Bar graphs show mean ±
1376 SEM. Statistical significance assessed by two-tailed paired t-test (A) with Benjamini-
1377 Hochberg false discovery rate correction.
1378
1379 **Supplemental Figure 11. Site specific EV communication strategies in plaque and**
1380 **marginal zones. A-B.** Heatmap depicting differential marginal and plaque EV-cell
1381 signaling strength stratified by tissue site; derived from layering differentially enriched
1382 EV proteins in marginal **(A)** and plaque **(B)** zones to atherosclerotic single cells in
1383 plaque and marginal regions, respectively. Strength of EV-derived signaling molecule
1384 and cell type shown on right and top bar graph, respectively. **C.** Chord diagrams
1385 representing differentially expressed EV ligand to macrophage ligand-receptor pairs.
1386 Arrows represent EV-ligand interactions. Individual cell populations annotated in legend.
1387 Marginal and plaque zones represented in left and right panels, respectively.

1388 **Supplemental Figure 12. Further characterization of EV release, contents, and**
1389 **pathway analysis in asymptomatic and symptomatic plaques. A.** Hematoxylin and
1390 eosin (H&E) and Movat pentachrome stain of asymptomatic (Patient 3 and 4) and
1391 symptomatic (Patient 5) of carotid plaque specimens. Large plaque with significant
1392 inflammation, but without a necrotic core (Patient 3). Large, calcified plaque with
1393 calcified/necrotic center with intraplaque hemorrhage (Patient 4). H&E staining with
1394 intraplaque hemorrhage indicated by green arrowhead and Movat pentachrome staining
1395 with intraplaque hemorrhage indicated by cyan arrowhead. Large, calcified plaque with
1396 calcified/necrotic center with intraplaque hemorrhage (Patient 5). H&E staining with
1397 intraplaque hemorrhage indicated by green arrowhead and Movat pentachrome staining
1398 with intraplaque hemorrhage indicated by cyan arrowhead. Scale bar (500 μm) as
1399 shown. **B.** Differences plot from the Wilcoxon test comparing asymptomatic and
1400 symptomatic plaque versus marginal EV concentrations (Figure 5C-D). **C-D.**
1401 Nanoparticle tracking analysis (NTA) of nanoparticle concentration between
1402 asymptomatic versus symptomatic cohorts in marginal **(C)** and plaque **(D)** zones. **E.**
1403 Protein-protein interaction network with all differentially enriched EV-proteins in
1404 asymptomatic and symptomatic plaque versus marginal zones. Represents full STRING
1405 network wherein edges indicate both functional and physical protein interactions with a
1406 medium confidence interaction score (0.400). **F.** Bar graph of all significant KEGG
1407 pathways (adjusted p-value<0.05) derived from shared asymptomatic and symptomatic
1408 plaque-derived EV-proteins (adjusted p-value<0.05). Cancer-, and infection- associated
1409 pathways were excluded from analysis.
1410

1411 **Supplemental Figure 13. Recipient cell repertoire in asymptomatic versus**
1412 **symptomatic (vulnerable) plaques. A-B.** Box plot of predicted EV-miRNA-mRNA
1413 target signature enrichment among cells of the atherosclerotic plaque, informed by
1414 integrating differentially detected EV-miRNA - mRNA targets in asymptomatic **(A)** and
1415 symptomatic **(B)** plaques with scRNA-seq of carotid atherosclerotic plaques.
1416
1417 **Supplemental Figure 14. Symptom (asymptomatic versus symptomatic) and site-**
1418 **specific (plaque versus marginal) differences in EV-ligand-receptor interactions.**
1419 **A.** Chord diagrams representing ligand-receptor pairs between differentially enriched
1420 EV-proteins (ligands) to ECs (receptor) in symptomatic marginal zones. Red arrows
1421 represent EV-ligand to receptor interactions. Individual cell populations annotated in
1422 legend. **B-D.** Chord diagrams representing ligand-receptor pairs between differentially
1423 enriched EV-proteins (ligands) to SMCs (receptor) in asymptomatic plaque zone **(B)**,
1424 symptomatic marginal zone **(C)** and symptomatic plaque zone **(D)**. Purple arrows
1425 represent EV-ligand to receptor interactions. Individual cell populations annotated in
1426 legend. **E-G.** Chord diagrams representing ligand-receptor pairs between differentially
1427 enriched EV-proteins (ligands) to macrophages (receptor) in asymptomatic plaque zone
1428 **(E)**, symptomatic marginal zone **(F)** and symptomatic plaque zone **(G)**. Yellow arrows
1429 represent EV-ligand to receptor interactions. Individual cell populations annotated in
1430 legend.
1431
1432 **Supplemental Figure 15. Approach to externally validate cell communication**
1433 **predictions in dataset from the Biobank of Karolinska Endarterectomy (BiKE).** A.

1434 CD63 protein expression in symptomatic (S) vs asymptomatic (AS) patients in both
1435 central (plaque zone) and distal (marginal zone) regions. B. NAMPT (visfatin) protein
1436 normalized to CD63 level by zone in S versus AS patients in both central (plaque zone)
1437 and distal (marginal zone) regions. C. VEGFA protein normalized to CD63 level by zone
1438 in S versus AS patients in both central (plaque zone) and distal (marginal zone) regions.
1439 Protein levels are expressed in arbitrary units (AU). CD63 zone values were determined
1440 based on CD63 protein levels in each of the central AS (0.86 AU set to 1.1), distal AS
1441 (0.79 AU set to 1), central S (1.20 AU set to 1.5) and distal S (0.96 AU set to 1.2).
1442 NAMPT and VEGFA protein levels were then multiplied by the corresponding CD63
1443 zone values for each group to account for CD63 expression in these zones. Statistical
1444 comparison was performed using a two-tailed t-test when comparing AS vs S and a
1445 paired t-test when comparing distal vs central zones as they were collected from the
1446 same patient. P-value threshold for significance was set to 0.05 and results are
1447 presented as mean ± standard deviation (SD). There were n=9 patients in the AS group
1448 and n=9 patients in the S group.
1449
1450 **Supplemental Figure 16. Bioinformatic and network analysis to delineate distinct**
1451 **and shared functions of EV-miRNAs and EV-proteins. A.** Bubble plots depicting top
1452 Gene Ontology pathways (by fold enrichment) for EV-miRNA (left panel), EV-proteins
1453 (middle panel), and network analysis (BIONIC network integration algorithm, 512
1454 embedded features, Louvain-clustered modules) to integrate whole EV-secretome
1455 (miRNA and proteins; right panel). **B.** Bubble plots depicting top Kyoto Encyclopedia of
1456 Genes and Genome pathways (by fold enrichment) for EV-miRNA (left panel), EV-

1457 proteins (middle panel), and network analysis (BIONIC network integration algorithm,
1458 512 embedded features, Louvain-clustered modules) to integrate whole EV-vesiculome
1459 (miRNA and proteins; right panel). Bubbles colored by q-value and sized by fold
1460 enrichment.
1461
1462 **Supplemental Figure 17. Overrepresentation analysis delineates distinct and**
1463 **shared pathways being modulated by plaque EV-miRNA and EV-proteome with**
1464 **symptom status-based distinctions in pathway identity and strength. A-B.**
1465 Overrepresentation analysis with Gene Ontology (GO) pathways using differentially
1466 expressed predicted EV-miRNA-mRNA targets **(A)** and EV-proteins **(B)** in asymptomatic
1467 and symptomatic groups. **C-D.** Overrepresentation analysis with Kyoto Encyclopedia of
1468 Genes and Genomes pathways using differentially expressed predicted EV-miRNA-
1469 mRNA targets **(C)** and EV-proteins **(D)** in asymptomatic and symptomatic groups.
1470
1471 **Supplemental Figure 18. Overrepresentation analysis finds endothelial and**
1472 **angiogenesis-based pathways as contributors to plaque vulnerability. A-C.** Subset
1473 analysis of differentially expressed EV-miRNAs **(A,B)** and EV-proteins **(C)** querying
1474 specific endothelial and angiogenesis based KEGG Pathways. Pairwise comparison of
1475 mean fold enrichment of EC-specific pathways in symptomatic versus asymptomatic
1476 plaques **(B)**. **D.** Subset analysis of differentially expressed EV-proteins querying specific
1477 endothelial and angiogenesis-based Gene Ontology Biological Process (GO-BP)
1478 Pathways. **E-F.** Subset analysis of differentially expressed EV-vesiculome (miRNA and
1479 proteins; Per-module) querying specific endothelial and angiogenesis-based Gene

1480 Ontology Biological Process (GO-BP; **E**) and Kyoto Encyclopedia of Genes and
1481 Genomes pathways (KEGG; **F**).
1482
1483 **Supplemental Figure 19. Functional validation of increased angiogenesis with**
1484 **plaque-derived vesicles employing a newly optimized low-input sprouting assay.**
1485 **A-B.** Pairwise comparison of mean fold enrichment of endothelial cell (EC)-specific
1486 pathways in EV-protein based Gene Ontology (GO; **A**) and Kyoto Encyclopedia of
1487 Genes and Genomes (KEGG**; B**) pathways in symptomatic versus asymptomatic
1488 plaques. Individual tests labelled above graph. **C-D.** Pairwise comparison of mean fold
1489 enrichment of EC-specific pathways in EV-vesiculome (miRNA and protein) based Gene
1490 Ontology (GO; **C**) and Kyoto Encyclopedia of Genes and Genomes (KEGG**; D**)
1491 pathways in symptomatic versus asymptomatic plaques. Individual tests and p-values
1492 labelled above graph. **E.** Schematic of sprouting angiogenesis assay depicting EV-
1493 enrichment from plaque and marginal zones of symptomatic patients, treatment of
1494 immortalized human umbilical endothelial cell (HUVEC) derived spheroids, followed by
1495 staining and quantification. **F.** Representative confocal microscopy images of HUVEC-
1496 spheroid angiogenesis after addition of EVs (2-4X10^{10} EVs; 24 h), vascular endothelial
1497 growth factor (VEGF; positive control), plaque zone (PZ) elute (PZ EV control), marginal
1498 zone (MZ) elute (MZ EV control), assay control (media only). Scale bar represents 100
1499 μm. **G.** Quantification of average sprout length (n=188-331 sprouts from 7–10 spheroids
1500 from 3 independent experiments). **H-J.** Quantification of sprout number **(H)**, sprout
1501 length **(I)**, and average sprout length **(J)** with addition of VEGF (50 ng/ml, positive
1502 control; *n*=6-8). Bar graphs show the mean±SEM. Violin plots show median ±

1503 interquartile range. Statistical significance assessed by 1-way ANOVA with Sidak

1504 multiple comparisons test **(**adjusted p-values shown, G). P-values meeting significance

1505 (<0.05) shown in bolded text **(G)**.

Figure 1

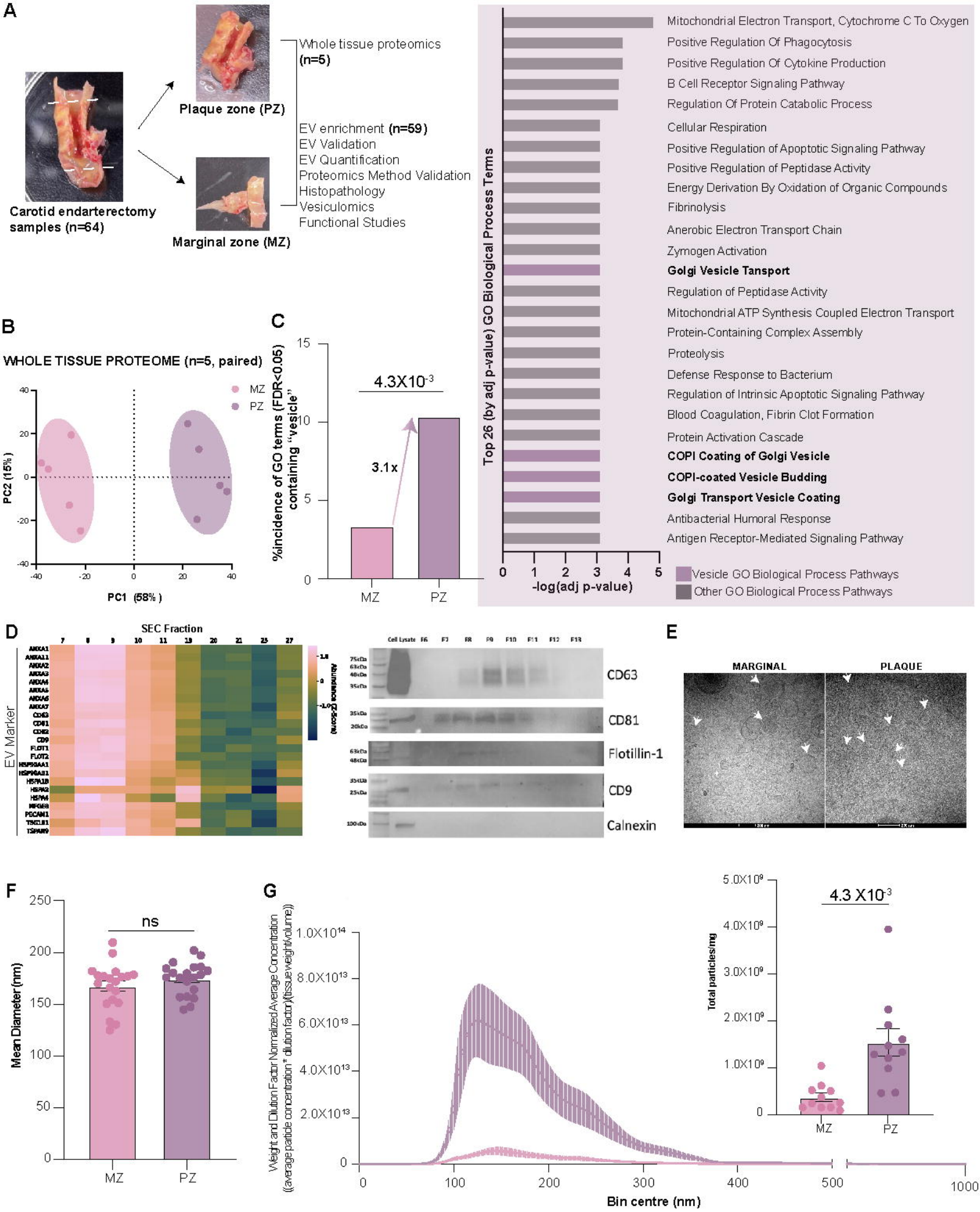
A
Carotid endarterectomy samples (n=64)
Plaque zone (PZ)
Marginal zone (MZ)
Whole tissue proteomics (n=5)
EV enrichment (n=59)
EV Validation
EV Quantification
Proteomics Method Validation
Histopathology
Vesiculomics
Functional Studies
Top 26 (by adj p-value) GO Biological Process Terms
Mitochondrial Electron Transport, Cytochrome C To Oxygen
Positive Regulation Of Phagocytosis
Positive Regulation Of Cytokine Production
B Cell Receptor Signaling Pathway
Regulation Of Protein Catabolic Process
Cellular Respiration
Positive Regulation of Apoptotic Signaling Pathway
Positive Regulation of Peptidase Activity
Energy Derivation By Oxidation of Organic Compounds
Fibrinolysis
Anerobic Electron Transport Chain
Zymogen Activation
Golgi Vesicle Tansport
Regulation of Peptidase Activity
Mitochondrial ATP Synthesis Coupled Electron Transport
Protein-Containing Complex Assembly
Proteolysis
Defense Response to Bacterium
Regulation of Intrinsic Apoptotic Signaling Pathway
Blood Coagulation, Fibrin Clot Formation
Protein Activation Cascade
COPI Coating of Golgi Vesicle
COPI-coated Vesicle Budding
Golgi Transport Vesicle Coating
Antibacterial Humoral Response
Antigen Receptor-Mediated Signaling Pathway
-log(adj p-value)
Vesicle GO Biological Process Pathways
Other GO Biological Process Pathways
B
WHOLE TISSUE PROTEOME (n=5, paired)
MZ
PZ
PC2 (15%)
PC1 (58%)
C
%incidence of GO terms (FDR<0.05) containing "vesicle"
4.3X10-3
3.1x
MZ
PZ
D
SEC Fraction
EV Marker
Cell Lysate
CD63
CD81
Flotillin-1
CD9
Calnexin
E
MARGINAL
PLAQUE
F
Mean Diameter (nm)
ns
MZ
PZ
G
Weight and Dilution Factor Normalized Average Concentration
Bin centre (nm)
Total particles/mg
4.3 X10-3
MZ
PZ

Figure 2

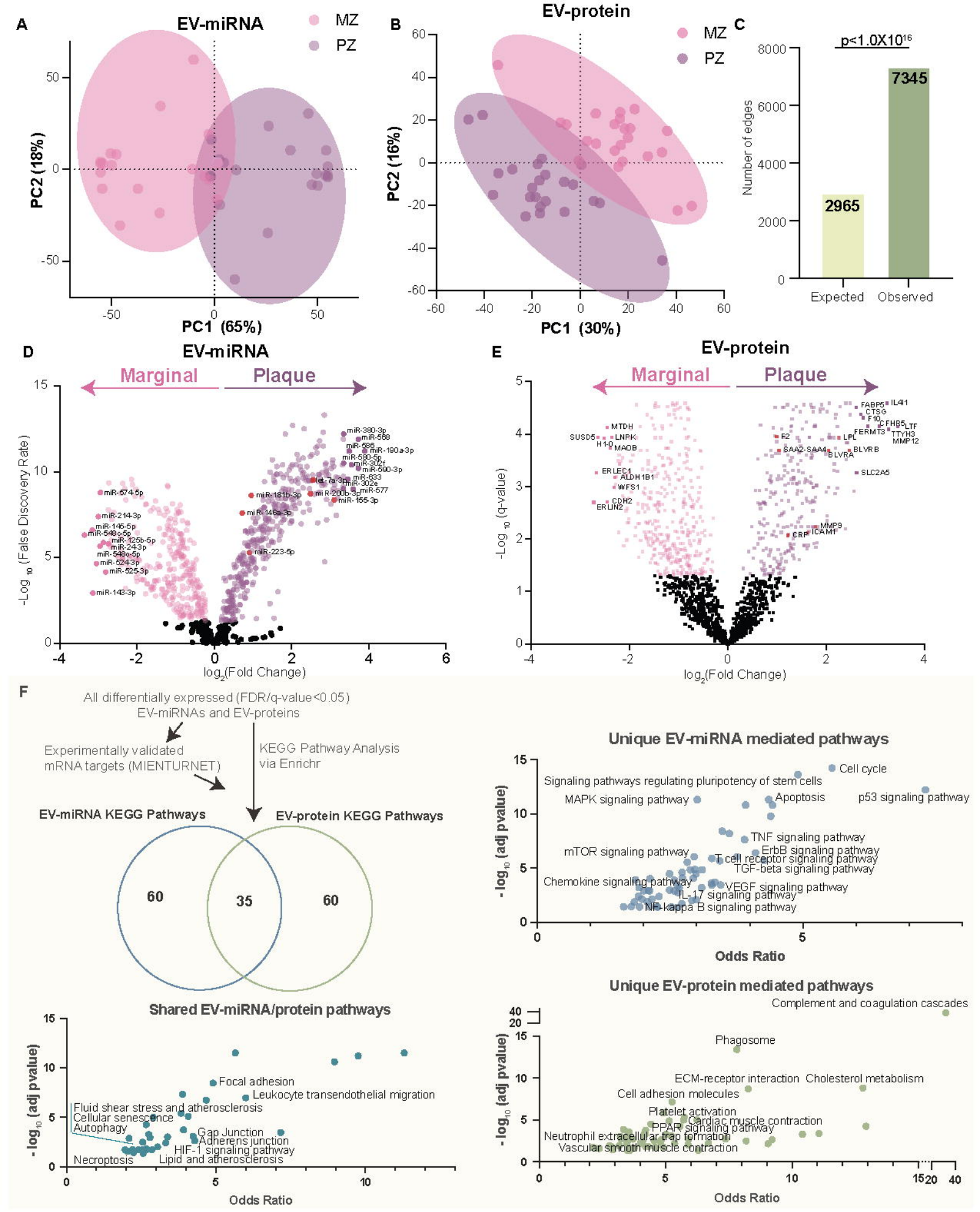
A
EV-miRNA
MZ
PZ
PC2 (18%)
PC1 (65%)
B
EV-protein
MZ
PZ
PC2 (16%)
PC1 (30%)
C
p<1.0X10^16
Number of edges
7345
2965
Expected
Observed
D
EV-miRNA
Marginal
Plaque
-Log 10 (False Discovery Rate)
log2(Fold Change)
miR-380-3p
miR-568
miR-586
miR-190a-3p
miR-580-5p
miR-302f
miR-590-3p
miR-633
let-7a-3p
miR-302e
miR-577
miR-181b-3p
miR-200b-3p
miR-155-3p
miR-146a-3p
miR-223-5p
miR-574-5p
miR-214-3p
miR-145-5p
miR-548o-5p
miR-125b-5p
miR-24-3p
miR-548o-5p
miR-524-3p
miR-525-3p
miR-143-3p
E
EV-protein
Marginal
Plaque
-Log 10 (q-value)
log2(Fold Change)
MTDH
SUSD5
LNPK
H1-0
MAOB
ERLEC1
ALDH1B1
WFS1
CDH2
ERLIN2
FABP5
IL4I1
CTSG
F10
CFHR5
LTF
FERMT3
TTYH3
MMP12
F2
LPL
SAA2-SAA4
BLVRB
BLVRA
SLC2A5
MMP9
ICAM1
CRP
F
All differentially expressed (FDR/q-value<0.05)
EV-miRNAs and EV-proteins
Experimentally validated
mRNA targets (MIENTURNET)
KEGG Pathway Analysis
via Enrichr
EV-miRNA KEGG Pathways
EV-protein KEGG Pathways
60
35
60
Unique EV-miRNA mediated pathways
Cell cycle
Signaling pathways regulating pluripotency of stem cells
MAPK signaling pathway
Apoptosis
p53 signaling pathway
TNF signaling pathway
mTOR signaling pathway
ErbB signaling pathway
T cell receptor signaling pathway
TGF-beta signaling pathway
Chemokine signaling pathway
VEGF signaling pathway
IL-17 signaling pathway
NF-kappa B signaling pathway
- log10 (adj pvalue)
Odds Ratio
Shared EV-miRNA/protein pathways
Focal adhesion
Leukocyte transendothelial migration
Fluid shear stress and atherosclerosis
Cellular senescence
Autophagy
Gap Junction
Adherens junction
HIF-1 signaling pathway
Necroptosis
Lipid and atherosclerosis
- log10 (adj pvalue)
Odds Ratio
Unique EV-protein mediated pathways
Complement and coagulation cascades
Phagosome
ECM-receptor interaction
Cholesterol metabolism
Cell adhesion molecules
Platelet activation
Cardiac muscle contraction
PPAR signaling pathway
Neutrophil extracellular trap formation
Vascular smooth muscle contraction
- log10 (adj pvalue)
Odds Ratio

Figure 3

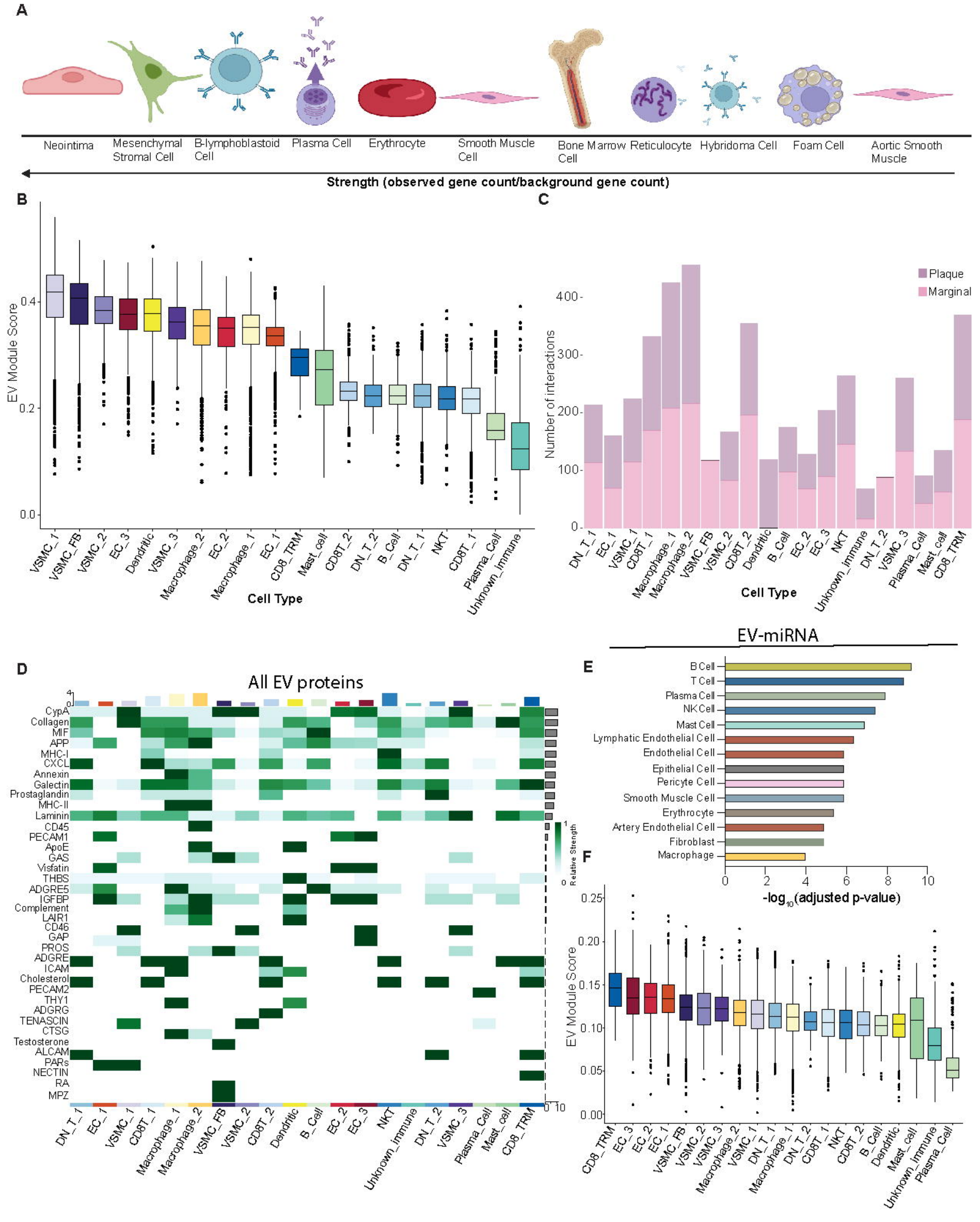
A
Neointima
Mesenchymal Stromal Cell
B-lymphoblastoid Cell
Plasma Cell
Erythrocyte
Smooth Muscle Cell
Bone Marrow Cell
Reticulocyte
Hybridoma Cell
Foam Cell
Aortic Smooth Muscle
Strength (observed gene count/background gene count)
B
EV Module Score
Cell Type
C
Plaque
Marginal
Number of interactions
Cell Type
D
All EV proteins
Relative Strength
E
EV-miRNA
B Cell
T Cell
Plasma Cell
NK Cell
Mast Cell
Lymphatic Endothelial Cell
Endothelial Cell
Epithelial Cell
Pericyte Cell
Smooth Muscle Cell
Erythrocyte
Artery Endothelial Cell
Fibroblast
Macrophage
-log10(adjusted p-value)
F
EV Module Score

Figure 4

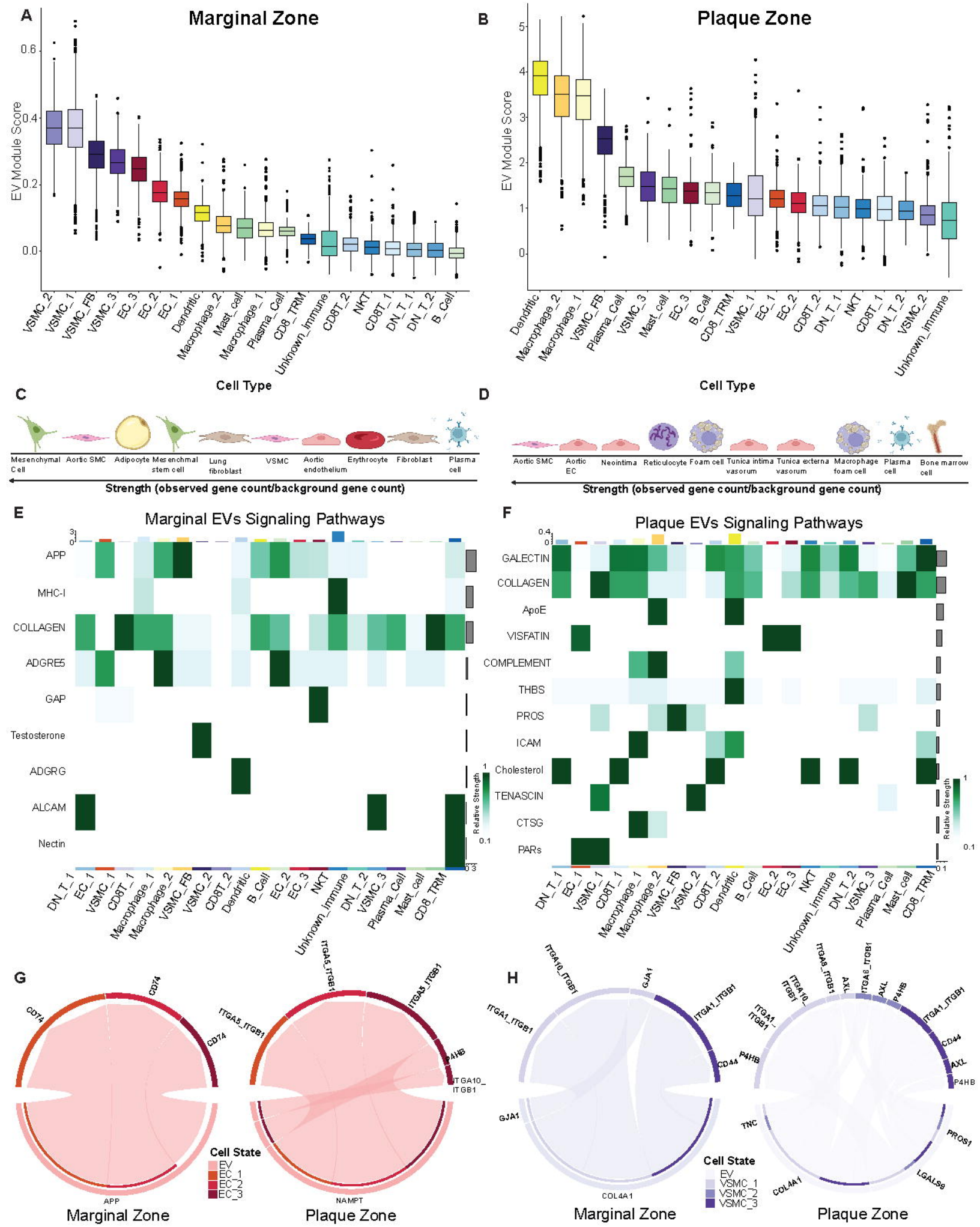
A
Marginal Zone
EV Module Score
Cell Type
VSMC_2
VSMC_1
VSMC_FB
VSMC_3
EC_3
EC_2
EC_1
Dendritic
Macrophage_2
Mast_cell
Macrophage_1
Plasma_Cell
CD8_TRM
Unknown_immune
CD8T_2
NKT
CD8T_1
DN_T_1
DN_T_2
B_Cell
B
Plaque Zone
EV Module Score
Cell Type
Dendritic
Macrophage_2
Macrophage_1
VSMC_FB
Plasma_Cell
VSMC_3
Mast_cell
EC_3
B_Cell
CD8_TRM
VSMC_1
EC_1
EC_2
CD8T_2
DN_T_1
NKT
CD8T_1
DN_T_2
VSMC_2
Unknown_immune
C
Mesenchymal Cell
Aortic SMC
Adipocyte
Mesenchmal stem cell
Lung fibroblast
VSMC
Aortic endothelium
Erythrocyte
Fibroblast
Plasma cell
Strength (observed gene count/background gene count)
D
Aortic SMC
Aortic EC
Neointima
Reticulocyte
Foam cell
Tunica intima vasorum
Tunica externa vasorum
Macrophage foam cell
Plasma cell
Bone marrow cell
Strength (observed gene count/background gene count)
E
Marginal EVs Signaling Pathways
APP
MHC-I
COLLAGEN
ADGRE5
GAP
Testosterone
ADGRG
ALCAM
Nectin
Relative Strength
F
Plaque EVs Signaling Pathways
GALECTIN
COLLAGEN
ApoE
VISFATIN
COMPLEMENT
THBS
PROS
ICAM
Cholesterol
TENASCIN
CTSG
PARs
Relative Strength
G
CD74
APP
ITGA5_ITGB1
P4HB
ITGA10_ITGB1
NAMPT
Cell State
EV
EC_1
EC_2
EC_3
Marginal Zone
Plaque Zone
H
ITGA10_ITGB1
GJA1
ITGA1_ITGB1
CD44
P4HB
COL4A1
AXL
TNC
PROS1
LGALS9
Cell State
EV
VSMC_1
VSMC_2
VSMC_3
Marginal Zone
Plaque Zone

Figure 5

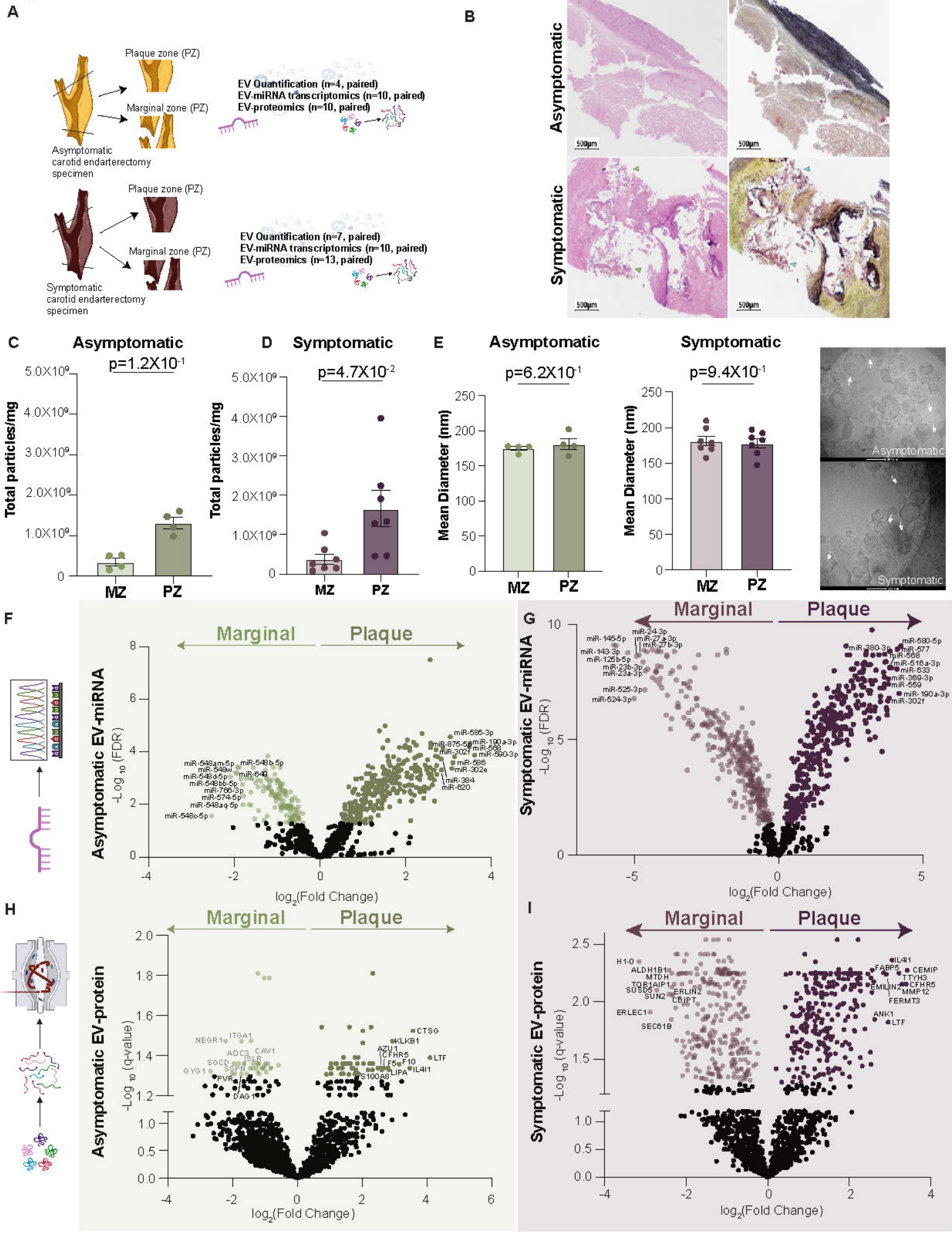
A
Plaque zone (PZ)
Marginal zone (PZ)
Asymptomatic carotid endarterectomy specimen
EV Quantification (n=4, paired)
EV-miRNA transcriptomics (n=10, paired)
EV-proteomics (n=10, paired)
Plaque zone (PZ)
Marginal zone (PZ)
Symptomatic carotid endarterectomy specimen
EV Quantification (n=7, paired)
EV-miRNA transcriptomics (n=10, paired)
EV-proteomics (n=13, paired)
B
H&E
Movat Pentachrome
Asymptomatic
Symptomatic
500µm
C
Asymptomatic
p=1.2X10-1
Total particles/mg
MZ
PZ
D
Symptomatic
p=4.7X10-2
E
Asymptomatic
p=6.2X10-1
Mean Diameter (nm)
Symptomatic
p=9.4X10-1
Asymptomatic
Symptomatic
F
Marginal
Plaque
Asymptomatic EV-miRNA
-Log 10 (FDR)
log2(Fold Change)
G
Symptomatic EV-miRNA
H
Asymptomatic EV-protein
-Log 10 (q-value)
I
Symptomatic EV-protein

Figure 6

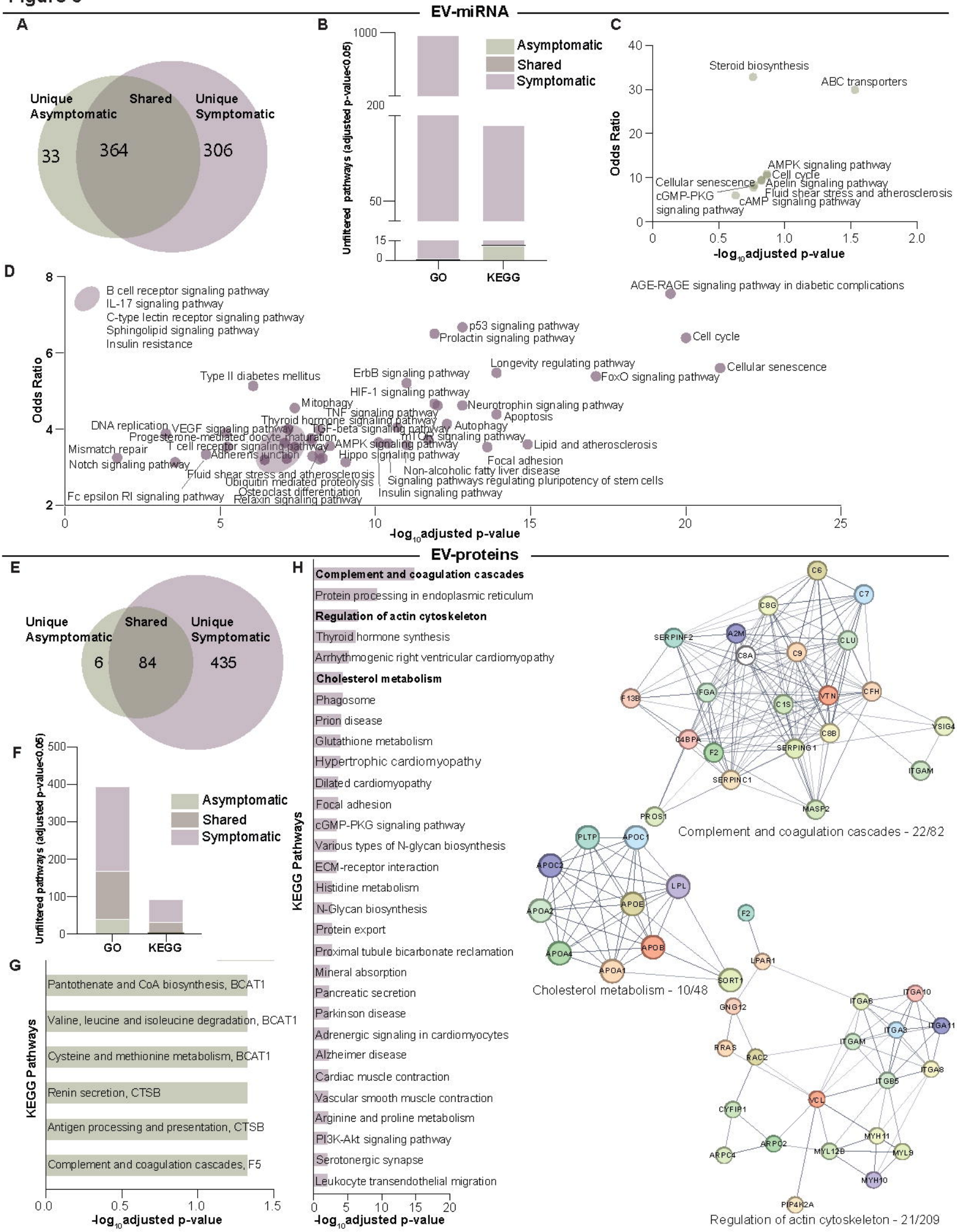
EV-miRNA
A
Unique Asymptomatic
Shared
Unique Symptomatic
33
364
306
B
Asymptomatic
Shared
Symptomatic
Unfiltered pathways (adjusted p-value<0.05)
1000
200
50
15
0
GO
KEGG
C
Odds Ratio
Steroid biosynthesis
ABC transporters
AMPK signaling pathway
Cell cycle
Cellular senescence
Apelin signaling pathway
cGMP-PKG
Fluid shear stress and atherosclerosis
cAMP signaling pathway
signaling pathway
-log10adjusted p-value
D
Odds Ratio
B cell receptor signaling pathway
IL-17 signaling pathway
C-type lectin receptor signaling pathway
Sphingolipid signaling pathway
Insulin resistance
AGE-RAGE signaling pathway in diabetic complications
p53 signaling pathway
Prolactin signaling pathway
Cell cycle
Longevity regulating pathway
Cellular senescence
Type II diabetes mellitus
ErbB signaling pathway
FoxO signaling pathway
HIF-1 signaling pathway
Mitophagy
Neurotrophin signaling pathway
TNF signaling pathway
Apoptosis
Thyroid hormone signaling pathway
DNA replication
VEGF signaling pathway
TGF-beta signaling pathway
Autophagy
Progesterone-mediated oocyte maturation
mTOR signaling pathway
T cell receptor signaling pathway
AMPK signaling pathway
Lipid and atherosclerosis
Mismatch repair
Adherens junction
Hippo signaling pathway
Focal adhesion
Notch signaling pathway
Non-alcoholic fatty liver disease
Fluid shear stress and atherosclerosis
Ubiquitin mediated proteolysis
Signaling pathways regulating pluripotency of stem cells
Osteoclast differentiation
Insulin signaling pathway
Fc epsilon RI signaling pathway
Relaxin signaling pathway
-log10adjusted p-value
EV-proteins
E
Unique Asymptomatic
Shared
Unique Symptomatic
6
84
435
F
Unfiltered pathways (adjusted p-value<0.05)
Asymptomatic
Shared
Symptomatic
GO
KEGG
G
KEGG Pathways
Pantothenate and CoA biosynthesis, BCAT1
Valine, leucine and isoleucine degradation, BCAT1
Cysteine and methionine metabolism, BCAT1
Renin secretion, CTSB
Antigen processing and presentation, CTSB
Complement and coagulation cascades, F5
-log10adjusted p-value
H
KEGG Pathways
Complement and coagulation cascades
Protein processing in endoplasmic reticulum
Regulation of actin cytoskeleton
Thyroid hormone synthesis
Arrhythmogenic right ventricular cardiomyopathy
Cholesterol metabolism
Phagosome
Prion disease
Glutathione metabolism
Hypertrophic cardiomyopathy
Dilated cardiomyopathy
Focal adhesion
cGMP-PKG signaling pathway
Various types of N-glycan biosynthesis
ECM-receptor interaction
Histidine metabolism
N-Glycan biosynthesis
Protein export
Proximal tubule bicarbonate reclamation
Mineral absorption
Pancreatic secretion
Parkinson disease
Adrenergic signaling in cardiomyocytes
Alzheimer disease
Cardiac muscle contraction
Vascular smooth muscle contraction
Arginine and proline metabolism
PI3K-Akt signaling pathway
Serotonergic synapse
Leukocyte transendothelial migration
-log10adjusted p-value
C6
C7
C8G
SERPINF2
A2M
CLU
C8A
C9
F13B
FGA
VTN
CFH
C1S
VSIG4
C8B
C4BPA
F2
SERPING1
ITGAM
SERPINC1
MASP2
PROS1
Complement and coagulation cascades - 22/82
PLTP
APOC1
APOC2
LPL
APOA2
APOE
F2
APOA4
APOB
LPAR1
APOA1
SORT1
Cholesterol metabolism - 10/48
GNG12
ITGAB
ITGA10
ITGA3
ITGA11
ITGAM
RRAS
RAC2
ITGA8
ITGB5
VCL
CYFIP1
MYH11
ARPC2
ARPC4
MYL12B
MYL9
MYH10
PIP4K2A
Regulation of actin cytoskeleton - 21/209

Figure 7

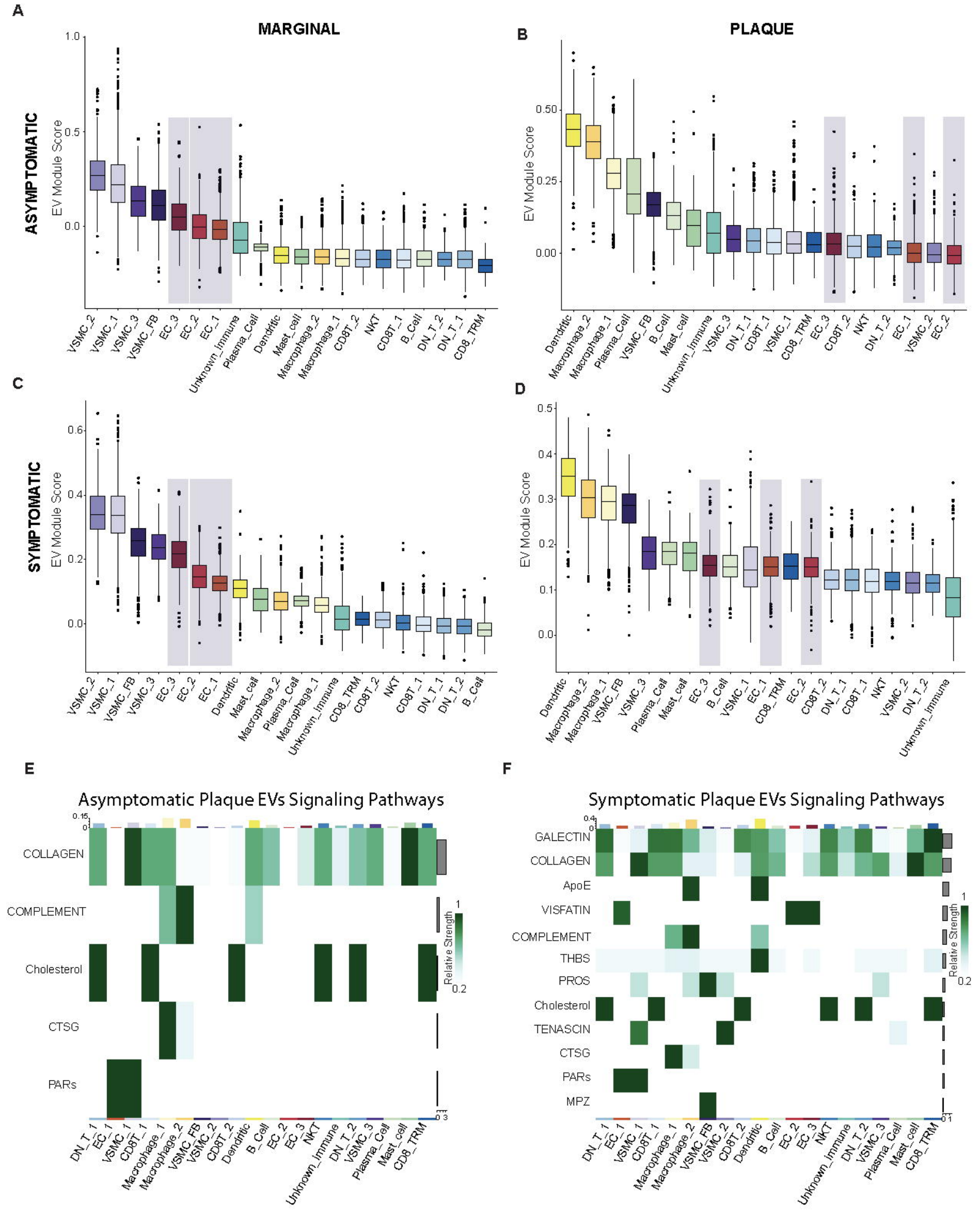
A
MARGINAL
ASYMPTOMATIC
EV Module Score
VSMC_2
VSMC_1
VSMC_3
VSMC_FB
EC_3
EC_2
EC_1
Unknown_Immune
Plasma_Cell
Dendritic
Mast_cell
Macrophage_2
Macrophage_1
CD8T_2
NKT
CD8T_1
B_Cell
DN_T_2
DN_T_1
CD8_TRM
B
PLAQUE
C
SYMPTOMATIC
D
E
Asymptomatic Plaque EVs Signaling Pathways
COLLAGEN
COMPLEMENT
Cholesterol
CTSG
PARs
Relative Strength
F
Symptomatic Plaque EVs Signaling Pathways
GALECTIN
ApoE
VISFATIN
THBS
PROS
TENASCIN
MPZ

Figure 8

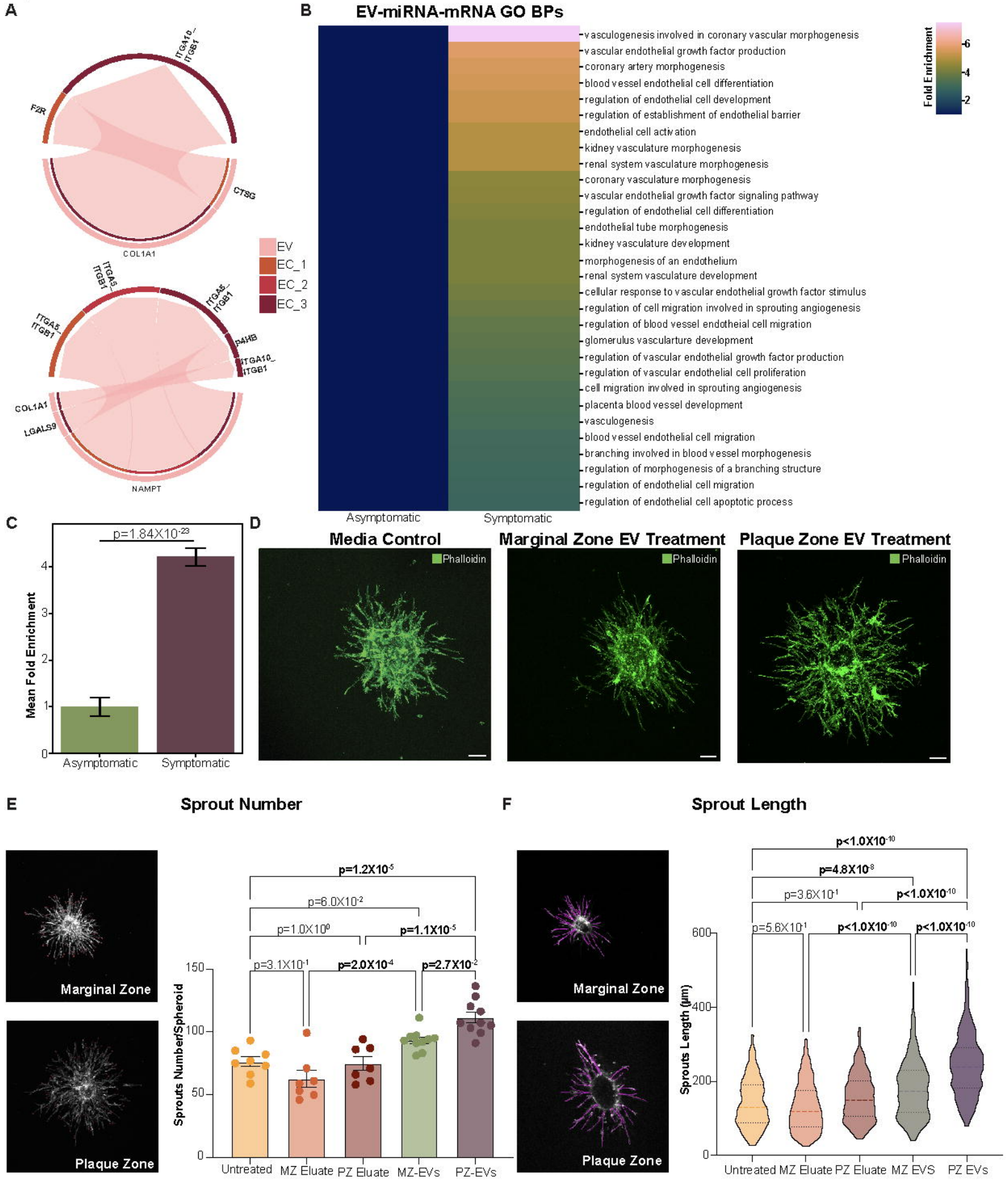
A
ITGA10_ ITGB1
F2R
CTSG
COL1A1
EV
EC_1
EC_2
EC_3
ITGA5_ ITGB1
ITGA5_ ITGB1
ITGA5_ ITGB1
P4HB
ITGA10_ ITGB1
COL1A1
LGALS9
NAMPT
B
EV-miRNA-mRNA GO BPs
vasculogenesis involved in coronary vascular morphogenesis
vascular endothelial growth factor production
coronary artery morphogenesis
blood vessel endothelial cell differentiation
regulation of endothelial cell development
regulation of establishment of endothelial barrier
endothelial cell activation
kidney vasculature morphogenesis
renal system vasculature morphogenesis
coronary vasculature morphogenesis
vascular endothelial growth factor signaling pathway
regulation of endothelial cell differentiation
endothelial tube morphogenesis
kidney vasculature development
morphogenesis of an endothelium
renal system vasculature development
cellular response to vascular endothelial growth factor stimulus
regulation of cell migration involved in sprouting angiogenesis
regulation of blood vessel endotheial cell migration
glomerulus vascularture development
regulation of vascular endothelial growth factor production
regulation of vascular endothelial cell proliferation
cell migration involved in sprouting angiogenesis
placenta blood vessel development
vasculogenesis
blood vessel endothelial cell migration
branching involved in blood vessel morphogenesis
regulation of morphogenesis of a branching structure
regulation of endothelial cell migration
regulation of endothelial cell apoptotic process
Asymptomatic
Symptomatic
Fold Enrichment
6
4
2
C
p=1.84X10-23
Mean Fold Enrichment
0
1
2
3
4
Asymptomatic
Symptomatic
D
Media Control
Marginal Zone EV Treatment
Plaque Zone EV Treatment
Phalloidin
Phalloidin
Phalloidin
E
Sprout Number
Marginal Zone
Plaque Zone
p=1.2X10-5
p=6.0X10-2
p=1.0X100
p=1.1X10-5
p=3.1X10-1
p=2.0X10-4
p=2.7X10-2
Sprouts Number/Spheroid
0
50
100
150
Untreated
MZ Eluate
PZ Eluate
MZ-EVs
PZ-EVs
F
Sprout Length
Marginal Zone
Plaque Zone
p<1.0X10-10
p=4.8X10-8
p=3.6X10-1
p<1.0X10-10
p=5.6X10-1
p<1.0X10-10
p<1.0X10-10
Sprouts Length (µm)
0
200
400
600
Untreated
MZ Eluate
PZ Eluate
MZ EVS
PZ EVs

Supplemental Figure 1

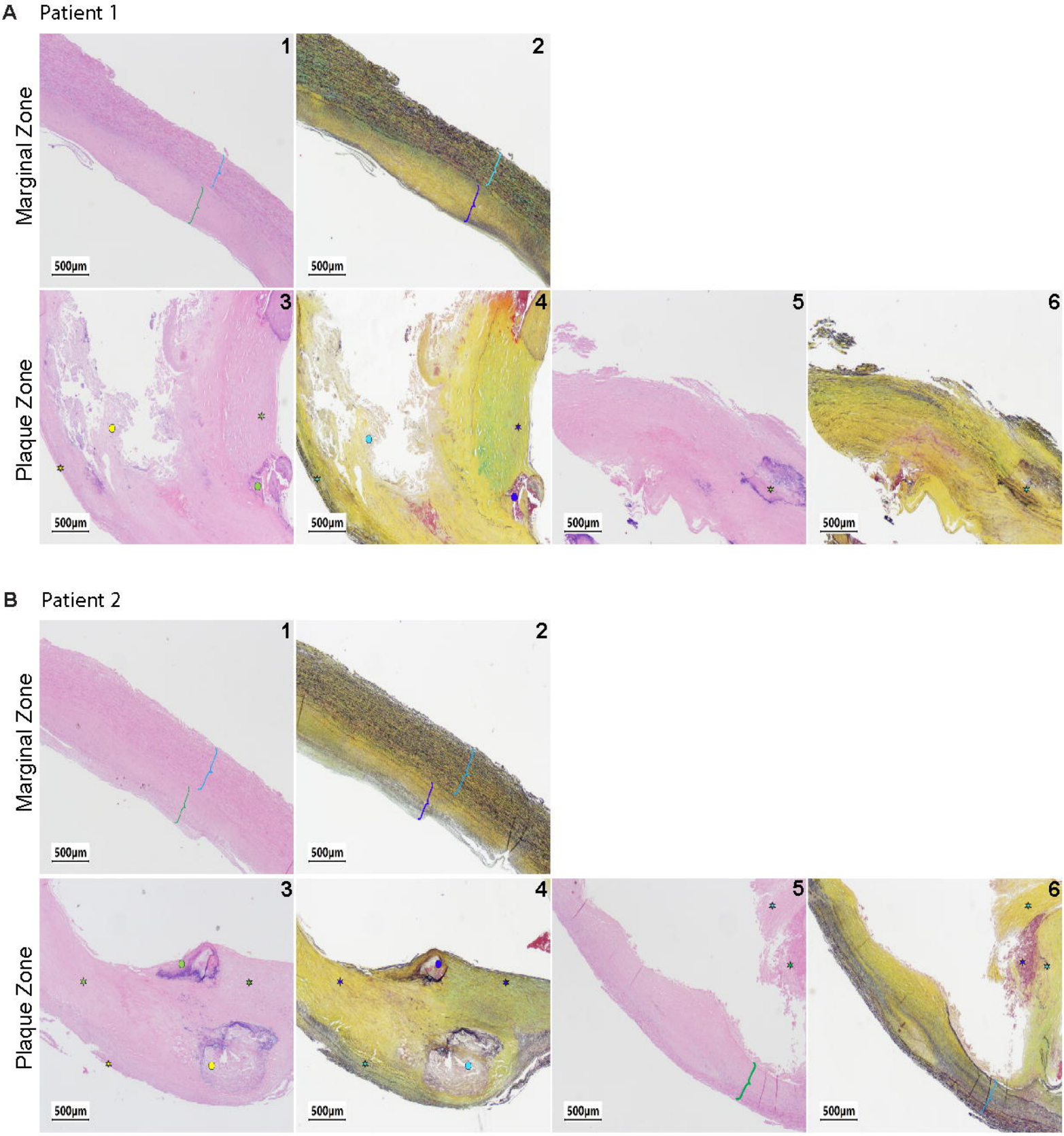

Supplemental Figure 2

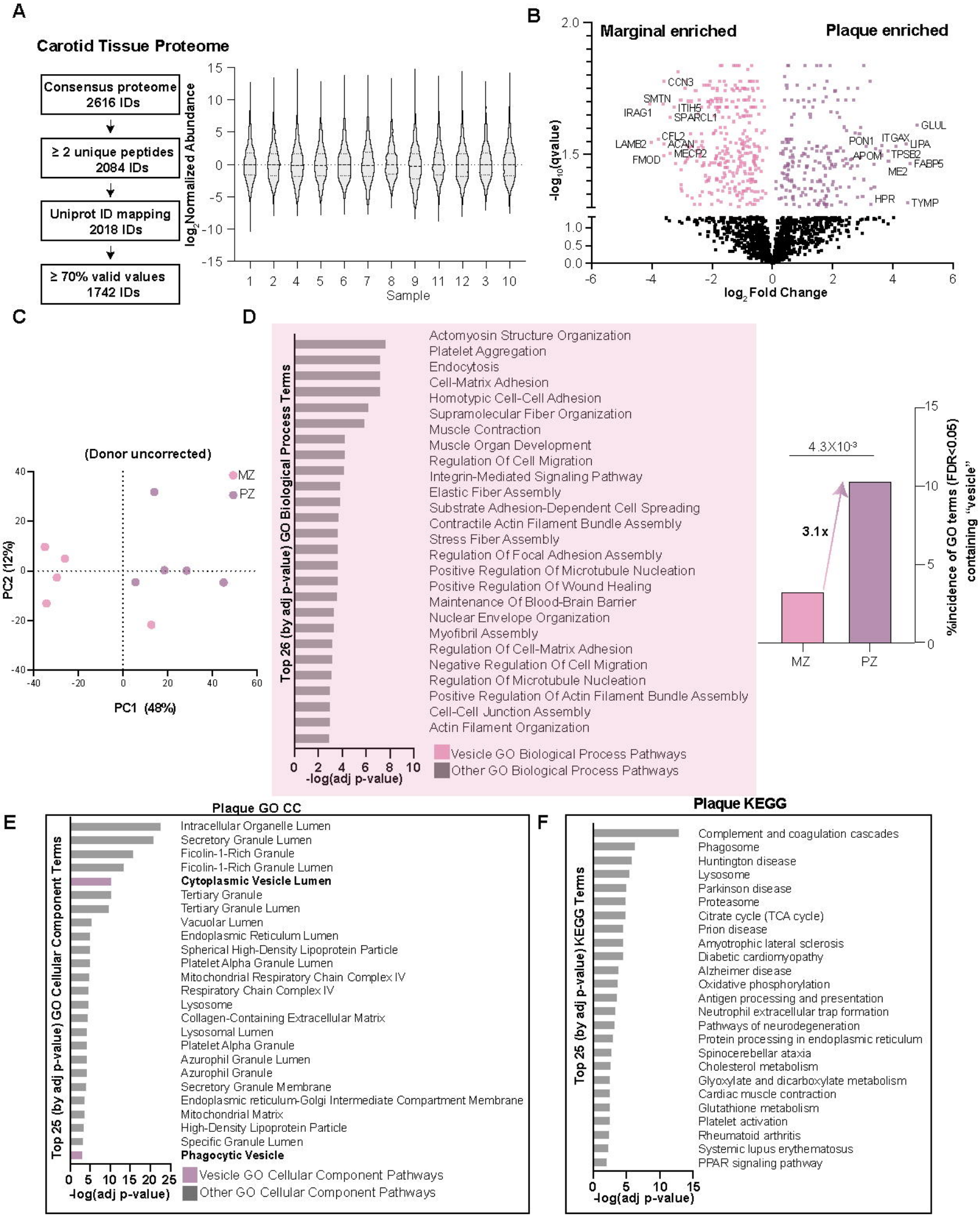

Supplemental Figure 3

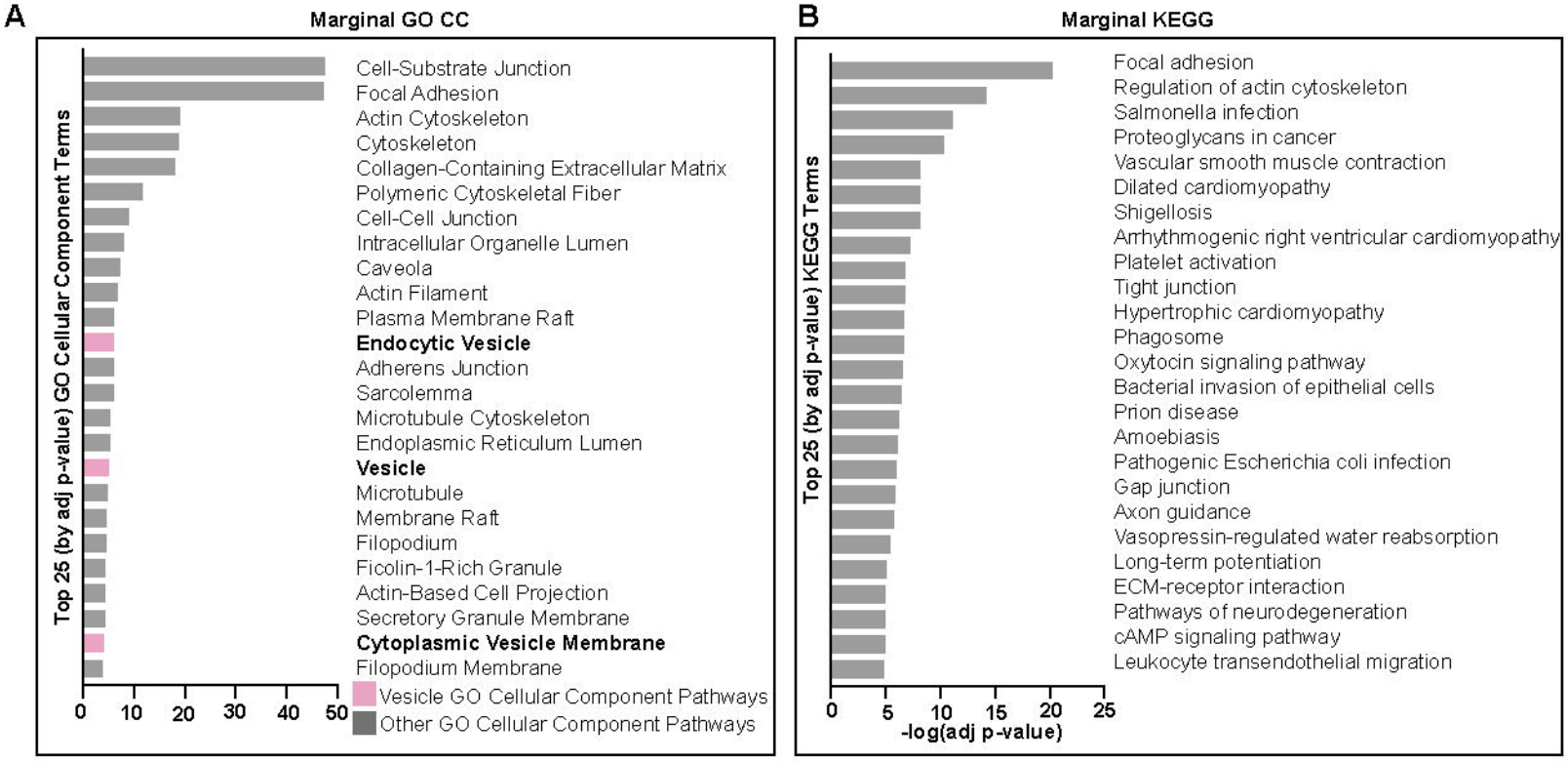

Supplemental Figure 4

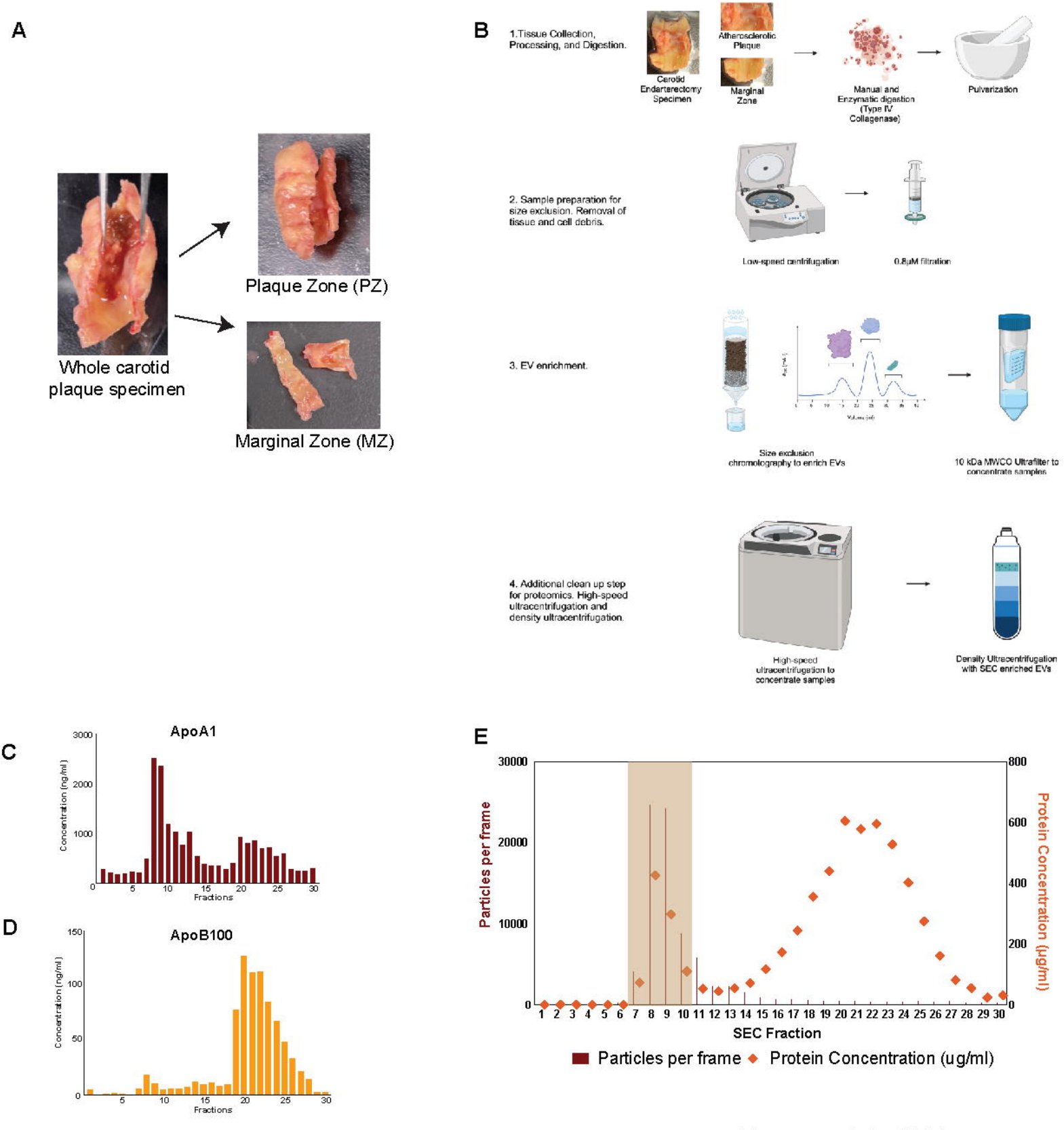

Supplemental Figure 5

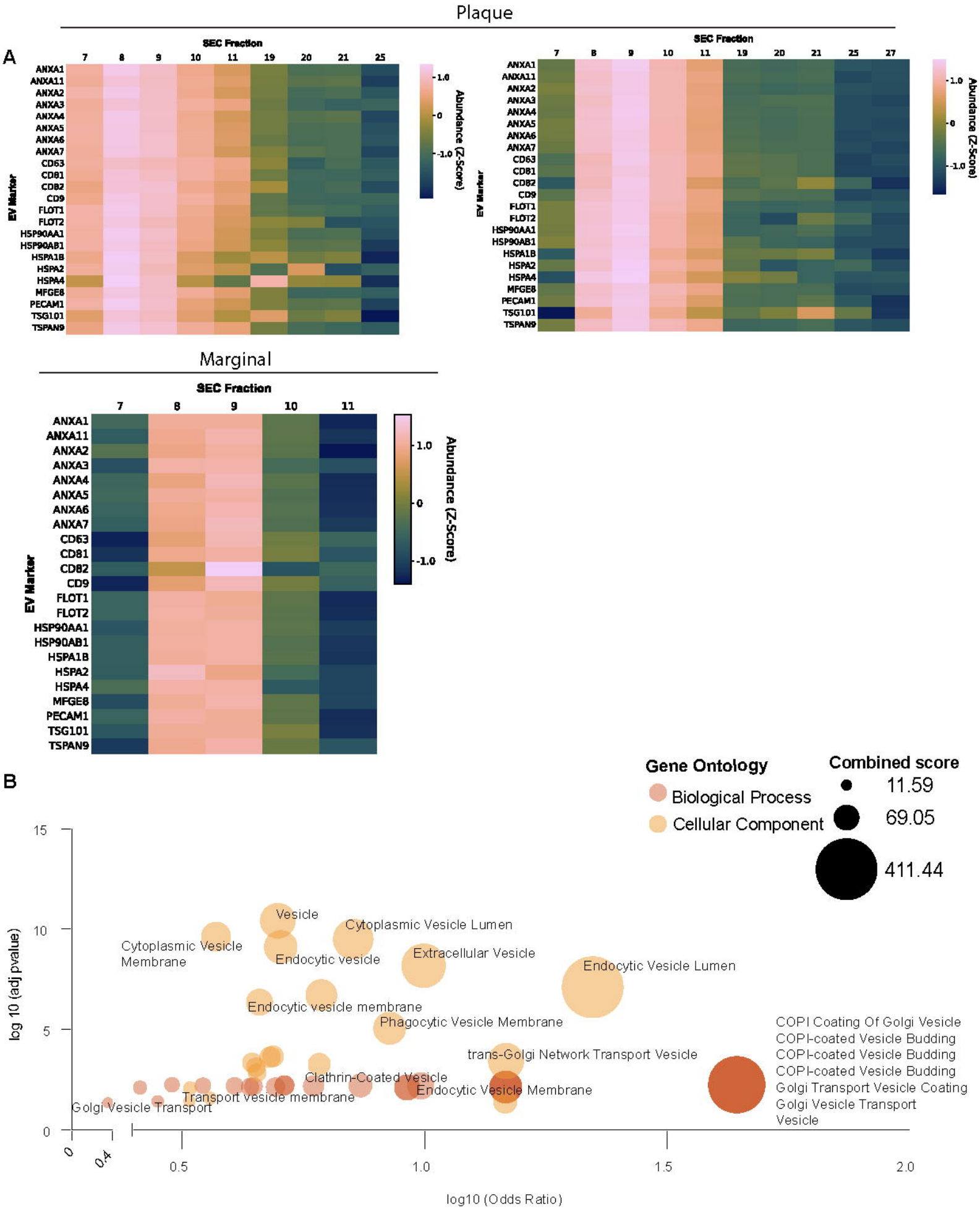

Supplemental Figure 6

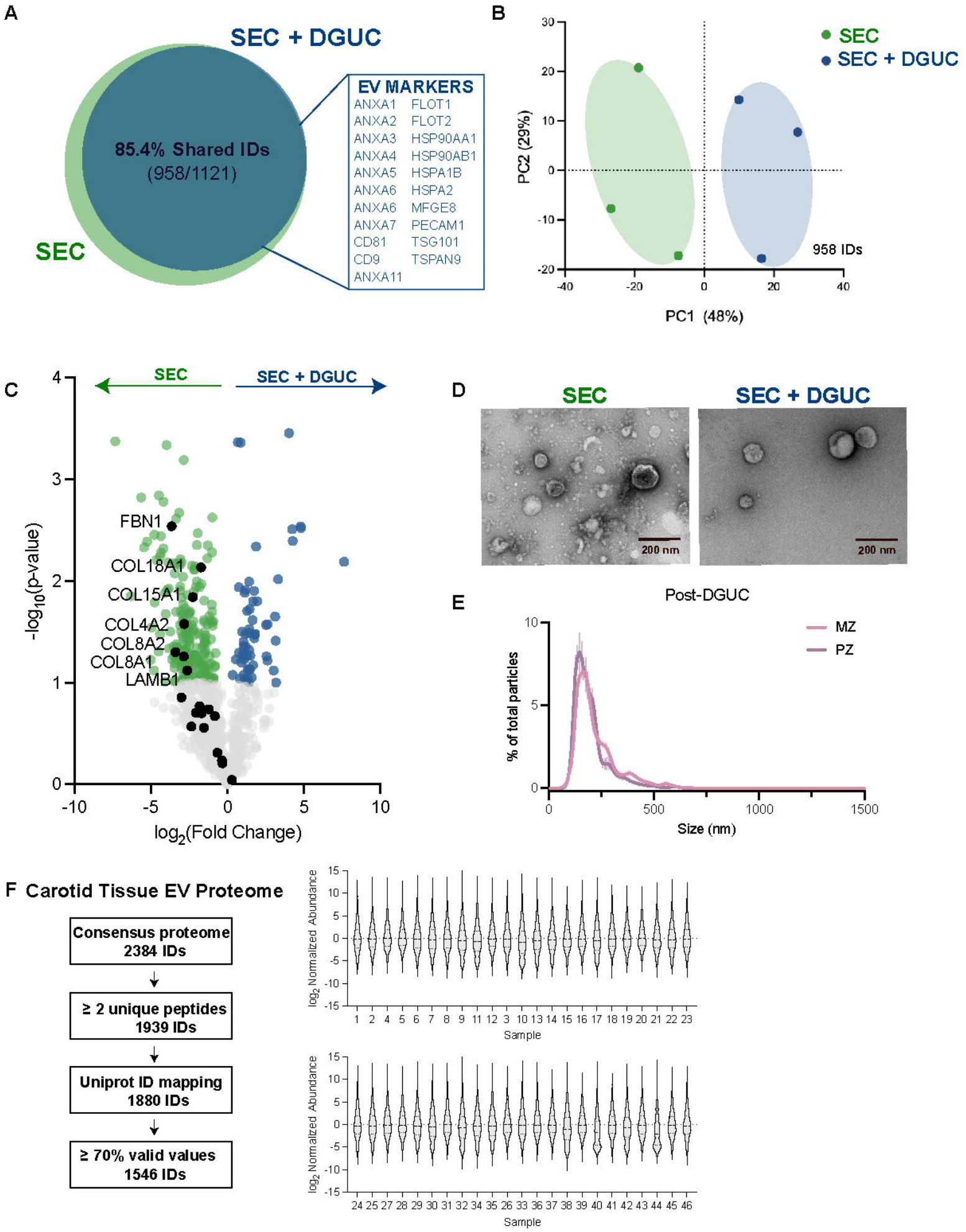

Supplemental Figure 7

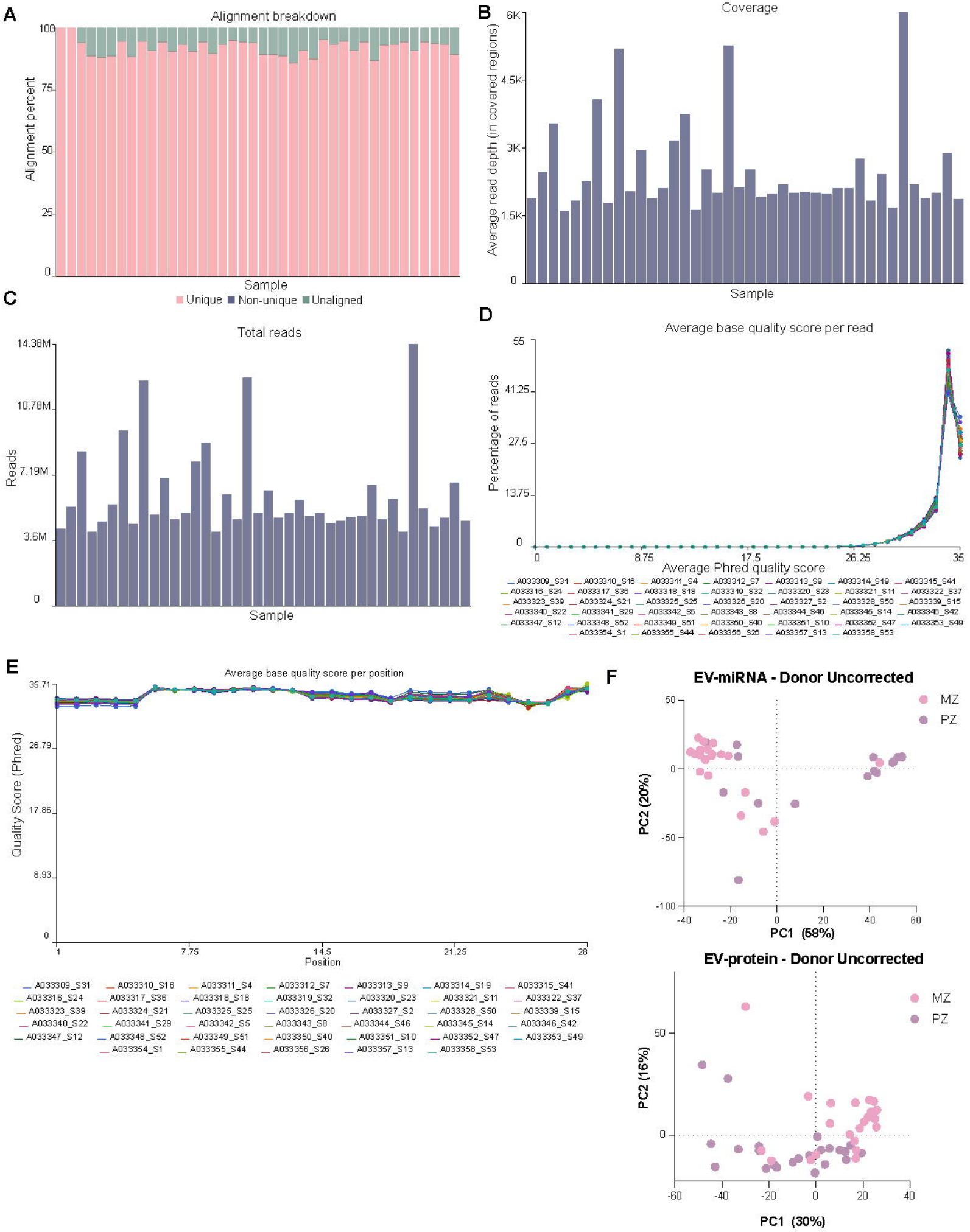

Supplemental Figure 8

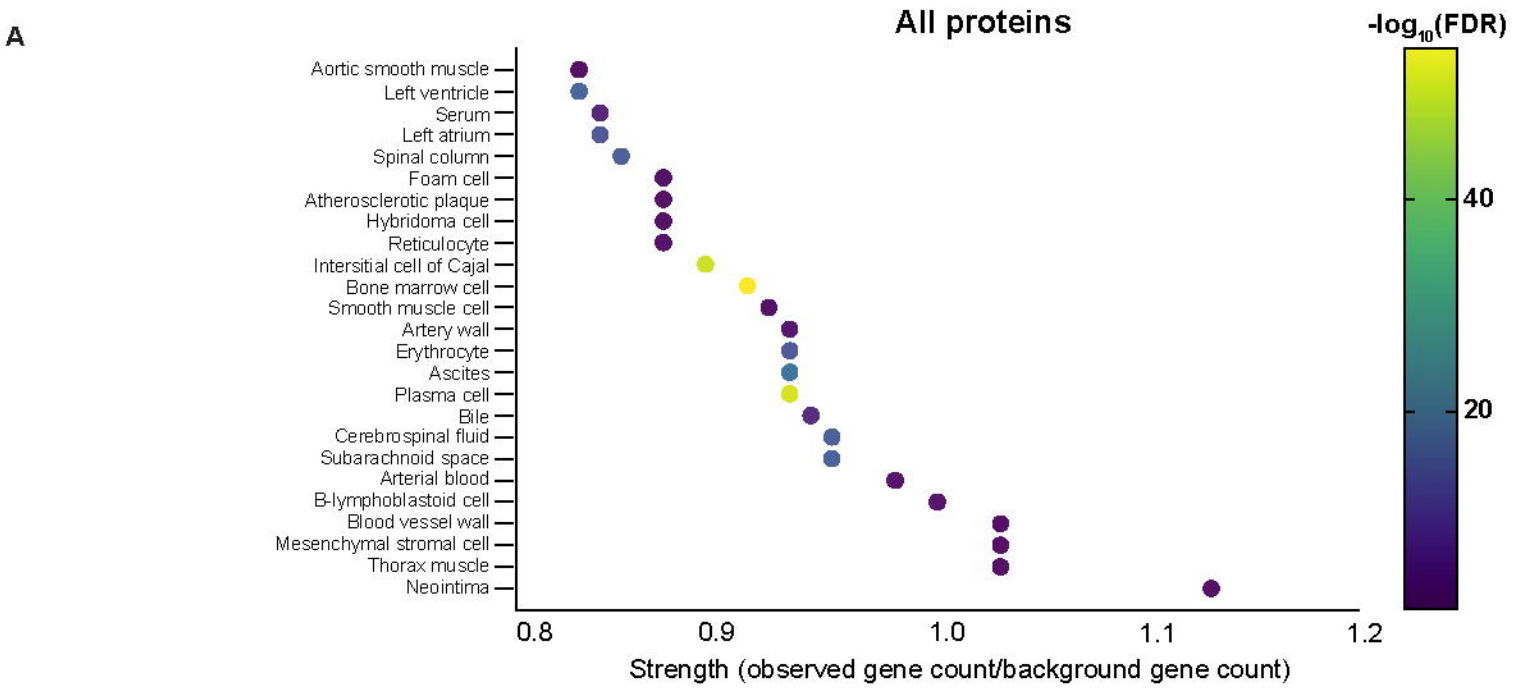

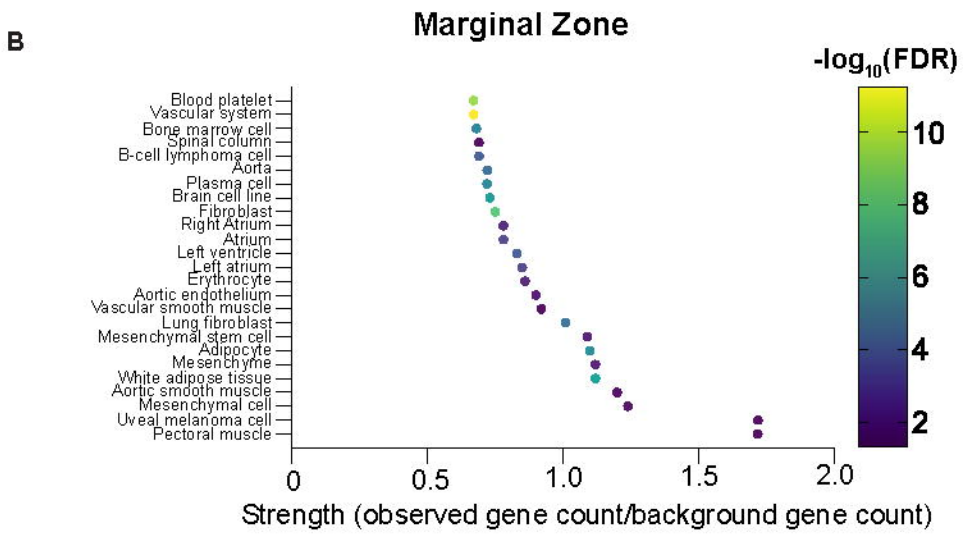

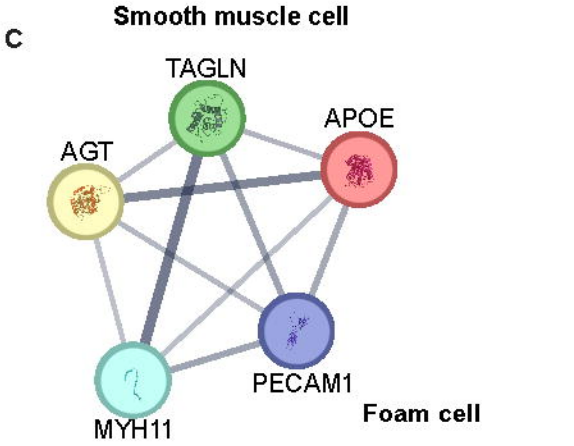

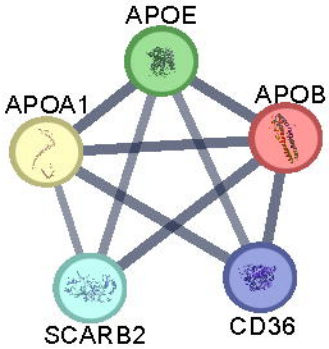

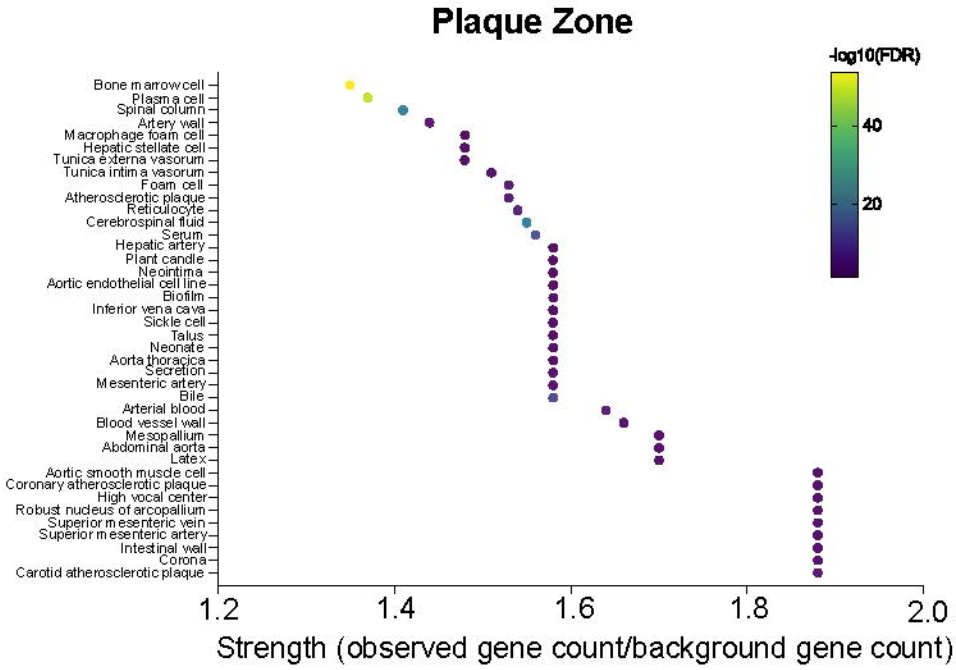

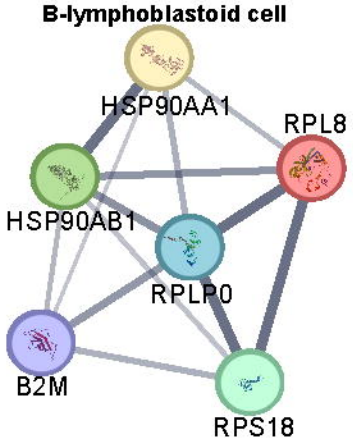

Supplemental Figure 9

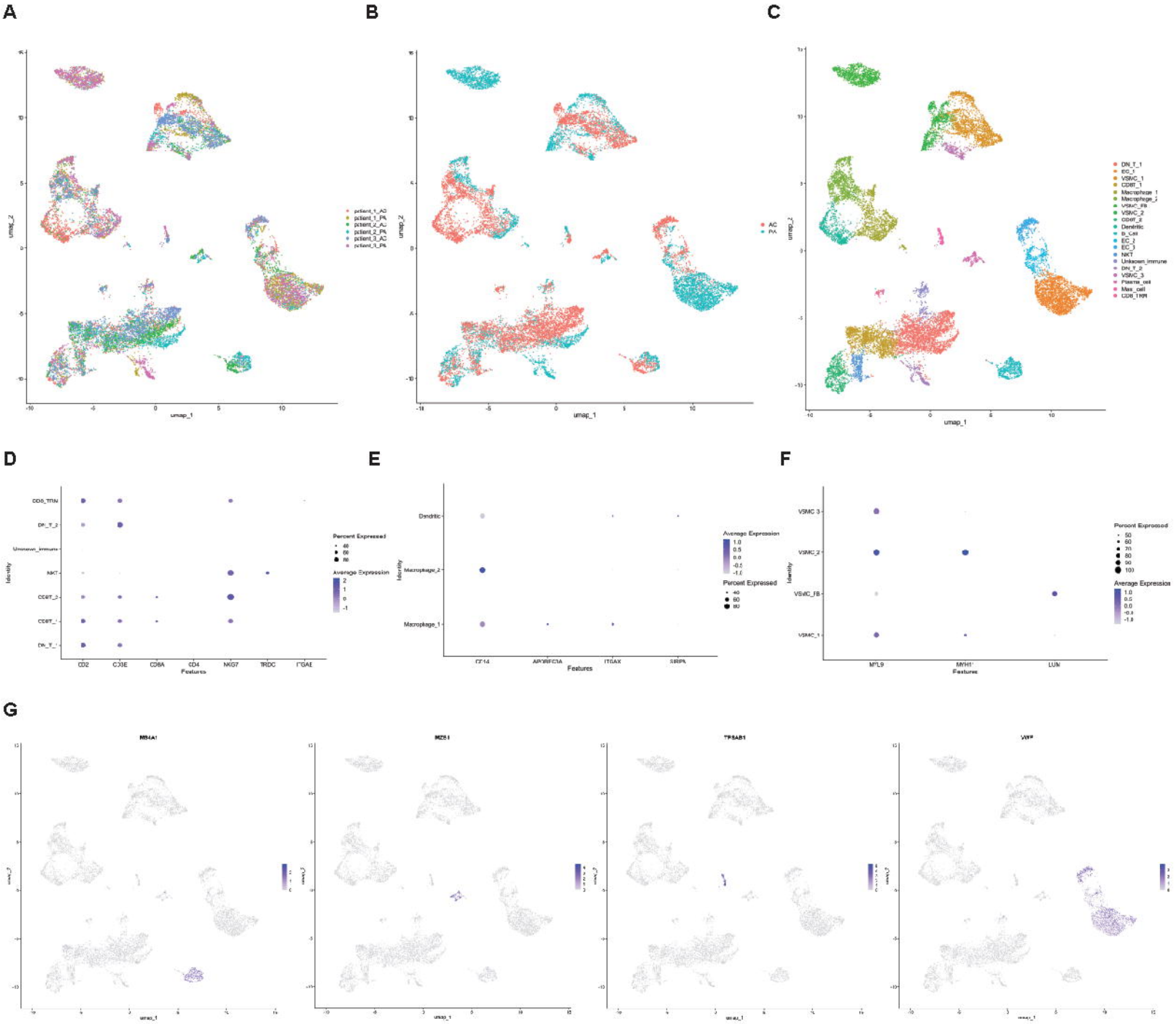

Supplemental Figure 10

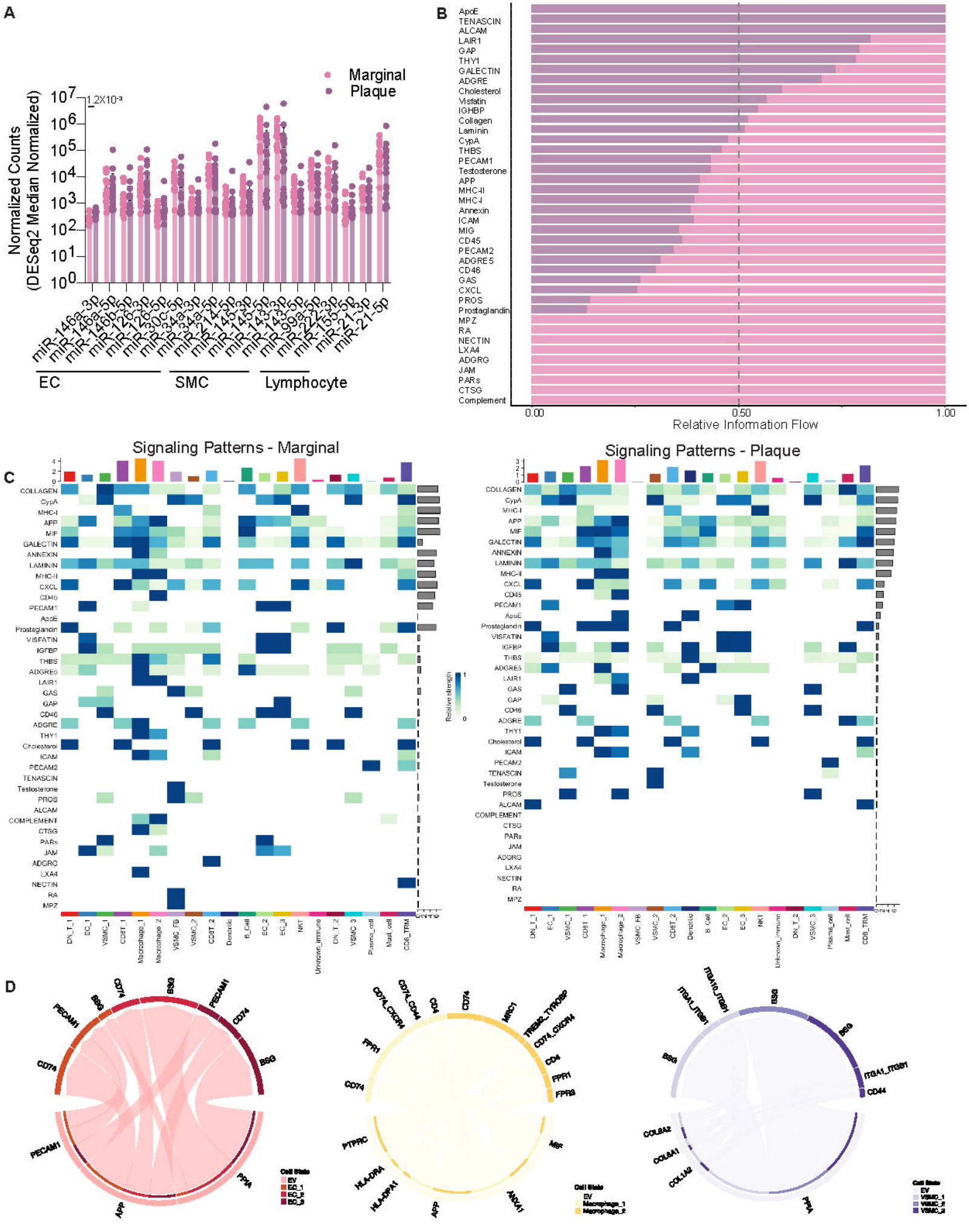

Supplemental Figure 11

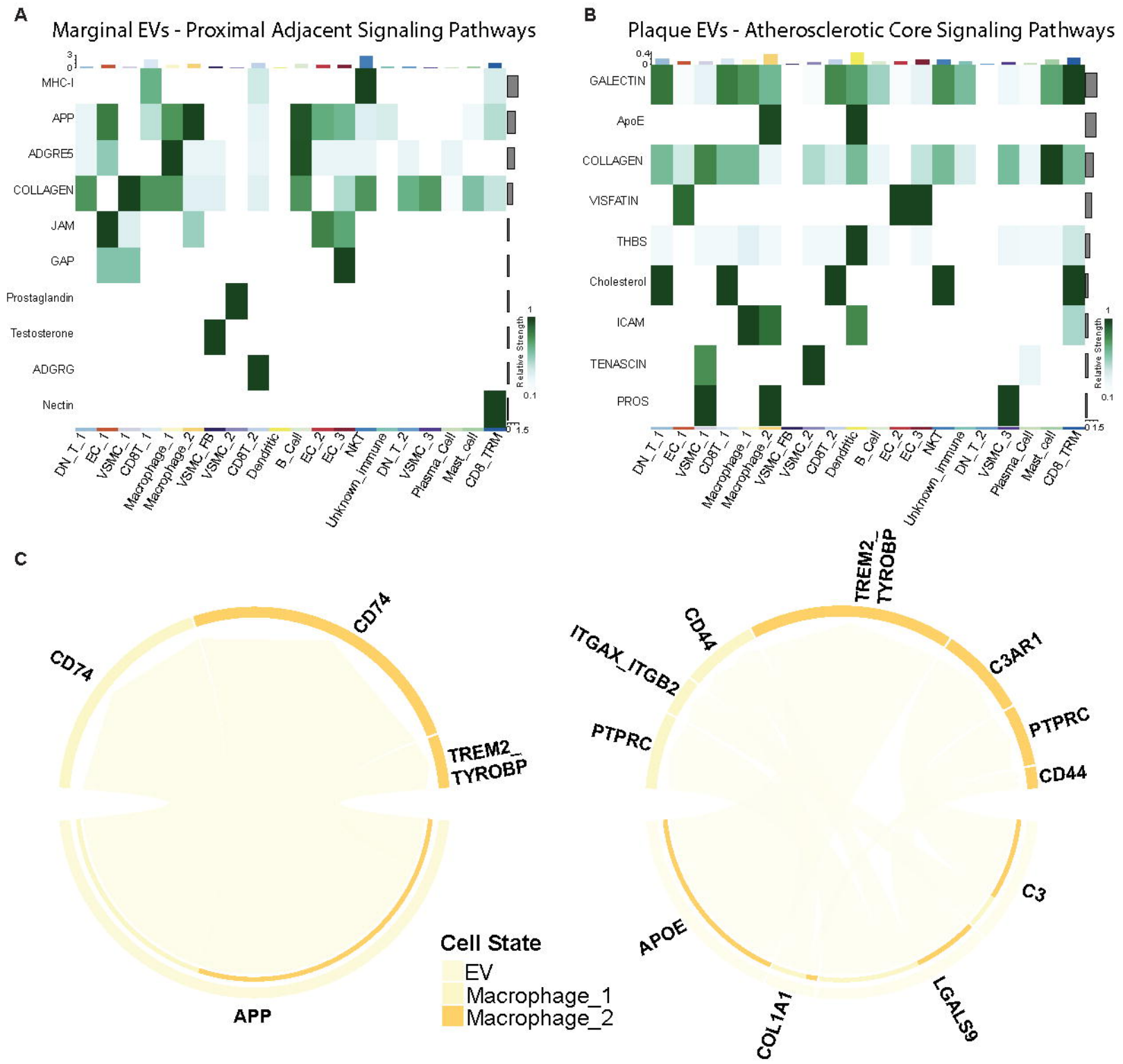

Supplemental Figure 12

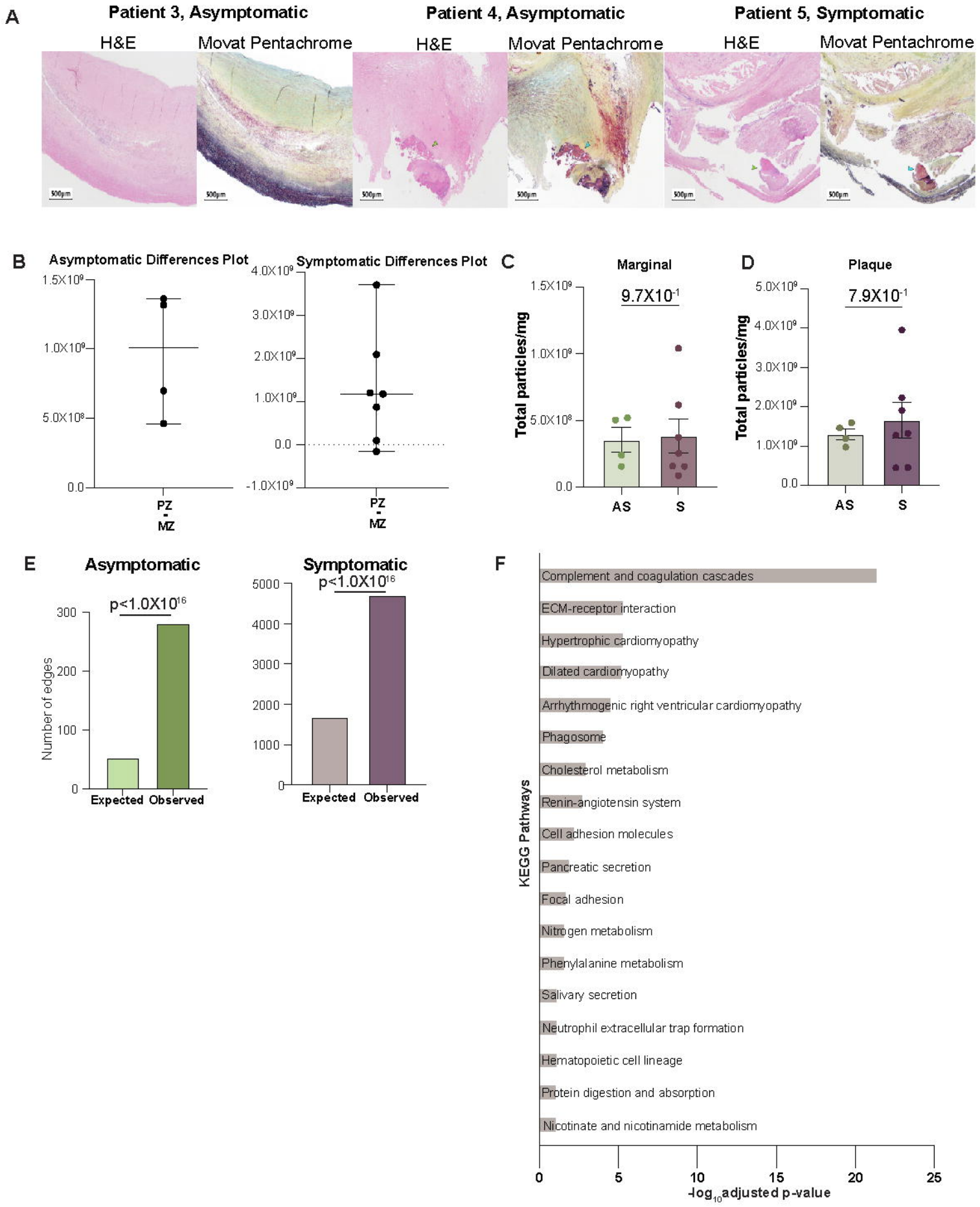

Supplemental Figure 13

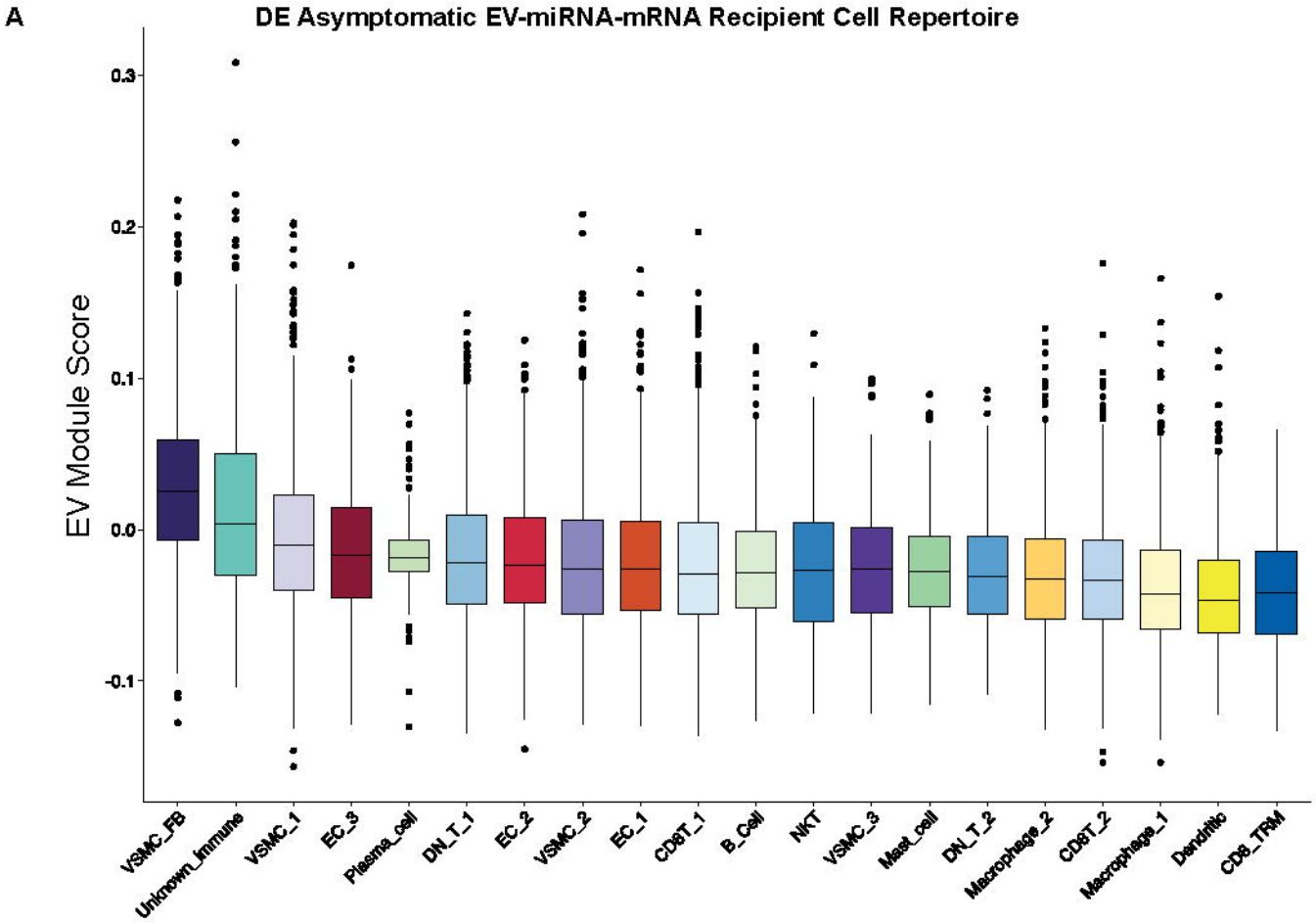

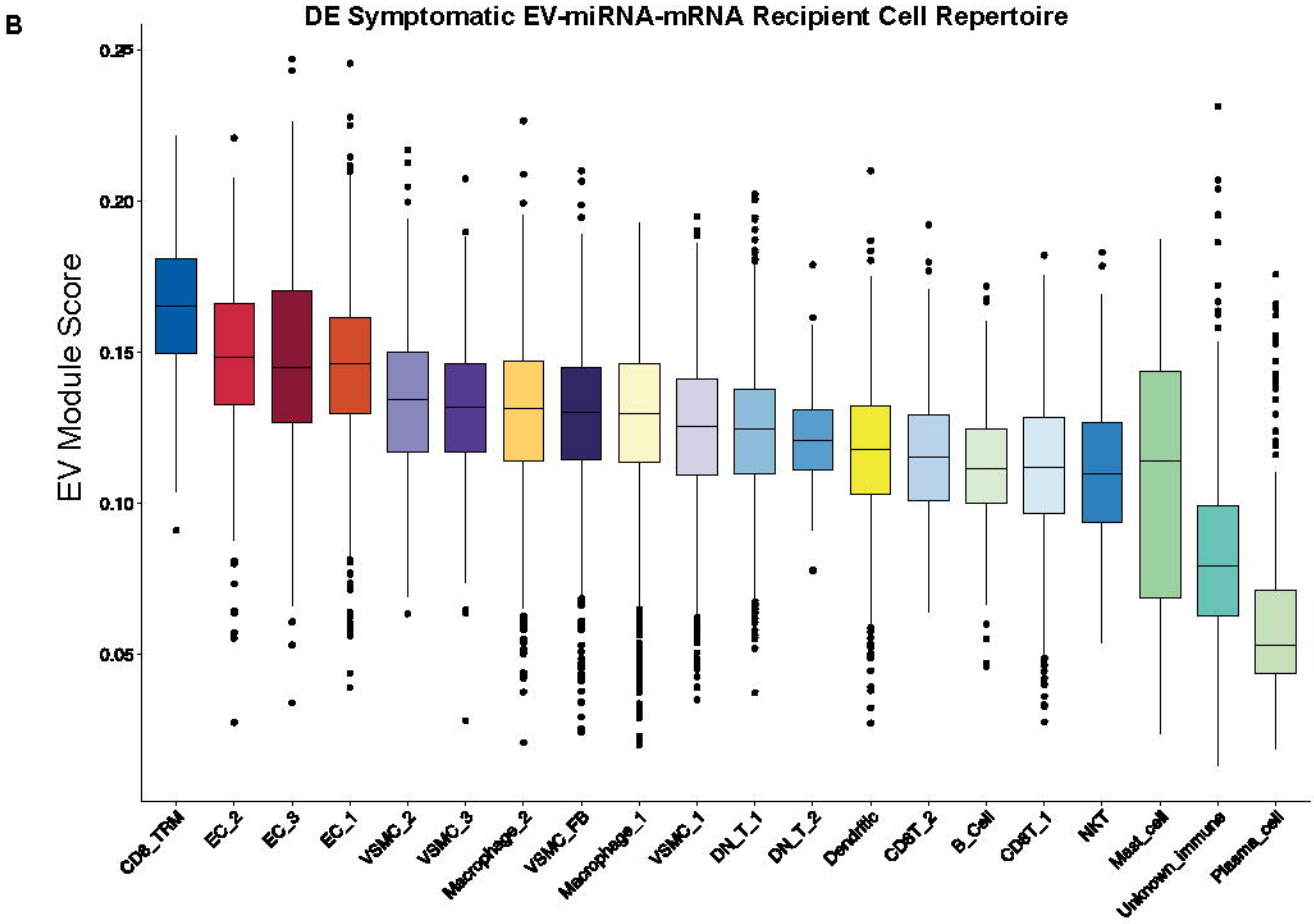

Supplemental Figure 14

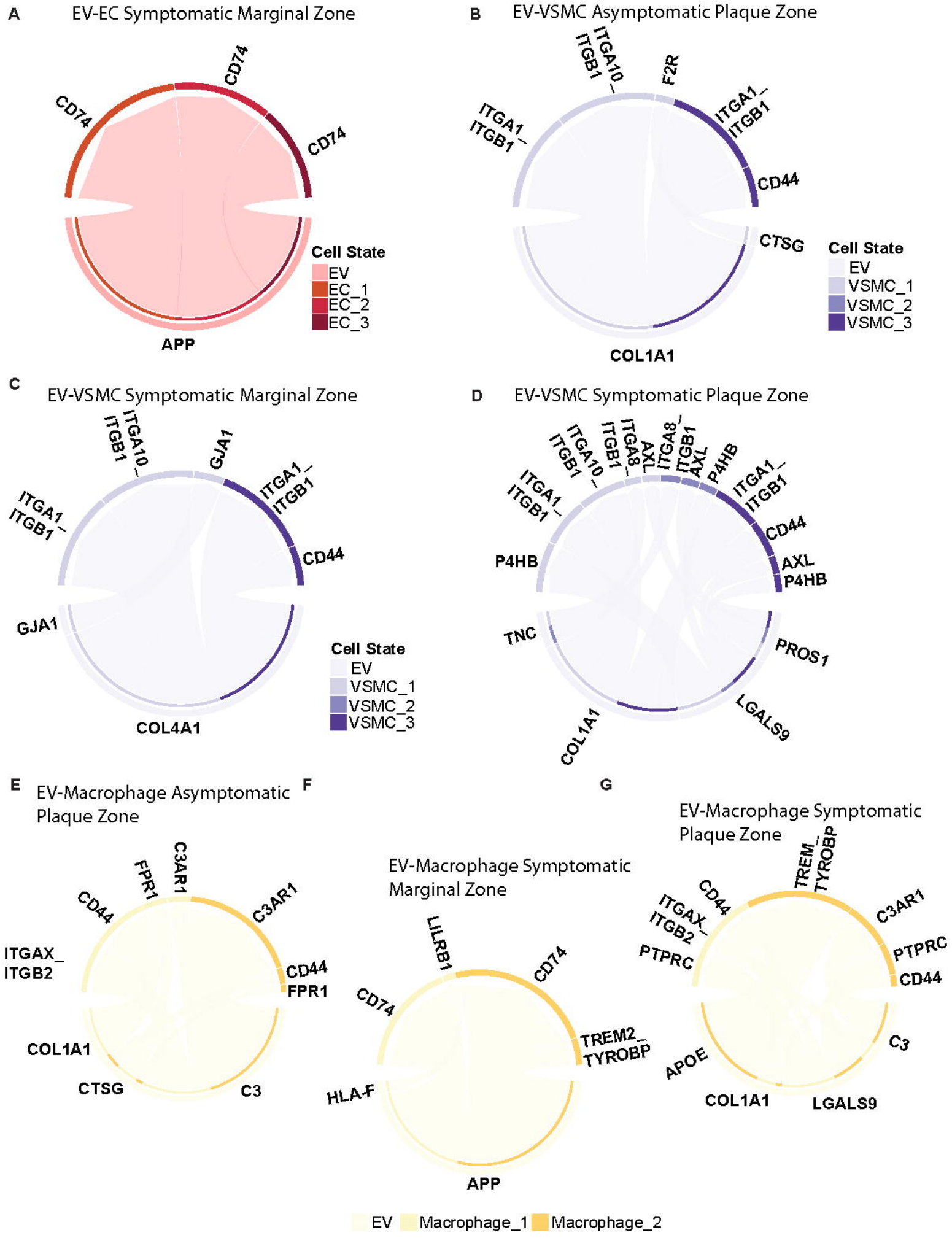

Supplemental Figure 15

EV marker CD63 in atherosclerotic plaques

Protein values normalized to CD63 levels

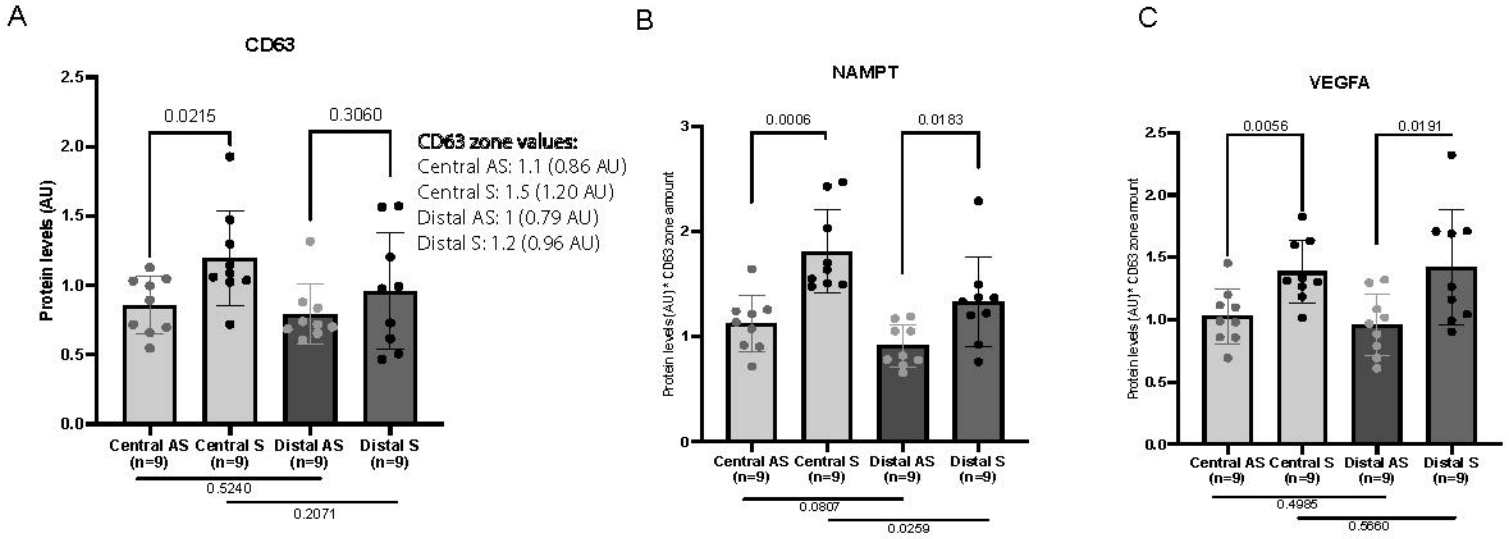

Supplemental Figure 16

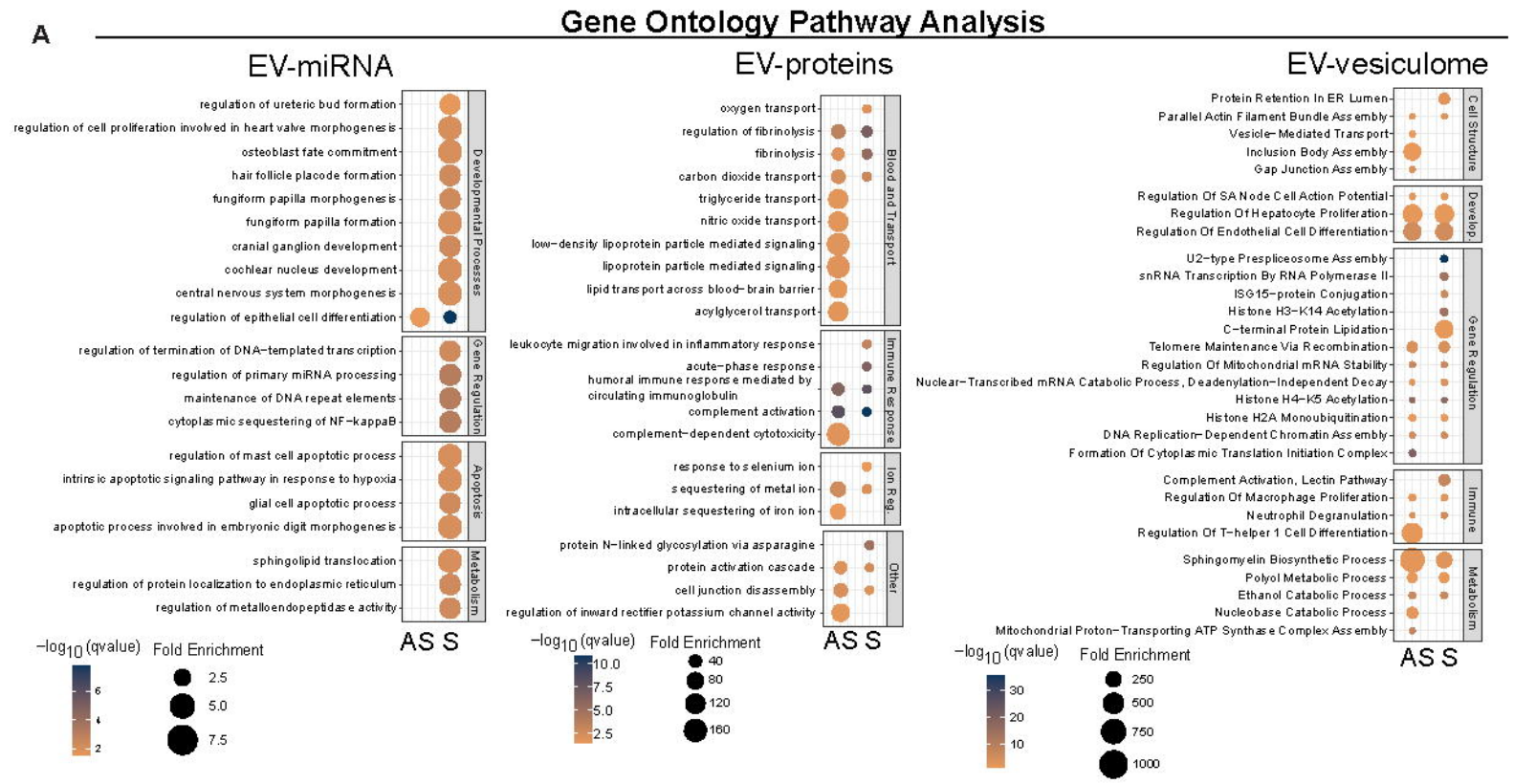

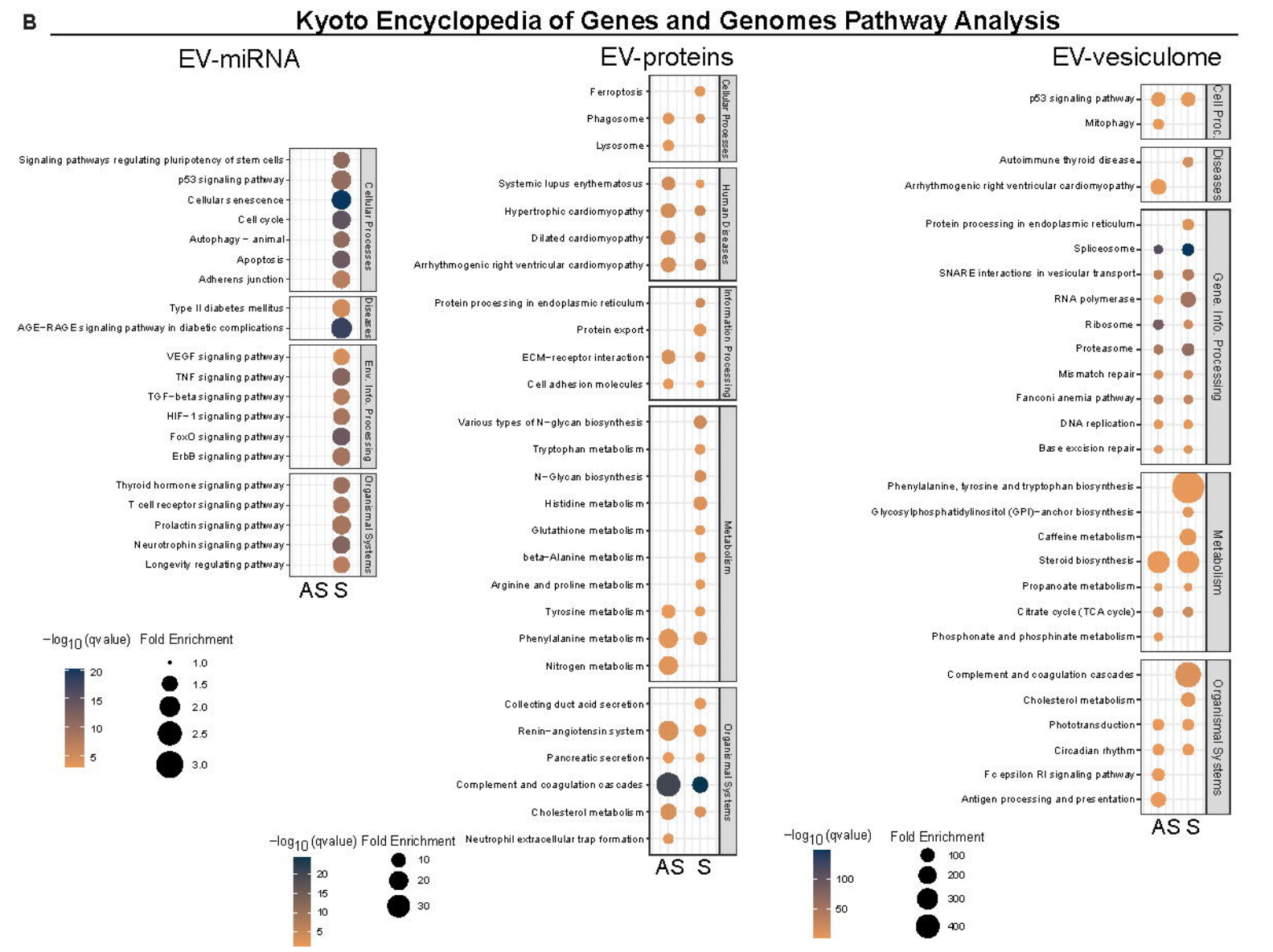

Supplemental Figure 17

Gene Ontology Overrepresentation Analysis

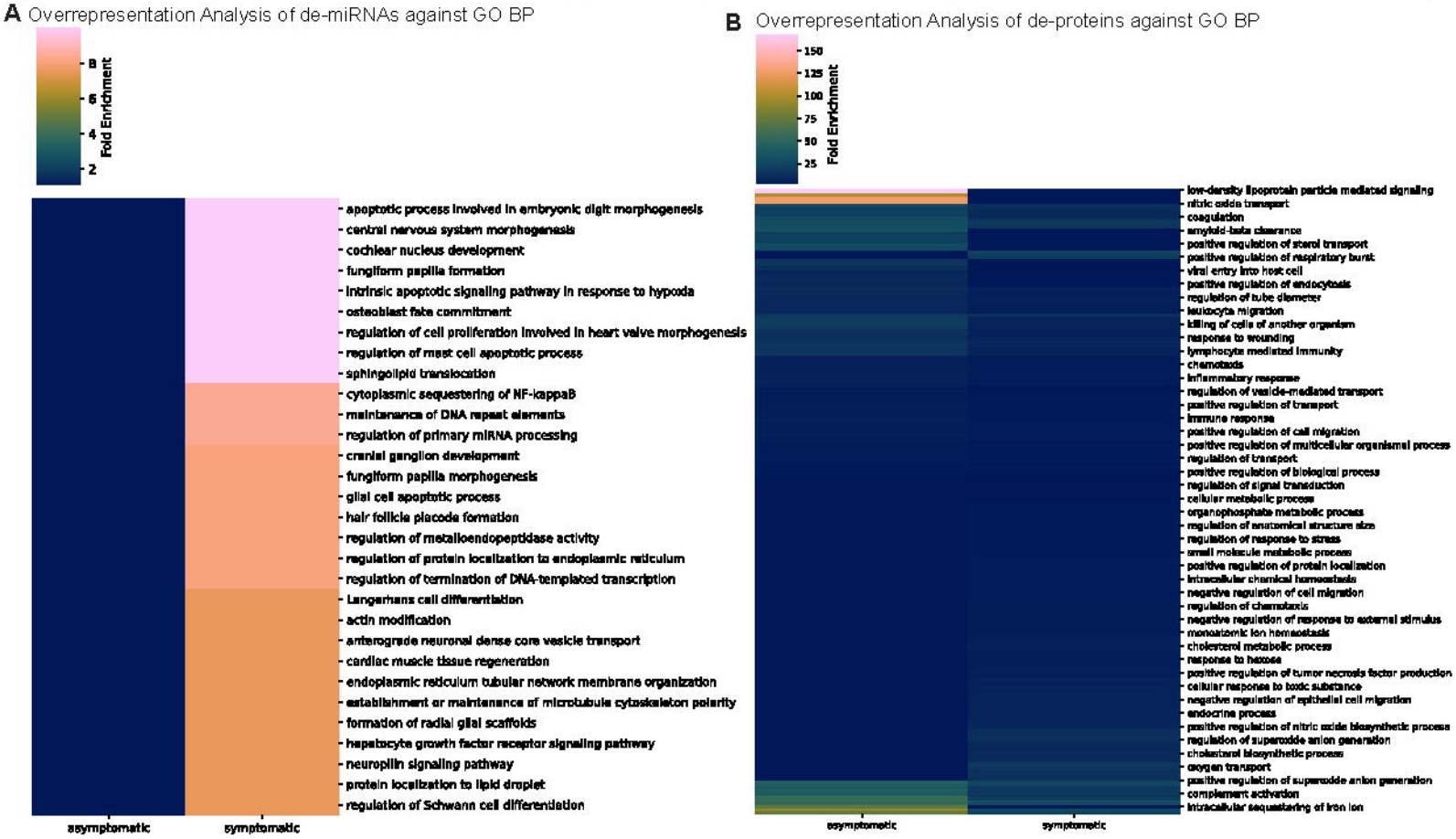

Kyoto Encyclopedia of Genes and Genomes Overrepresentation Analysis

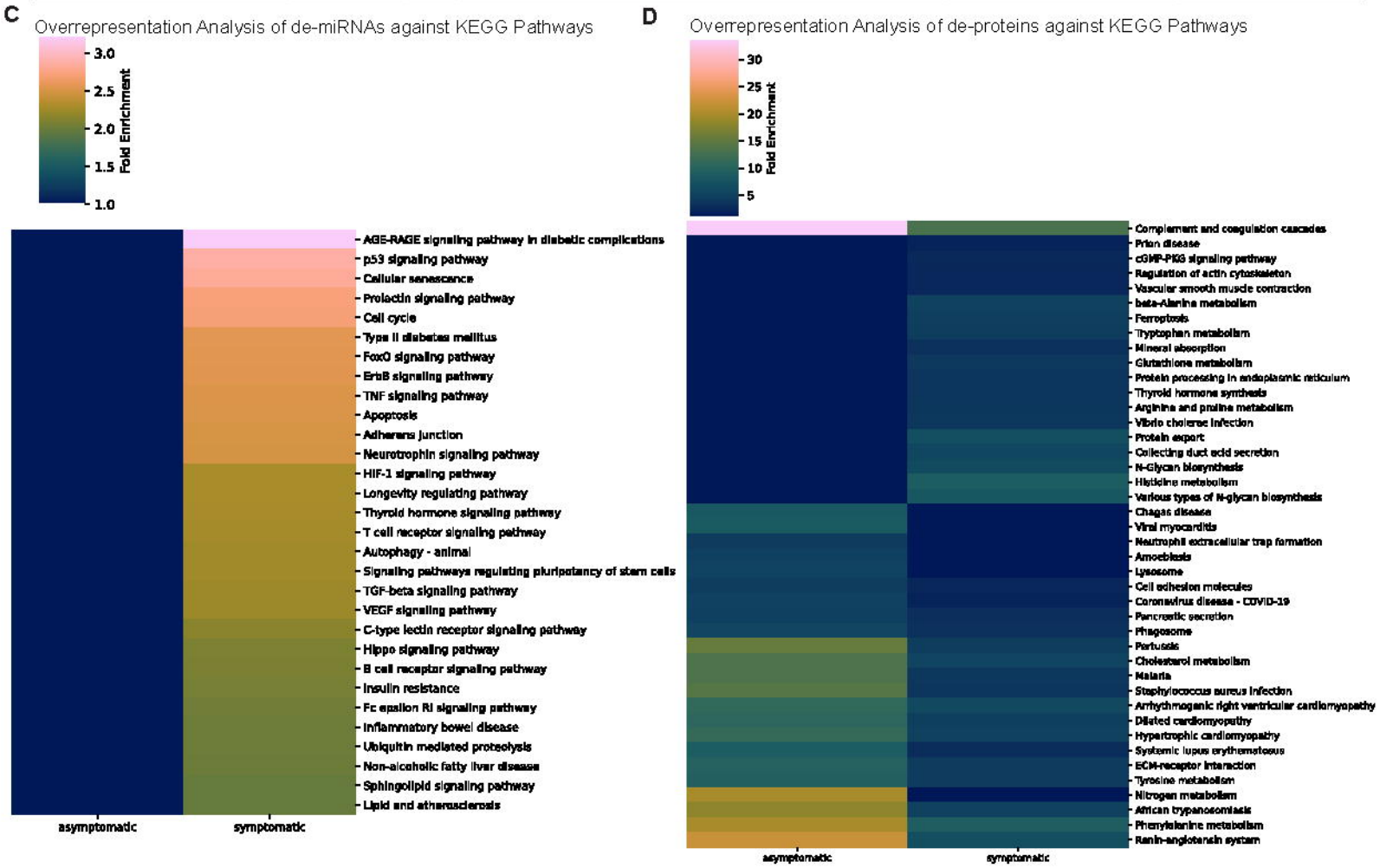

Supplemental Figure 18

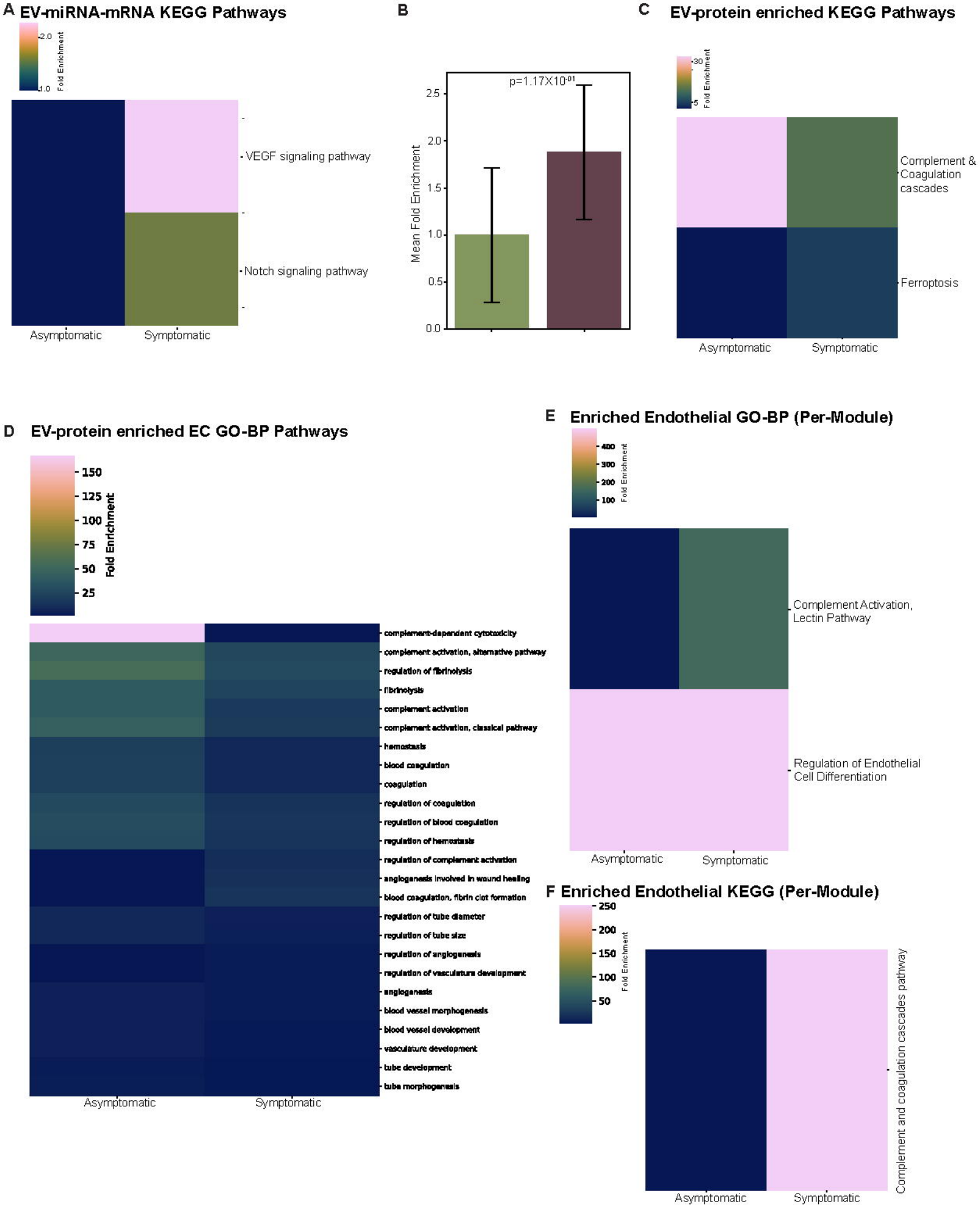
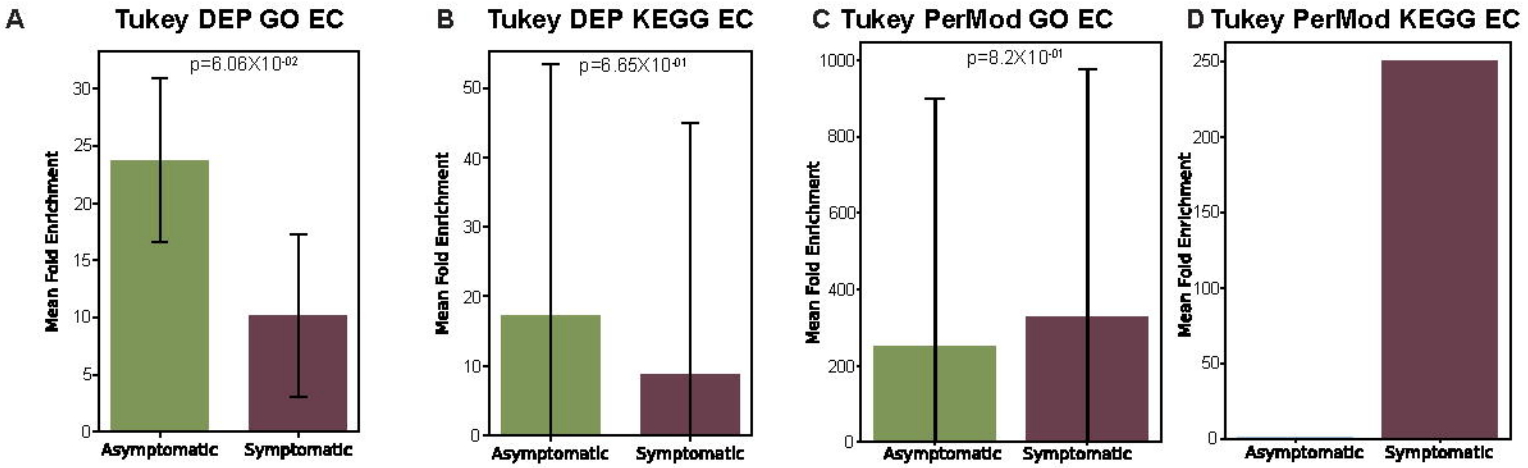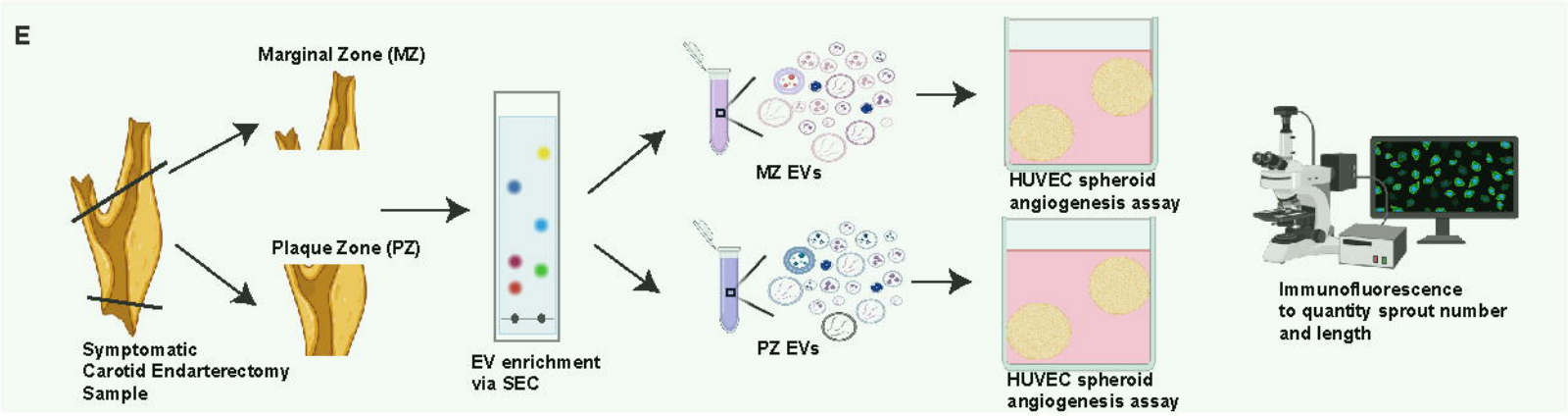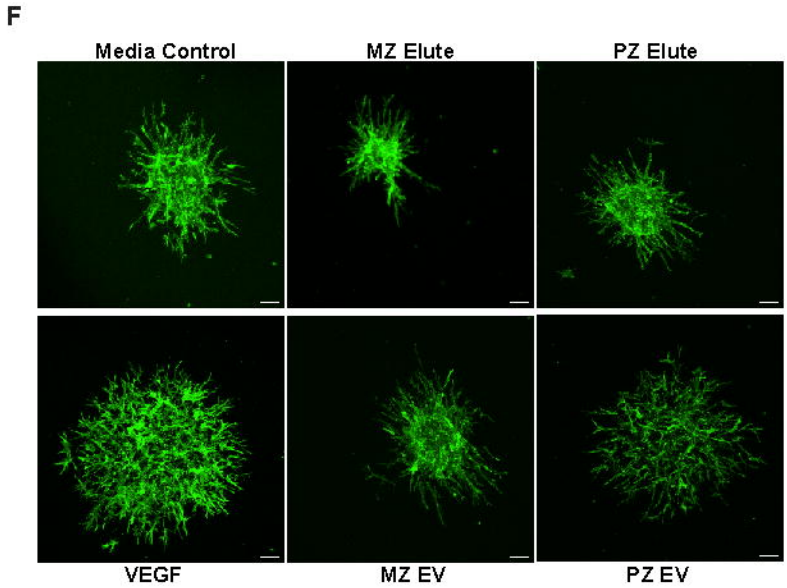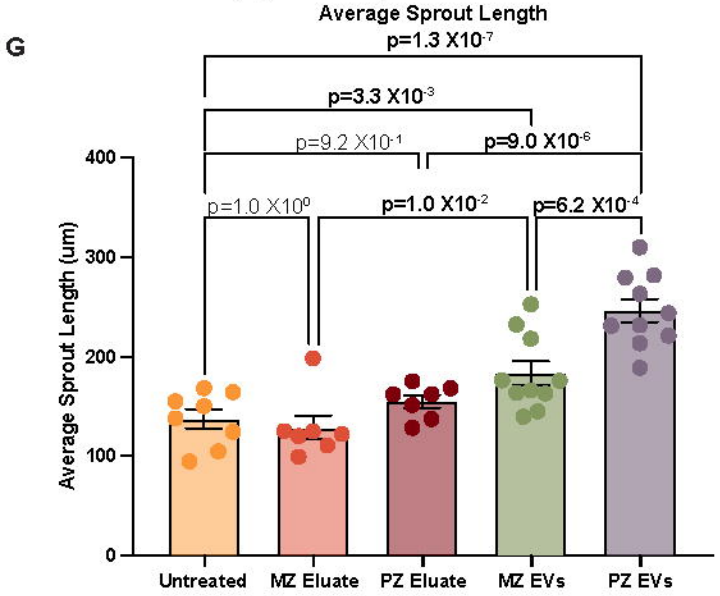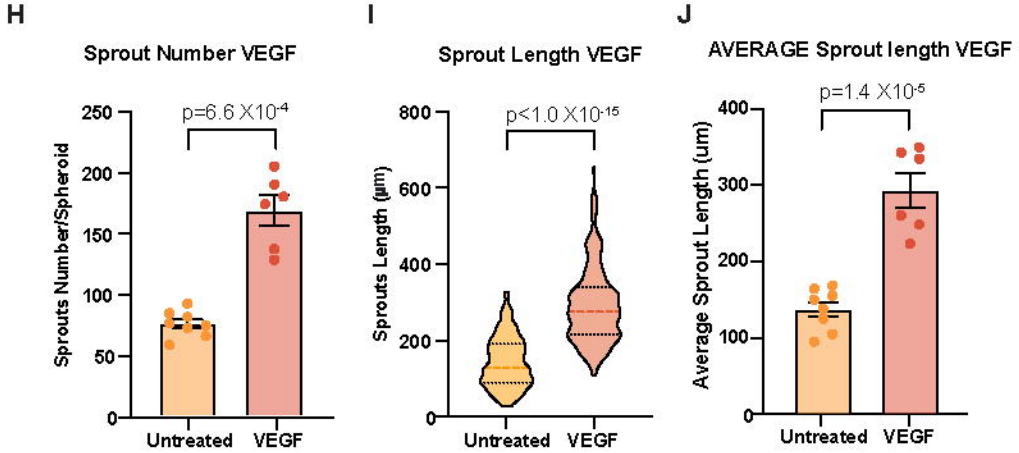
Supplemental Figure 19